Biochemical and structural attributes of *leishmanial* seryl and glutamyl tRNA synthetases

Thesis submitted to the University of Hyderabad for the degree of Doctor of Philosophy (PhD)

by

Bandigi Narsimulu

(Registration No. 16LTPH01)

Supervisor:

Dr. Insaf Ahmed Qureshi

Department of Biotechnology & Bioinformatics

School of Life Sciences,

University of Hyderabad

Hyderabad 500 046, India

University of Hyderabad
Hyderabad- 500 046, India

CERTIFICATE

This is to certify that this thesis entitled **"Biochemical and structural attributes of *leishmanial* seryl and glutamyl tRNA synthetases"** submitted by **Mr. Bandigi Narsimulu** bearing registration number **16LTPH01** in partial fulfilment of the requirements for award of Doctor of Philosophy in the Department of Biotechnology and Bioinformatics, School of Life Sciences, is a bonafide work carried out by him under my supervision and guidance.

This thesis is free from plagiarism and has not been submitted previously in part or in full to this or any other University or Institution for award of any degree or diploma.

Parts of his research work have been:

A. Published in the following research articles:

1. **Narsimulu B,** Qureshi R, Jakkula P, Sign P, Arifuddin M, **Qureshi IA** (2023). Exploration of seryl tRNA synthetase to identify potent inhibitors against leishmanial parasites. ***International Journal of Biological Macromolecules* 237(1): 124118.**
2. **Narsimulu B,** Qureshi R, Jakkula P, Are S, **Qureshi IA** (2022). Biophysical and structural characterization of ribulose-5-phosphate epimerase from *Leishmania donovani.* ***ACS Omega* 7(1):548-564.**
3. Jakkula P, **Narsimulu B**, **Qureshi IA** (2021). Biochemical and structural insights into 6-phosphogluconate dehydrogenase from *Leishmania donovani*. ***Applied Microbiology and Biotechnology* 105(13):5471-5489.**

B. Posters presented in International Conferences:

1. **Narsimulu B**, **Qureshi IA.** Evaluation of salicylate as a potent inhibitor for glutamyl-tRNA synthetase of *Leishmania donovani.* In: NextGen therapeutics & diagnostics to commercialization, NIPER, Hyderabad. April 20-22, 2022. **(Best Poster Award)**
2. **Narsimulu B,** Pranay J, **Qureshi IA.** Biophysical and biochemical characterization of 6-phosphogluconate dehydrogenase from *Leishmania donovani.* In: International

Symposium on Malaria Biology & 29th National Congress of Parasitology on Basic and Applied Aspects at University of Hyderabad, Hyderabad, India. November 1-3, 2018.

Further, the student has passed the following courses towards fulfilment of coursework requirement for Ph.D.

Course code	Name	Credits	Pass/Fail
BT 801	Analytical Techniques	4	Pass
BT 802	Research Ethics, Data Analysis and Biostatistics	3	Pass
BT 803	Lab work & Seminar	5	Pass

Supervisor

Dr. INSAF A. QURESHI
Associate Professor
Dept. of Biotechnology & Bioinformatics
School of Life Sciences
University of Hyderabad
Hyderabad-500 046, India.

Head of Department

HEAD
Dept. of Biotechnology & Bioinformatics
University of Hyderabad
Hyderabad.

Dean of School

संकाय अध्यक्ष / Dean
जीव विज्ञान संकाय / School of Life Sciences
हैदराबाद विश्वविद्यालय / University of Hyderabad
हैदराबाद / Hyderabad-500 046.

University of Hyderabad
Hyderabad- 500 046, India

DECLARATION

I, **Bandigi Narsimulu**, hereby declare that this thesis entitled **"Biochemical and structural attributes of *leishmanial* seryl and glutamyl tRNA synthetases"** submitted by me under the guidance and supervision of **Dr. Insaf Ahmed Qureshi**, is an original and independent research work. I also declare that it has not been submitted previously in part or in full to this University or any other University or Institution for the award of any degree or diploma.

Date:

Signature of the student

Name: Bandigi Narsimulu

Regd No. 16LTPH01

Signature of the Supervisor

Dr. INSAF A. QURESHI
Associate Professor
Dept. of Biotechnology & Bioinformatics
School of Life Sciences
University of Hyderabad
Hyderabad-500 046, India.

Acknowledgements

Completion of this doctoral dissertation would not have been possible without the support of several people. I would like to express my sincere thanks to all of them.

First of all, I would like to express my deepest gratitude towards my research supervisor, **Dr. Insaf Ahmed Qureshi**, for his constant guidance throughout my Ph.D. His support during the critical phases of my Ph.D is phenomenal. He lightened up the way in my darkest times and encouraged me a lot in the academic life. I am also very grateful for his scientific advice knowledge and many insightful discussions about research and life. The everlasting discussions and the freedom of my thoughts to design and plan experiments made me more research oriented and gave a lot of self-confidence to build my own research aptitude. He always made himself available to clarify doubts despite his busy schedules, and I consider it is a great opportunity to do my doctoral programme under his guidance and to learn from him research expertise.

I would like to thank my doctoral committee members, **Drs. N. Prakash Prabhu** and **M. Venkataramana** for their insightful evaluation and critical suggestions for improving my work.

I am also thankful to **Drs. Mohd. Akif, Bindu Madhava Reddy, Nooruddin Khan, and Irfan Ahmad Ghazi** and for allowing me to use their lab facilities.

I wish to thank the present and former **Heads and Deans** of the **Department of Biotechnology and Bioinformatics and School of Life Sciences**, University of Hyderabad, respectively for providing me with all the essential facilities.

I am thankful to **Drs. Santhosh Gattredi, Sayanna are, and Saleem** for their support during experiments, data analysis.

I am thankful to my lab members **Pranay, Janish, Jyotisha, Fauzia** along with present and former M.Sc and M. Tech students for their support and for creating a peaceful and amiable work atmosphere in the lab.

I am also thankful to **Dr. Rahila Qureshi** for her help during cell culture experiments and for data analysis.

I am grateful to **Prof. Swati Saha,** University of Delhi South Campus, New Delhi for providing genomic DNA of *Leishmania donovani.*

I would like to thank my friends **Shankar, Kumar, chaitanya, Pankaj, Nachiket, Shiraj, Matin** and other SLS friends for their support and making the campus life cheerful and memorable.

I also extend my thanks to Biotechnology office staff, **Mr. Rajashekar, Mr. Shekar, and Mr. Rahul** for their help in time.

I greatly acknowledge **UGC** for providing me financial support (JRF and SRF).

I also thank all the funding bodies (**ICMR, CSIR, DST, UPE, DBT and PURSE**) for their financial assistance to the department and school.

I am much indebted to **my parents** and **wife** for their love and support. I am thankful to my elder brother **Bandigi Balamurali** for providing me the moral support and encouragement from my childhood. He is like teachers to me and without him, I would not have achieved this.

Bandigi Narsimulu

Dedicated to My Parents

CONTENTS

Page No.

List of Figures and Tables

Page No.

Figures

Tables

Abbrevations

µl	Micro litre
µM	Micro molar
Å	Angstrom
aaRS	Aminoacyl tRNA synthetase
ATP	Adenosine 5' triphosphate
bp	Base pair
cm	Centimetre
CD	Circular Dichroism
ºC	Degree centigrade
DNA	Deoxy ribonucleic acid
DTT	1, 4-dithiothreitol
EDTA	Ethylene diamine tetraacetic acid
GROMACS	GROningen Machine for Chemical Simulations
IPTG	Isopropyl β-d-1-thiogalactopyranoside
kb	Kilo Base
Kilo Dalton	Kilo Dalton
M	Molar
mg	Milli gram
min	Minutes
ml	Milli liter
mM	Milli molar
ns	Nano second
nm	Nano meter
OD	Optical density
PDB	Protein data bank
PPase	Inorganic pyrophosphatase
aaRS	Aminoacyl-tRNA synthetase
SDS-PAGE	Sodium dodecyl sulphate-Polyacrylamide gel electrophoresis
*Ld*SerRS	Seryl-tRNA synthetse of *Leishmavnia donoani*
*Hs*SerRS	Seryl-tRNA synthetse of *Homo sapiens*
*Ld*GluRS	Glutamyl-tRNA synhetase of *Leishmavnia donovani*

cDNA	Circular deoxy ribonucleic acid
PPi	Inorganic pyrophosphate
pCMB	para chloromercuri benzoic acid
AMP	Adinosine mono phosphate
EF1&2	Elongation factor 1 & 2

1. Introduction and review of literature

Leishmaniasis, a vector-borne disease, is one of the prevalent neglected tropical diseases (NTDs) in the majority of underdeveloped countries. According to the WHO, more than 50,000 new cases are reported globally each year [**1**]. Leishmaniasis is spread by trypanosomatid parasites of genus *Leishmania*, which are free-living, obligatory, tiny, unicellular microorganisms that can enter human macrophages and result in life-threatening infections. The main risk factors for this disease include immune system weakness, inadequate shelter, poor diet, and lack of awareness [**2**].

1.1 History

Leishmaniasis has a long history dating back to first century AD. The first indicator of leishmaniasis was cutaneous and mucocutaneous leishmaniasis. Skin lesions and facial deformities were the most common symptoms of the disease affecting agricultural farmers during the 15th and 16th centuries. The disease was given different names like White leprosy, Andean sickness, Valley sickness and Black fever [**3]**. It was further classified as Aleppo boil in 1756 by Alexander Russell, and as black fever in African countries and kala-azar in India in the mid-18th century [**4**].

Leishmania was noticed individually by a Scottish pathologist William Leishman and the Irish doctor Donovan. This infection was officially dubbed Leishmaniasis in the year of 1901. Among them, William Leishman worked as a medical officer in India for the British Army. Having collected ovoid bodies from the spleens of patients suffering from fever, muscular atrophy, and inflamed spleens, he named this disease Dum Dum fever. Charles Donovan observed similar characteristics in a patient suffering from prolonged fever a few months later, which was detected using Leishmania's stain. Later, Ronald Ross coined the term *Leishmania donovani* on behalf of both the doctors who discovered this parasite [**5]**. Based on where the disease is most prevalent, leishmaniasis has been divided into Old world (Africa, Mediterranean basin and the Middle East) and New world (Central America, Mexico and South America) leishmanial infections [**6**].

1.2 Taxonomic classification

The *Leishmania* protozoan parasites are associated with order Kinetoplastida and are responsible for a number of infectious illnesses that affect people. Kinetoplastida is further split into two sub-orders, one of which is Trypanosomatidae. This sub-order has a number of parasites belonging to nine different genera that affect plants as well as lower and higher

vertebrates [**7**]. Among them, two genera are mainly responsible for infections in human, namely, *Trypanosoma* and *Leishmania*.

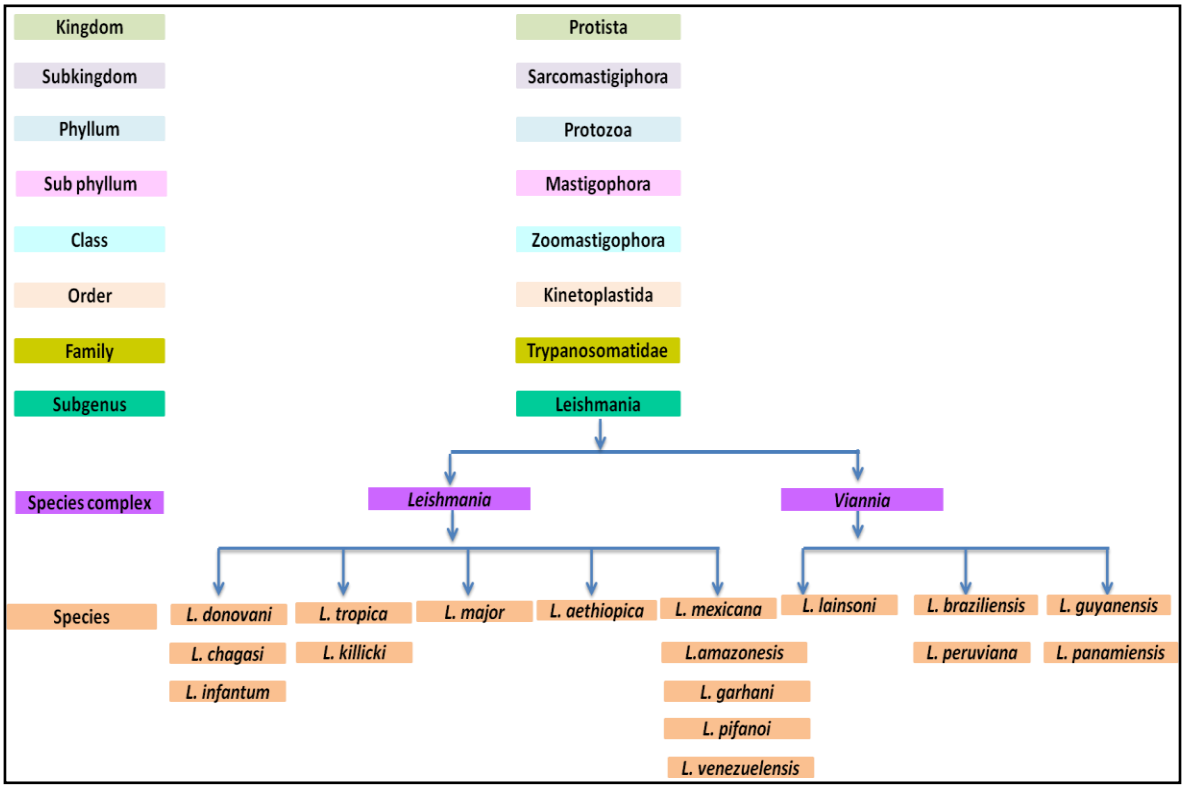

Figure 1: Classification of *Leishmania donovani*

Leishmaniasis is spread through the bite of infected female Phlebotomine sandflies [**8**]. In mammals, cutaneous leishmanisiasis (CL) is majorly caused by *L. major*, *L. mexicana* and *L. braziliensis* while *L. donovani*, *L. chagasi*, and *L. infantum* are principal agents for fatal visceral leishmaniasis (VL) **(Fig. 1)**.

1.3 Prevalence

Leishmaniasis is classified by WHO as a type-I disease, which is the most ignored and contagious tropical disease [**9**]. Around 89 nations are home to 12–15 million cases of leishmaniasis worldwide **[10]**. VL is endemic in Africa, Asia, America, and the Mediterranean region affecting approximately 50,000 to 90,000 people worldwide annually, however only a tiny fraction (19–37%) was reported to health centres. From 2011 (2, 00, 000-4, 00, 000 new infected cases) till 2017 (50, 000-90, 000), the number of reported VL infections decreased significantly worldwide [**11, 12**]. In light of this, Indian sub-continent (Bangladesh, India, and Nepal) has set a goal to eradicate VL by 2015 with WHO assistance **[13].** Globalization and

changes in environmental conditions have caused an upsurge in *Leishmania* cases over the past 25 years and also spreading it to new areas.

1.4 Geographical distribution

Most of the Mediterranean, tropical and subtropical countries are affected by the neglected tropical illness leishmaniasis, whereas it hasn't been reported in either Australia or Antarctica **[14**]. The disease spreads to mammals, including humans, by sandflies and there are more than 20 different species of *Leishmania* that infect mammals as hosts during the parasite life cycle [**15**]. While many parasitic infections are spread through laboratory infection, organ transplantation, or even blood transfusion, the former uses vectors including sandflies of the species Phlebotomus (Old World) or Lutzomyia (New World) **[16]**. Two epidemiological patterns exist for visceral leishmaniasis (VL) such as anthroponotic VL that spreads mostly between human and to a lesser extent between people to animals. The second one is zoonotic VL, which is spread from animal to people and, to a limited proportion, between animals. Anthroponotic VL, caused by *Leishmania donovani*, is present in India, Nepal, East Africa and Bangladesh [**17**]. The zoonotic type is characteristic of *Leishmania infantum*, found in South America and Mediterranean basin [**18**]. This disease mostly disseminated from southern Texas to new Argentina and other places including the Middle East, Africa and Asia [**19**]. The majority of cutaneous leishmaniasis (CL) cases are reported in Iran, Saudi Arabia, Algeria, Syria and Afghanistan while mucocutaneous leishmaniasis (MCL) is reported in Brazil [**20, 21**]. *L. donovani* is responsible for visceral leishmaniasis (VL) with the majority of cases occurring in the seven nations i.e. India, Kenya, Sudan, Brazil, Somalia, Iran, and South Sudan [**22**] **(Fig. 2)**.

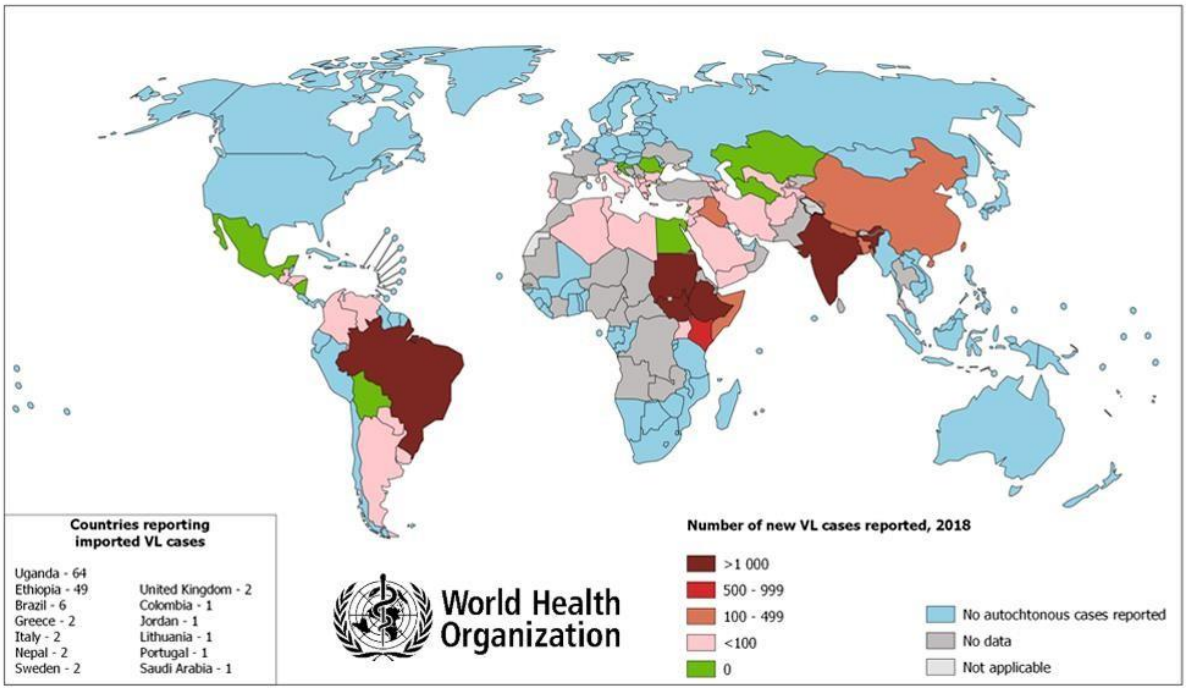

Figure 2: Worldwide prevalence of leishmaniasis (WHO Report 2018)

1.5 Visceral leishmaniasis in India

In India, visceral leishmaniasis (VL) has been the most common medical consequence. It is commonly known as kala-azar in the Indian subcontinent and can affect people of all ages. About 7, 60, 432 cases of VL were recorded between 1987 and 2011. Out of 676 districts, 54 were infected in India, in which, 34 districts belonged to the north-eastern state of Bihar reflecting 70% of the overall VL cases [**23**]. The number of yearly reported VL cases drastically declined from 77,102 in 1992 to 12,140 in 2002 with a mean of 30417.28 per annum, while the rate of mobility and mortality was higher in the years 1992 and 2007. It is a widespread infection in 52 places throughout four Indian states, with the worst cases occurring in Jharkhand (4 regions), West Bengal (6 areas), Uttar Pradesh (11 districts), and Bihar (31 areas) [**24**] **(Fig. 3)**. *L. donovani* typically causes VL in humans by the bite of an infected sand fly vector called *Phlebotomus argentipes* [**25**]. Asymptomatic people do not lead to the spread, however, there is one symptomatic case within every 8-9 asymptomatic cases and thus, it is necessary to clarify their involvement in the transmission of infection [**26**]. Only a small number of Post kala azar dermal leishmaniasis (PKDL) instances have been recorded in the Indian subcontinent, and there isn't much information accessible about them. Recently, leishmaniasis-HIV co-infection was reported with 5.6% of VL cases tested positive for HIV infection [**27, 28**].

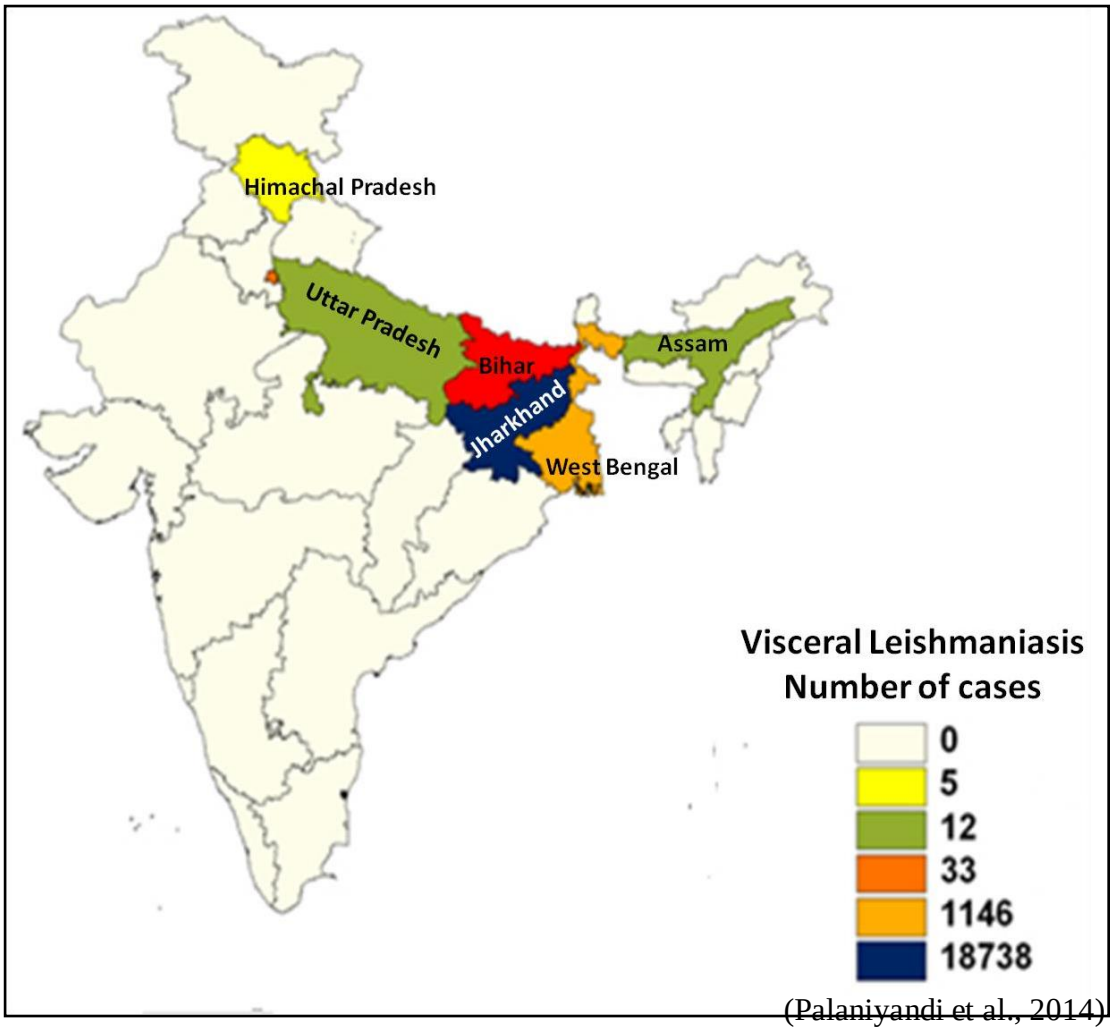

(Palaniyandi et al., 2014)

Figure 3: Indian states with VL prevalence

1.6 Disease transmission

Leishmania parasites are transmitted to individuals through the bite of phlebotomine sand flies. Up to 98 species primarily found in the genera *Lutzomyia* and *Phlebotomus* have been identified as human leishmaniasis vectors [**29**]. Sand flies belonging to the genus *Phlebotomus* may survive in tropical, subtropical, and temperate climates. Commonly, sandflies suck the blood meal in the evening and their activity is shown in the hottest periods of the day. The growth of a parasite within the midgut can only be supported by female sandflies that feed on the blood of animals. The parasite grows inside the sandfly's gut before being injected into the skin during the next blood meal, which it seeks out by hunting down a blood meal from an infected animal or person [**30**]. Humans are included in the anthroponotic mode of transmission, whereas the dog is the main source of zoonotic transmission [**31**].

1.7 Life cycle of *Leishmania*

Humans and invertebrates serve as the hosts for the protozoan dimorphic intracellular parasite species known as *Leishmania donovani* [**32, 33**] In the *Leishmania* life cycle, promastigotes and amastigotes are the two morphological forms [**34**]. In the human circulatory system and macrophages, the amastigotes stage is frequently seen that lacks flagella and is intracellularly immobile. In the mononuclear phagocytic cells, a brief oval structure measuring 3-6 mm in length and 1-3 mm in diameter is present. Promastigotes are extracellular, motile, 15-20 µm long flagellated forms of *Leishmania* that are found in the sandfly's nutrient track. They are noticeably bigger than amastigotes and demonstrate the longitudinal binary fission mode of multiplication [**35, 36**]. The beginning of the parasite life cycle occurs when a healthy person is bitten by an infected female sandfly, which injects procyclic promastigotes into the bloodstream where *Leishmania* parasites successfully invade and multiply within human mononuclear phagocytic cells [**37, 38**]. Mammalian macrophages and other mononuclear phagocytic cells are the hosts for promastigote where it transforms into amastigote.

Due to the huge quantity of amastigotes that proliferate within the cells, the location of parasite discharge causes the cell bursts, re-invasion of nearby macrophages, and activation of the adaptive immune system. After the sandfly bites an infected person, the amastigotes enter the sandfly's midgut that is covered by the type-I peritrophic membrane (PM) [**39**]. The amastigotes quickly multiply, change into procyclic promastigotes, and then transform into nectomonad promastigotes. Nectomonads distinguish into leptomonad promastigotes when they go into the front region of the sandfly gut, undergo rapid multiplication, and locate the stomodeal valve. Leptomonads transform into haptomonads and metacyclics after colonisation [**40**], which enter the sandfly's proboscis and inject these promastigotes during blood meal **(Fig. 4)**. The difference in temperature and pH between the mammalian host and the insect host is conducive to leishmanial differentiation [**41, 42**].

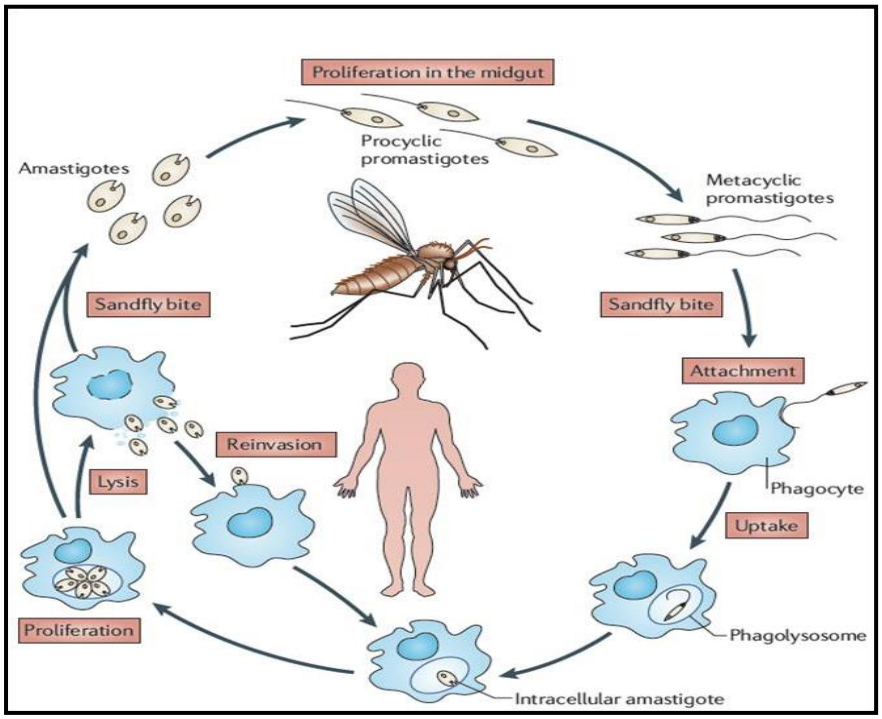

(Kaye et al., 2011)

Figure 4: *Leishmania* parasite life cycle. The parasite completes its life cycle in two hosts under various conditions.

1.8 Pathogenesis

Different clinical symptoms of leishmaniasis arise by the interaction of the host's immune system and the pathogenic species type [**43**]. This heterogeneity may be caused by changes in the genetic content that emerged over evolution, which may explain why certain species choose to infiltrate visceral organs while others prefer to attack the skin [**44**]. The cutaneous and visceral leishmaniasis causing pathogens differ in the types of macrophages they attack depending on their affinities for particular macrophage surface receptors, albeit how they do this remains unclear [**45, 46**]. Additionally, the host's ability to respond through adaptive and natural immunity, which is mostly under hereditary control, has an impact on clinical symptoms [**43**]. Based on how the disease develops, leishmaniasis can be divided into four types, namely, cutaneous, visceral, mucocutaneous, and post-kala-azar leishmaniasis.

1.8.1 Visceral Leishmaniasis (VL)

The visceral form is the most severe and deadliest among the distinct form of leishmaniasis with around 30,000 to 50,000 new cases per year (WHO, 2019). Notably, India, Sudan, Ethiopia, Brazil, Somalia, and Kenya account for more than 90% of all VL infections. The time it takes for VL to incubate varies and the clinical symptoms may appear in 10 days to

less than a year after exposure [**47**]. The major signs of the disease generally include spleen enlargement and liver swelling. Additionally, weight loss, moderate fever, and anorexia were observed in children from one week to one year [**48**]. The aggregation of phagocytes inside of the infected organs and the manifestation of reticuloendothelial hyperplasia, a defining hallmark of splenomegaly and hepatomegaly are the typical symptoms of VL [**49**]. If VL is not properly or effectively treated, it can result in secondary infections, a sharp decline in platelet count, and mortality within one to two years. Based on increased skin pigmentation, VL is known as kala azar in the Indian subcontinent [**50**]. According to a WHO report, any VL patient who is also co-infected with HIV may represent a more advanced form of leishmaniasis infections **[51]**. The recent research from India and Brazil has revealed that up to 16% of individuals presenting with VL are also co-infected with HIV infection [**52**].

1.8.2 Post kala azar dermal leishmaniasis (PKDL).

Post kala azar dermal leishmaniasis (PKDL) is a rare post-complication of VL prompted by *L. donovani*. Nearly 5–15% of PKDL instances were seen in India, whereas that number rises to 55% in Sudan [**53**]. Following an immune response to the parasites in human, the PKDL remain in the skin and serve as a reservoir for the illnesses. Patients with PKDL infection still have parasites in their skin even after treatment and TH-2 cells were found to be stimulated to overexpress IL-10 and TH-1 cells consistently [**27**]. Infected people have an erythematous, maculopapular and hypopigmented or macular rash all over their mouth, trunk, and sometimes the entire body [**54**]. About 60 percent of VL cases in east Africa (Sudan and Ethiopia) and 10 percent in Asia (India, Bangladesh and Nepal) are complicated by dermatosis (hypopigmented erythematous rash that covers their mouths and trunks) and can spread to covering the entire bodies [**55**].

1.9 Treatment options

Since a few decades ago, pentavalent antimonials like sodium meglumine antimoniate or sodium stibogluconate have been utilised specifically for the treatment of VL. As a result of ineffectiveness of these drugs, the treatment period is extended and the dosage is increased via intravenous or intramuscular infusion for more than 28-30 days [**56**]. Moreover, over usages of sodium stibogluconate medicine in India has led to development of resistance to it. However, the recent research focusses on creating therapeutic compounds with a shorter half-life and fighting drug resistance [**57**]. In the sub-continental region of India, liposomal amphotericin B (LAMB) was used only once, followed by oral miltefosine from 2002 and paromomycin injection from 2006. Additionally, in Africa, paromomycin coupled with

sodium gluconate is the initial therapy option for 17 days [**58**]. LAMB significantly outperformed sodium stibogluconate as the first-line treatment for all types of VL caused by *L. donovani* and *L. infantum* in Asia. Ambisome is currently the only LAMB formulation approved for use in the treatment of VL by the WHO and US Food and Drug Administration (FDA) [**59**]. However, classic amphotericin B deoxycholate, which was later created, is more toxic than LAMB and acts against VL. There are still more medications like pentamidine isethionate and paramomycin sulphate that are used as a second line of treatment only, due to their toxicity and high expense in South Asia [**60**]. Nevertheless, chemotherapy remains the predominant treatment for visceral leishmaniasis because there is no effective vaccine to prevent it. Pharmacotherapy continues to face hurdles due to a number of reasons, including toxicity, rising HIV co-infections, growing drug resistance, and expensive treatment (hospitalisation and medication) [**52**]. Therefore, it is urgently necessary to identify new therapeutic targets for the treatment of this illness, which entails characterizing and investigating parasitic enzymes of crucial metabolic pathways that can be blocked or inactivated. The aminoacyl tRNA synthetases (aaRSs), major enzymes involved in the protein synthesis pathway of *Leishmania*, had been the focus of the current investigation.

1.10 Protein synthesis pathway

One of the fundamental biological processes that take place in a cell is the protein production pathway. The role of the ribosome in protein synthesis in a cell was identified by Palade and other scientists in the year 1979 [**61**]. The protein synthesis process is composed of the two steps naming transcription and translation, where mRNA and protein synthesis take place respectively. The synthesized proteins can perform a wide range of functions in the cell, including those of enzymes, antibodies, structural proteins, hormones, and transport proteins [**62**] **(Fig. 5)**. Errors in the protein synthesis pathways are the root cause of several serious illnesses that affect humans, such as Sickle Cell Anemia, Duchenne Muscular Dystrophy, and Diamond-Blackfan Anemia [**63**]. The translation machinery is made up of ribosomes, elongation factors and aminoacyl-tRNA synthetases (aaRSs). In a variety of microorganisms, the biological route of protein translation has been well-verified as a drug target. The majority of drugs physically bind to rRNA which is a component of ribosomal RNA, and prevent microbial protein translation [**64**]. Since several parasites actively and continuously reproduce, they are highly dependent on protein synthesis and might be susceptible to interference with the translation machinery **[65, 66]**. The three locations where the protein synthesis pathway is active in apicomplexan parasites are the cytoplasm, apicoplasts, and mitochondria [**67, 68**].

The upper small intestines of many mammalian hosts are colonized by the anaerobic (mitochondria-deficient) protozoan known as *Giardia lamblia*. The binding of mRNA and tRNA to 16S-like small-subunit RNA is essential for protein synthesis, and a large number of aminoglycoside antibiotics have been identified to target this area that leads to the arrest of parasitic protein synthesis. Conversely, additional compounds involved in the process of protein translation may serve as therapeutic targets. A prime example of such target for both current and upcoming antimicrobial treatments is the aminoacyl-tRNA synthetases (aaRSs) [**69**].The process of protein translation is thus halted when aaRSs are disrupted. The aaRSs perform a critical role in the mechanism of protein translation by catalyzing the linkage of a particular amino acid to its specific tRNA. Each amino acid has its own aminoacyl-tRNA synthetase enzyme during the stages of protein synthesis.

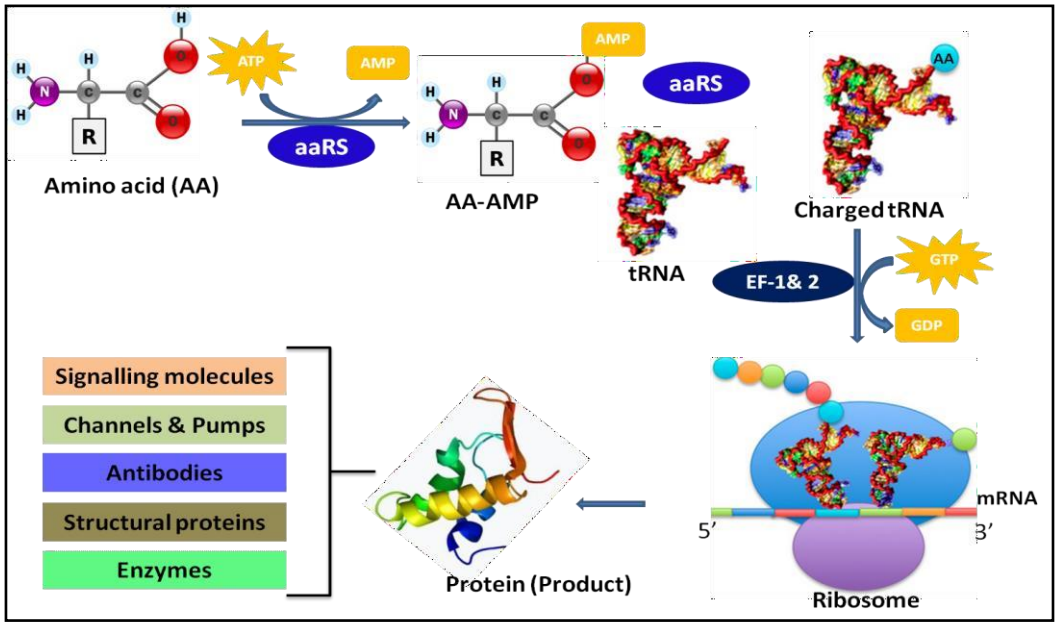

Figure 5: Protein synthesis machinery. aaRSs: animoacyl tRNA synthetase; AA: amino acid (Substrate); AA-AMP: amino acid linked adenylate mono phosphate; EF1 & 2: elongation factors. 11Significance of aminoacyl tRNA synthetases (aaRSs)

1.11 Aminoacyl tRNA synthetases

Each of the 20 standard amino acids has a unique tRNA synthetase in the majority of species **[70]**. The aaRSs enzymes are made up of a catalytic core domain and a few other domains for certain functions such as oligomerization, tRNA binding and amino acid proofreading and these sites might be considered as drug targets **(Fig. 6)**.

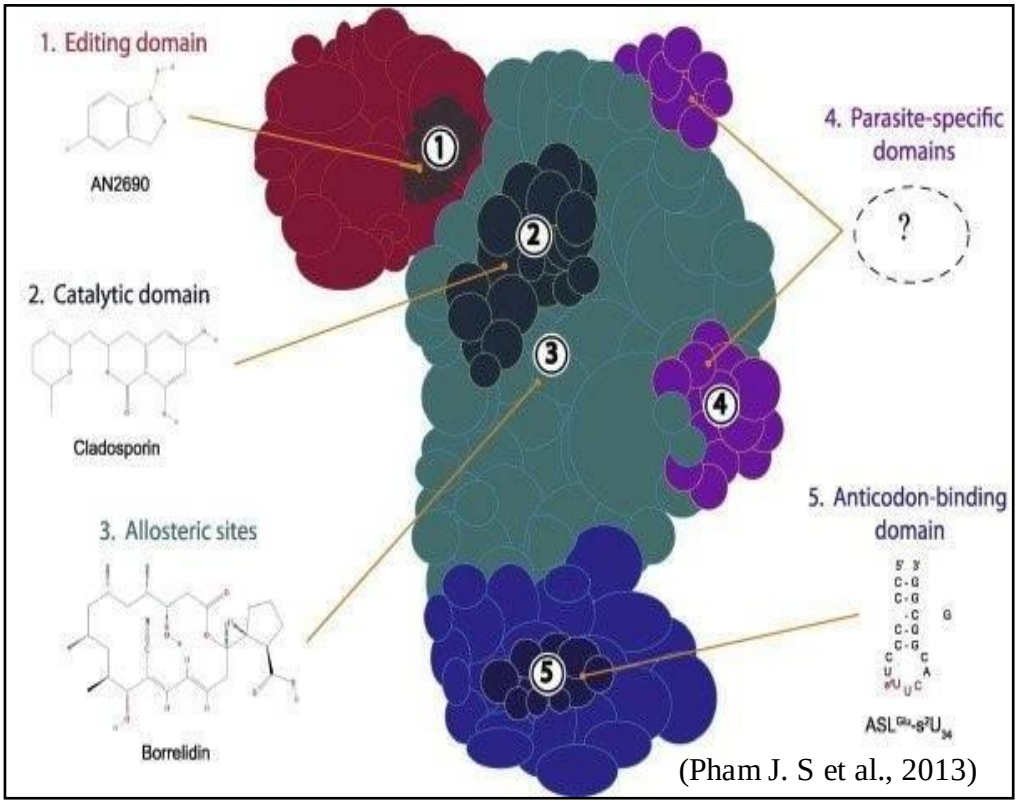

Figure 6: Schematic illustration of aminoacyl tRNA synthetases. The catalytic domain (cyan), anticodon binding domain (indigo), editing domain (red), and parasite-specific domains (purple) are only a few of the several aaRSs domains that are depicted. Numbers 1, 2, 3 and 4 represent potential points like editing site, active site, allosteric sites, parasite-specific domains and anticodon-binding site respectively for interaction between aaRS and the compound.

However, they all basically perform the same chemical reactions [**71**]. Thus, 20 aaRSs are divided into two classes based on evolutionarily dissimilar catalytic cores [**72**]. Another difference between the two groups of enzymes may be seen in the direction in which the tRNAs attach to the active sites. The 2' hydroxyl of the ribose at the acceptor end is where the class I enzymes connect the activated amino acids, whereas the 3' hydroxyl terminus is needed in the class II enzymes [**73**]. According to structural characterization, the active site of class I enzymes has a Rossmann fold that is made up of sequential β-strands and α-helices and the two sequence motifs, HIGH (His-Ile-Gly-His) and KMSKS (Lys-Met-Ser-Lys-Ser) were highly conserved and engaged in ATP contact in an extended conformation. While the core of class II enzymes is made up of three motifs that are each composed of seven regular anti-parallel β-sheets and binds ATP in bent form [**74**]. Each class of enzymes could perhaps be subdivided into the, b, and c subclasses. It seems that every category of enzymes exhibits a propensity to identify chemically similar amino acids. For instance, enzymes of the subclass Ia

detect aliphatic amino acids (Leu, Val, and Ile), sulfur-containing polar residues (Met and Cys), and Arg. The charged amino acid residues such as Lys and Glu as well as its derivative Gln, belong to subclass Ib enzymes. Aromatic amino acids are detected by subclass Ic enzymes (Tyr and Trp). Additionally, class II enzymes exhibit the characteristics identical to that of class I enzymes, allowing them to be further split into three subclasses non-polar (Gly), polar (Thr, His, and Ser,) and aliphatic (Pro and Ala) amino acids. Subclass IIb is capable of identifying amino acids with charged side chains (Lys and Asp and its derivative Asn), one aromatic amino acid (Phe) is recognised by the subclass IIc synthetases [**75, 76**]. Additionally, many studies have proved that aaRSs are also involved in several essential non-translational cellular activities like signal transduction, transcription, RNA splicing, inflammation, apoptosis and angiogenesis [**77**].

Furthermore, aaRSs are known to function as ambidextrous molecules participating in immune regulation and diseases [**78**]. Majority of the eukaryotic species have two genes for each of the 20 common aminoacyl tRNA synthetases (mitochondrial and cytosolic). With the exception of Lys, Asp, and Trp, trypanosomatids only have a single copy gene for each amino acid [**79, 80**]. Gene knock out studies of histidyl tRNA synthetase in trypanosomatids such as *Trypanosoma brucei* and *T. cruzi* showed a complete arrest of growth in the bloodstream forms of the parasite suggesting its essential role in cell survival [**81**]. Aminoacyl-tRNA synthetases are attractive targets for globally important pathogens including *Plasmodium* sp., *Mycobacterium tuberculosis*, which causes malaria and tuberculosis respectively [**82, 83**]. An important example of aaRS inhibitor is mupirocin, a gram-positive bacterial isoleucyl-tRNA synthetase (IleRS) inhibitor that is used as an antibacterial medication to treat *Staphylococcus aureus* on the skin [**84, 85**]. A number of potential drug binding sites on aaRSs are described including an ATP-binding site, a neighbouring amino acid interacting site, and a groove for tRNA identification and binding. Tryptophan-derived indolmycin is generated from *Streptomyces griseus* and has antibacterial effects on both gram-positive and gram-negative microbes inhibiting tryptophan tRNA synthetase [**86**] and furanomycin, which decreases isoleucyl tRNA synthetase activity [**87**]. Recently, the search for new anti-trypanosomal medications pushed scientists closer to focusing on aaRSs based on which inhibiting agents of these enzymes were developed that showed a post-treatment decrease in pathogen proliferation [**88**].

1.12 Significance of aminoacyl tRNA synthetases

Aminoacyl tRNA synthetases (aaRSs) are the crucial components of the protein translational machinery. They attach amino acids to their associated transfer RNA covalently. The process of aminoacylating tRNA involves two steps: first, the aaRS hydrolyzes ATP to activate an amino acid; and second, it esterifies the activated amino acid to the 3' terminal of the tRNA, producing aminoacylated tRNA as the final product (aa-tRNA). In addition to their aminoacylation capabilities, around half of the aaRSs have an editing function also that discharge mismatched amino acids from their corresponding tRNA [**89**]. When a tRNA is mischarged with non-cognate amino acid, aaRSs stimulate the deacylation pathway of the tRNA to stop mistranslation [**90**]. Deficiency of editing mechanism results in the synthesis of mis- and unfolded proteins, which can aggregate in the neuronal cytoplasm leading to neurodegenerative disorders like Alzheimer's and Parkinson's disease [**91**]. Previously, aaRSs were often thought as merely routine enzymes, but they are now understood as key players in number of biological and pathological functions, including cancer, angiogenesis, and immunological response [**92**].

1.13 Seryl tRNA synthetase (SerRS)

The amino acid, serine, is covalently linked to its cognate tRNA by the seryl tRNA synthetase (SerRS). Furthermore, this enzyme contributes to the addition of selenocysteine to proteins [**93**]. The serylation reaction of $tRNA^{Sec}$ has been explained in detail in *Escherichia coli* and *Homo sapiens*, but the system has not been characterized in protozoans or lower eukaryotes [**94, 95**]. SerRS belongs to class II aminoacyl tRNA synthetase. Along with other class II enzymes like lysyl tRNA synthetase of *P. falciparum* and aspartyl-tRNA synthetase of *L. donovani*, seryl tRNA synthetase also usually exists as homodimers [**96, 97**]. The catalytic domain of SerRS contains an antiparallel β-sheet construction and exhibits three conserved motifs [**98**]. In addition to this, a coiled-coil domain is present at the N-terminal region which plays an important role in the recognition of the long variable loop of $tRNA^{Ser}$ [**99**]. In the case of eukaryotes, SerRS has a short extra segment, which is involved in protein stability and amino acid recognition [**100**]. Additionally, the catalytic core of enzymes is almost conserved from bacteria to humans. Previous research has suggested that certain tRNA synthetases have acquired new activities by adding other domains to the core domain [**97**]. An array of crystal structure of apo, binary and tertiary complexes of SerRS have been reported in *Thermus thermophilus* [**101**] *E. coli* [**102**] and humans [**103**], which gives information of the amino acid specificity and mechanism of serine activation. Subsequently, high-resolution structure of

E. coli SerRS with seryl–adenylate analogue provided insights into the molecular interaction between active site residues and analogue [**104**]. Most of the inhibitors of aaRSs showed competitive binding at the active site where cognate amino acid binds, but only very few inhibitors have crossed the stage of clinical development [**105**]. Inhibitors like SB-217452 and serine hydroxamine (SHX) were found to be the most effective against SerRS of *Staphylococcus aureus* [**106**]. Cladosporin, a secondary metabolite and antifungal antibiotic, is produced by *Cladosporium cladosporioides* and *Aspergillus flavus* [**107, 108**]. Recently, cladosporin was discovered to be a novel inhibitor for aaRS and it exhibited potent antimalarial activity against *Plasmodium falciparum* by targeting lysyl-tRNA synthetase activity and inhibiting protein synthesis [**109**]. Moreover, pyrimidine-based compounds have been reported as potent inhibitors for SerRS of *Klebsiella pneumonia* [**110**].

1.14 Glutamyl-tRNA synthetase

The glutamyl-tRNA synthetase (GluRS) is a member of the class I tRNA synthetase, which facilitates the transfer of glutamate to its associated tRNA. Generally, class-I enzymes exists as monomer or dimer [**111**]. There are two different kinds of GluRS, one of which is discriminatory and the other being non-discriminatory. While the discriminatory form of GluRS (D-GluRS) catalyses the glutamylation of $tRNA^{Glu}$ to produce Glu-$tRNA^{Glu}$ [**122**], the non-discriminatory form (ND-GluRS) is important for charging both $tRNA^{Glu}$ and $tRNA^{Gln}$ with glutamate. This misacylated Glu-$tRNA^{Gln}$ is successively converted into Gln-$tRNA^{Gln}$ through glutamyl-tRNA amidotransferase (Glu-AdT) via the incorporation of amide to glutamate [**113**]**.** The transamidation process is an indirect technique to make glutamine. If the misacylated Glu-$tRNA^{Gln}$ is not converted to Gln-$tRNA^{Gln}$, it becomes poisonous, making this Glu-AdT a critical enzyme [**114**]. The majority of bacteria and chloroplasts in all known archaea lack GlnRS, and this deficiency is often replaced by ND-GluRS and Glu-AdT. However, ND-GluRS is always accompanied by Glu-AdT [**115**]. The crystal structures of GluRS, complexed with $tRNA^{Glu}$, L-glutamate have been well characterized in *Thermus thermophilus* [**116**]. Multienzyme complexes of glutamyl-tRNA synthetases are found in higher eukaryotic organisms, for instance, Glu-prolyl tRNA synthetase, the biggest chimeric protein in *Drosophila*, has glutamyl-tRNA synthetase activity in its N-terminal domain and prolyl-tRNA synthetase activity in its C-terminal region [**117**]. Similarly, humans have only a single gene (locus EPRS) that codes for the glutamyl (class-I) and prolyl (class-II) tRNA synthetases [**118**]. Additionally, in most of the bacteria and plants GluRS also plays an important role in synthesis of d-aminolevulinic acid (ALA), the first common precursor of all

tetrapyrrole biosynthesis [**119**]. The role of GluRS in parasite survival and growth was also reported in *T. brucei* after its mRNA knockdown in mammalian stage wherein abnormalities in terms of growth, morphology, cell cycle, and DNA content were observed [**120**]. Furthermore, the importance of GluRS has also been studied in *Plasmodium berghei* and indicated as a potential drug target as it aminoacylates both $tRNA^{Glu}$ and $tRNA^{Gln}$ of the apicoplast [**121**]. On the basis of its importance in other organisms, the present study highlights the purification of leishmanial SerRS and GluRS along with their mutant enzymes followed by their characterization and inhibition studies using ureidosulfocoumarin and salicylate compounds individually. In addition, 3D-structure prediction and molecular docking studies were performed followed by MD simulations to validate the docking studies.

1.15 Objectives

Objective 1

Cloning and purification of seryl and glutamyl tRNA synthetases of *L. donovani*

Objective 2

Enzyme kinetics and inhibition studies of recombinant proteins

Objective 3

Structural characterization of leishmanial seryl and glutamyl tRNA synthetases

2. Materials and Methods

2.1 Materials

2.1.1 Strains, plasmids and enzymes.

The expression vector pET-28a(+) was obtained from Novagen, Madison, USA. Restriction enzymes (*BamH*I, *Sac*I and *Xho*I), *Taq* DNA polymerase, T4 DNA ligase and Phusion polymerase were procured from Thermo Scientific (USA). The bacterial strain *E. coli* XL1-Blue (Stratagene, USA) was utilized for cloning and *E. coli* BL21 (DE3) (Novagen) cells were used for protein expression. GeneJET Plasmid Miniprep and GeneJET Gel Extraction kits employed during cloning methods were obtained from Thermo Scientific (USA) and the primers used for the amplification were acquired from GCC Biotech (India) Pvt. Ltd.

2.1.2 LB (Luria-Bertani) media

The LB medium was utilized for cultivating the bacterial cells, which was prepared by mixing 10 g of NaCl, 10 g of tryptone and 5 g of yeast extract in 900 ml of double distilled water and then volume was adjusted to 1000ml.

2.1.3 Antibiotic stocks

The Kanamycin (50 mg/ml) stock was prepared in sterile milliQ water, while other antibiotics like tetracycline (12.4 mg/ml) were dissolved in 70% ethanol and stored at -20°C. Both antibiotics and culture media components were acquired from HiMedia Laboratories (India).

2.1.4 Enzymes assays

All components of enzyme assay such as L-Serine, L-Glutamate, ATP and PPase were bought from Sigma Aldrich (München, Germany). The monovalent salts (NaCl, KCl, LiCl, CsCl, K2HPO4), HEPES and DTT were purchased from HiMedia Laboratories (India) and divalent salts ($MgCl_2$, $MnCl_2$, $CoCl_2$, $CaCl_2$, and $NiCl_2$) were received from Merck fortes, India. The glutamyl tRNA synthetase inhibitor compounds (Salicylate and p-Chloromercurio benzoic acid) were bought from HiMedia Laboratories (India).

2.1.5 Cell lines and reagents

The human monocytic cell line THP-1 and murine macrophages RAW264.7 were obtained from National Centre for Cell Science (NCCS), Pune, India and cultured in RPMI-1640 and DMEM media, respectively. All cell culture reagents were acquired from HiMedia Laboratories (India) and DMSO reagent was bought from Sigma Aldrich.

2.2 Methodology

2.2.1 Sequence and phylogenetic analysis

The protein sequences of *Ld*SerRS (XP 003858988) and *Ld*GluRS (XP 003863040) were taken from NCBI database (https://www.ncbi.nlm.nih.gov/) and introduced to ProtParam (https://web.expasy.org/protparam/) and TOPCONS (http://topcons.cbr.su.se/) tools to analyse molecular weight, isoelectric point (pI), signal peptide, and transmembrane region of recombinant proteins. Phylogenetic and evolutionary relationships were studied employing MEGA X software (https://www.megasoftware.net/) with neighbor-joining method. Subsequently, multiple sequence alignment was conducted for SerRS of *Trypanosoma. brucei*, *Giardia lamblia*, *Cryptosporidium parvum*, *Homo sapiens* and *L. donovani*, whereas sequences of GluRS were aligned from different organisms like *T. cruzi*, *P. falciparum*, *T. thermophilus*, *H. sapiens* and *L. donovani* by Clustal Omega alignment tool (https://www.ebi.ac.uk/Tools/msa/clustalo/). The output alignment file was evaluated by ESPript (https://espript.ibcp.fr/ESPript/ESPript/) to understand the sequence homology, significant motifs and residues involved in binding of substrate and cofactors.

2.2.2 Cloning and site directed mutagenesis

The genomic DNA of *L. donovani* (Strain: MHOM/IN/80/DD8) was used to generate gene-specific primers employing polymerase chain reaction to amplify the full-length ORF of seryl tRNA synthetase of 1425 nucleotides and the truncated ORF of glutamyl tRNA synthetase containing 1518 nucleotides (**Table 1**). In a similar manner, the ORF of human SerRS (comprising 1545 nucleotides) was amplified from cDNA (synthesized from the mRNA obtained from human brain astrocytes nerve cell). After purification of PCR product, the amplicons of *Ld*SerRS and *Hs*SerRS were digested with *BamH*I and *Xho*I, while *Ld*GluRS was restricted using *Sac*I and *Xho*I. In addition, pET28a(+) expression vector that adds a hexa-histidine tag to the N-terminus of recombinant protein was digested with the same restriction enzymes to produce the requisite sticky ends followed by gel extraction. Digested products were ligated by T4 DNA ligase at 22°C for 2 hr and transformed into *E. coli* XL1-Blue competent cells. The positive clones were identified by colony PCR and restriction digestion followed by DNA sequencing prior to transformation into *E. coli* BL21 (DE3) cells. Site directed mutagenesis of *Ld*SerRS was performed at the conserved ATP binding site in which R295 was mutated to lysine and alanine, while E297 was substituted with aspartate and alanine employing primers containing specific mutation. Simultaneously, ATP interacting H60 of *Ld*GluRS was changed to alanine and arginine employing primers containing specific

mutation. Concurrently, mutants were generated by PCR amplification of *Ld*SerRS and *Ld*GluRS constructs through initial denaturation at 98°C (30 Sec) followed by a total of 18 cycles of denaturation at 98°C (10 Sec), annealing at 65°C (1 min) and primer extension at 72°C (3.5 min) with final extension for 10 min. The end products of PCR were incubated with *Dpn*I restriction enzyme for 1 hr at 37°C for cleavage of methylated template DNA and then transformed into XL1-Blue competent cells. All mutations were confirmed by DNA sequencing succeeded by transformation into *E. coli* BL-21(DE3) cells for expression.

Table 1: Oligonucleotide primers used in this study

Primers	Sequence (5′ to 3′)
*Ld*SerRS_FP	ATT GGA TCC ATG GGG CTC GAC ATT CAG CTG
*Ld*SerRS_RP	ATA CTC GAG TTA CTC CTT ATC GGC CGT AGG
*Ld*SerRS_E297D_(FP)	TCG TGC TTC CGA AAG GAT GCC GGT GCG CAC GGC
*Ld*SerRS_E297D_(RP)	GCC GTG CGC ACC GGC ATC CTT TCG GAA GCA CGA
*Ld*SerRS_R295K_(FP)	CGT CTC GTC GTG CTT CAA AAA GGA GGC CGG TGC G
*Ld*SerRS_R295K_(RP)	CGC ACC GGC CTC CTT TTT GAA GCA CGA CGA GAC G
*Ld*SerRS_E297A_(FP)	GTG CTT CCG AAA GGC GGC CGG TGC GCA CG
*Ld*SerRS_E297A_(RP)	CGT GCG CAC CGG CCG CCT TTC GGA AGC AC
*Ld*SerRS_R295A_(FP)	GTC TCG TCG TGC TTC GCA AAG GAG GCC GGT GC
*Ld*SerRS_R295A_(RP)	GCA CCG GCC TCC TTT GCG AAG CAC GAC GAG AC
*Ld*GluRS_FP	ATA GAG CTC GCT GAG AAA GGT AAG GTG GTG ACC C
*Ld*GluRS_RP	ATT CTC GAG ACT ACC ATC CGG GAT TGA GAT GAG C
*Ld*GluRS_H60R_FP	GCT AGC GGG TTC CTG CGT ATC GGC CAT GCG AAA G
*Ld*GluRS_H60R_RP	CTT TCG CAT GGC CGA TAC GCA GGA ACC CGC TAG C
*Ld*GluRS_H60A_FP	GCT AGC GGG TTC CTG GCT ATC GGC CAT GCG AA
*Ld*GluRS_H60A_RP	TTC GCA TGG CCG ATA GCC AGG AAC CCG CTA GC
*Hs*SerRS_FP	ATA GGA TCC ATG GTG CTG GAT CTG GAT TTG TTT CGG C
*Hs*SerRS_RP	AAT CTC GAG TCA AGC ATC GGT GAC CTC CAT GTT CTG

2.2.3 Expression and purification

For expressing the recombinant proteins, a single colony of each of *E. coli* BL21(DE3) cells harbouring constructs of *Ld*SerRS, *Hs*SerRS and mutant proteins was added into 20 ml of

Luria-Bertani (LB) broth comprising 50 µg/ml kanamycin succeeded by incubation for 16-18 hrs at 37°C with shaking. The primary culture (7.5 ml) was added into 750 ml of LB broth and then grown up to OD_{600} of 0.5 followed by induction with 0.2 mM IPTG at 18ºC for 20 hrs. Cells were harvested by centrifugation at 5,000 rpm for 10 min and pellet was resuspended in 50 ml of lysis buffer [30 mM HEPES pH 7.5, 300 mM KCl, 20 mM imidazole, 2 mM β-ME, 1 mM PMSF, lysozyme (0.25 mg/ml) and 5% (v/v) glycerol]. Simultaneously, *Ld*GluRS and its mutant enzymes were obtained from *E. coli* BL-21(DE3) cells induced with 0.4 mM IPTG followed by suspending pellet into lysis buffer [30 mM HEPES pH 7.5, 300 mM KCl, 20 mM imidazole, 2 mM BME, 1 mM PMSF, lysozyme (0.25 mg/ml), 0.5% lauroylsarcosine and 5% (v/v) Glycerol].

Subsequently, cells were lysed employing sonication and then centrifuged at 10,000 rpm for 30 min. Resultant supernatant was filtered with 0.2 micron syringe filters and injected into a pre-packed HisTrap HP 5 ml column (GE Healthcare) on AKTA Purifier equilibrated with buffer A containing 30 mM HEPES pH 7.5, 300 mM KCl and 20 mM imidazole. Non-specific proteins bound to resin were washed away with a gradient of 10, 20 and 30% of buffer B (30 mM HEPES pH 7.5, 300 mM KCl, 500 mM imidazole), while respective 60% and 35% of buffer B was employed for elution of *Ld*SerRS and *Ld*GluRS. Highly pure eluted fractions were combined and subjected to HiLoad 16/600 Superdex 200 pg column (GE Healthcare) equilibrated with 20 mM HEPES pH 7.5 and 100 mM KCl. Finally, concentration of obtained protein was estimated at 280 nm using NanoDrop 2000c (Thermo Scientific) with their respective molar absorption extinction coefficients and molecular weights.

2.2.4 Intrinsic fluorescence measurements

Intrinsic fluorescence emission spectra of purified proteins (*Ld*SerRS and *Ld*GluRS) were measured through Jasco Spectrofluorometer (FP-8500) with 5 µM protein in 10 mM HEPES pH 7.5 and 100 mM KCl. The path length of cuvette was 10 mm and the readings were taken at 25ºC. The wavelength of 280 nm was utilized for protein excitation and the emission was recorded from 300 to 400 nm, where scanning speed of 100 nm/min and slit widths of 5 nm were used as parameters for all the fluorescence experiments. Intrinsic fluorescence with different buffers (pH 3.5-9.5) was executed to measure the folding dynamics properties of recombinant proteins. Simultaneously, thermal stability of proteins with and without ligand was analysed at temperature ranging from 20 to 90ºC. Initially, purified protein was incubated with saturated concentration of ligands on ice for 30 min succeeded by recording of spectra at every 5°C interval. In addition, protein sequences were subjected to WESA server

(https://pipe.rcc.fsu.edu/wesa/) for delineating the position of tryptophan residues in both leishmanial proteins. For quenching studies, purified protein was incubated with increasing concentration of quenchers (acrylamide and potassium iodide) from 0 to 0.5 M for 30 min succeeded by recording the spectra. The output data of quenching studies were analysed by Stern-Volmer plot with quencher concentrations on X-axis and F_o/F_1 values on Y-axis. Additionally, unfolding studies of purified proteins were monitored in the presence of urea (0 - 8 M) as well as guanidine hydrochloride (0-5 M) to determine the Gibbs free energy (ΔG) and mid transition concentration (C_m).

2.2.5 Enzyme assay and kinetics

The enzymatic activity of recombinant proteins was performed through an *in vitro* aminoacylation reaction employing the malachite green phosphate detecting method as reported earlier **[96]** with minor modifications. The enzyme assays were conducted at 25°C in 96-well plate using multimode plate reader (Tecon spark). For aminoacylation assay of *Ld*SerRS, 2 µl of native protein and its mutants was added into 50 µl reaction buffer comprising of 30 mM HEPES pH 7.5, 150 mM NaCl, 30 mM KCl, 15 mM $MgCl_2$, 1 mM DTT, 100 µM ATP, 2 U/mL inorganic pyrophosphatase (PPase; Sigma) and 5 mM L-serine to obtain the final concentration of 5 µM purified protein followed by incubation at 37 ºC for 30 min. Simultaneously, 4 µl of purified *Ld*GluRS and its mutant proteins were dispensed in to 50 µl total reaction mixture containing 30 mM HEPES pH 7.5, 150 mM NaCl, 30 mM $MgCl_2$, 40 mM KCl, 1 mM DTT, 100 µM ATP, 2 U/mL inorganic pyrophosphatase, 1 mM L-glutamate to get the final concentration of 5 µM recombinant protein succeeded by incubation at 37 °C for 30 min. Reactions were discontinued by adding 100 µl malachite green (Reagent A: 10 mM ammonium molybdate in 1N HCl; Reagent B: 0.042 % malachite green in 1 % poly vinyl alcohol), kept for colour development at room temperature for 30 min and then absorbance was measured at 620 nm. Simultaneously, gradient concentrations (0-50 µM) of KH_2PO_4 were combined with malachite green solution and incubated for 30 min at room temperature to obtain standard curve for phosphate to estimate the product during reaction. The enzymatic activity of *Ld*SerRS and *Ld*GluRS was also determined at different pH (3.5–9.5) and temperature (10–90 °C). Concurrently, effect of monovalent (NaCl, LiCl KCl, CsCl) and divalent ($MgCl_2$, $MnCl_2$, $CoCl_2$, $CaCl_2$, $CuCl_2$, and $FeCl_2$) metal ions on the activity of recombinant proteins were evaluated. Subsequently, kinetic studies were performed for native proteins and their mutant enzymes (R295K, R295A, E297D and E297A of *Ld*SerRS; H60R and H60A of *Ld*GluRS) with substrate and cofactor. Kinetic parameters were calculated by

estimating the initial reaction rates of substrate/cofactor with respect to time. A graph of ligand concentrations versus initial reaction velocities was plotted and subsequent non-linear regression analysis through the equation ($V = V_{max}*[S]/(K_m + [S])$) was employed to compute maximum reaction velocity (V_{max}) and binding affinity (K_m). The turnover number (k_{cat}) was obtained with division of V_{max} by total enzyme concentration ($k_{cat} = V_{max}/[E]t$), while the catalytic efficiency was deduced by dividing k_{cat} with K_m.

2.2.6 *In vitro* inhibition of aminoacylation reaction

In order to identify specific inhibitors for leishmanial parasite, inhibition studies were performed with the ureidosulfocoumarin derivatives **[122]** against recombinant proteins (*Ld*SerRS and *Hs*SerRS). Briefly, all compounds (**Comp 5a-z)** were dissolved in 100% DMSO and aminoacylation assay was performed with varying concentrations to identify effective inhibitors against *Ld*SerRS. Subsequently, a plot with log inhibitor concentration on X-axis and normalized percentage activity values on Y-axis was drawn to calculate the IC_{50} values for *Ld*SerRS and *Hs*SerRS. Furthermore, inhibition kinetics was performed with screened hit compounds and the respective Line weaver-Burk plots were used to unravel the mode of inhibition. Simultaneously, salicylate **[123]** and p-Chloromercuriobenzoate (pCMB) **[124]** were assessed with *Ld*GluRS and its mutants to determine the IC_{50}, mode of inhibition, and inhibition constant (K_i) values for inhibitor.

Furthermore, the binding studies of Comp 5l towards *Ld*SerRS and *Hs*SerRS were performed by incubating the purified proteins with varying concentrations of compound for 30 min followed by recording the emission spectra from 300-400 nm. The data was fitted into a modified Stern-Volmer equation to calculate the binding constant (K_b) and number of binding sites using GraphPad Prism version 8.0 (https://www.graphpad.com/). In addition, physicochemical properties and druglikeness of identified compounds (Comp 5l and salicylate) were assessed through SwissADME program **[125]**. To analyse the cytotoxicity, MTT (3-(4, 5-dimethylthiazol-2-yl)-2, 5- diphenyltetrazolium bromide) assay was executed in triplicates with different concentrations of Comp 5l (1–20 μM) in murine macrophage RAW264.7 according to previous report **[126]**.

2.2.7 Circular dichroism (CD) analysis

Secondary structural content of native (*Ld*SerRS and *Ld*GluRS) and their mutant proteins was determined by CD spectrophotometer (JASCO 1500) devised with a Peltier temperature control unit employing far-UV range (195-250 nm) with a scanning speed of 50 nm/min for

two accumulations. CD spectra were recorded in 10 mM HEPES pH 7.5 and 100 mM KCl with a quartz cell of 2.0 mm path length using 5.0 µM of protein followed by evaluation using DichroWeb (http://dichroweb.cryst.bbk.ac.uk). The variations in secondary structural elements of the proteins were recorded in the buffer comprising 100 mM KCl with pH ranging from 3.5 to 9.5. Similarly, conformational changes for recombinant proteins along with its mutants were analysed in the presence of substrate and cofactor. Consequently, thermal-stability of native and mutant proteins were monitored by observing changes in ellipticity at 222 nm from 20 to 90ºC with 1ºC/min ramp rate. The obtained data was normalized and fit into a two-state equilibrium unfolding model to determine thermal melting temperature of proteins. Moreover, unfolding of the proteins in the presence of urea (0 - 8 M) was monitored by recording the spectra from 250 to 220 nm to estimate the Gibbs free energy (ΔG).

2.2.8 Homology modelling and docking study

The three-dimensional structure of *Ld*SerRS was retrieved from AlphaFold protein structure database (https://alphafold.ebi.ac.uk/) and its stereo-chemical quality was evaluated through PROCHECK [**127**]. Simultaneously, Crystal structure of *T. thermophilus* glutamyl tRNA synthetase (PDB ID: 1J09) was employed to generate three-dimensional structure of *Ld*GluRS using Modeller 10.2 **[128].** The best model was selected based on its DOPE score followed by analysis of stereo-chemical properties and then subjected to energy minimization through the GROMACS suite v. 5.1.4 **[129]**. Selected model structures were further used as a receptor for the molecular docking to identify the atomic interactions with various ligands employing AutoDock Vina 1.1.2 **[130]**. The corresponding coordinates of ATP (vent form), ATP and L-Glu were taken from PDB ID of 3LSS, 1J09 and 2CUZ (https://www.rcsb.org/), while structural coordinates of L-Ser and salicylate were obtained from PubChem database (https://pubchem.ncbi.nlm.nih.gov/). Simultaneously, the chemical structure of identified hit Comp 5l was drawn using ChemDraw Pro 8.0 **[131]** and converted into 3D coordinates employing Discovery Studio (https://discover.3ds.com/discovery-studio-visualizer-download). The grid box dimension for *Ld*SeRS was assigned as the center (16 × 10 × 18) and size (58.754, 57.358 and 73.981) with 1Å spacing, while the centre (14 × 12 × 15) and size (51.704, 54.318 and 71.951) was used for *Ld*GluRS with 1Å spacing. The docked conformations were visualized and evaluated using PyMOL (https://pymol.org/2/) and LigPlot (https://www.ebi.ac.uk/thornton-srv/software/LigPlus/).

2.2.9 Molecular dynamics simulations

Molecular dynamic simulations (MDS) of apo *Ld*SerRS and *Ld*GluRS as well as complex forms with substrate, cofactor and inhibitors were performed using GROMACS software **[129]**. The protein topology was generated using GROMOS96 43a1 force field, while the ligand topologies were prepared from the PRODRG (http://davapc1.bioch.dundee.ac.uk/cgi-bin/prodrg) server followed by generating the complex file. A cubic box was used in MDS with the SPC/E water model **[132]** by placing the protein/protein-ligand complex at the centre. These systems were neutralized with the addition of an appropriate number of sodium ions and then energy minimized using the steepest descent algorithm for 50,000 steps to improve hydrogen bond network. A separate indexing was done for the protein-ligand systems and the parameters were appended in their topology files. Two equilibration steps i.e. NVT and NPT were executed for 100 ps followed by MD production at 300 K for 100 ns (*Ld*SerRS and its complexes) and 50 ns (*Ld*GluRS and its complexes). After MDS, the trajectory files along with root mean square deviation (RMSD), root mean square fluctuation (RMSF) and radius of gyration (Rg) were analysed to understand the stability, fluctuation and compactness of the complexes in comparison to the apo form.

2.2.10 Statistical analysis

The experiments were performed in either duplicate or triplicate, while the data were reported as the mean standard deviation (SD) of three distinct assessments. Statistical analysis was executed with Microsoft Excel and GraphPad Prism version 6.0. Subsequently, statistical significance ($P < 0.01$) was determined by one way ANOVA for all the experiments.

Chapter-I

3. Cloning and purification ofseryl and glutamyl tRNA synthetases of *Leishmania donovani*

3.1 Result

3.1.1 Sequence and phylogenetic analysis of *Ld*SerRS and *Ld*GluRS

SerRS of *L. donovani* encompasses 474 amino acids containing neither signal peptide nor transmembrane domain with the calculated molecular weight as 53202 Da. The protein demonstrated corresponding theoretical isoelectric point and instability index as 6.2 and 44.30 inferring that most of the residues are negatively charged along with its slightly unstable nature. *Ld*SerRS displayed two domain organizations i.e. N-terminal tRNA anticodon domain (1-135) and C-terminal tRNA synt-2 domain (136-474). To enhance our knowledge pertaining to the evolutionary relatedness across the known SerRS proteins, a phylogenetic tree was constructed employing SerRS protein sequences from 20 different entities. The phylogenetic study revealed that *Ld*SerRS is closely associated with its homologues of *L. infantum, L. major, T. cruzi* and *T. brucei,* while apicomplexan parasites like *Cryptosporidium parvum* and *Plasmodium falciparum* were found in different group of phylogenetic tree. Bacterial seryl tRNA synthetases were found in separate clade of the phylogenetic tree, whereas mammalian organisms such as *Homo sapiens* and *Rattus norvegicus* exhibited higher divergence from *Ld*SerRS as they are present in other cluster **(Fig. 7A).** To elucidate the catalytic core of *L. donovani* SerRS, multiple sequence alignment was executed that displayed presence of three motifs *viz*. I (201-240 residues), II (284-314 residues), and III (420-450) in *Ld*SerRS. Remarkably, most of the residues that interact with substrate/cofactor were present in motif-II and III. Among the aligned sequences, SerRS of protozoan parasites showed a deletion of 34 amino acids at C-terminal in comparison to human SerRS **(Fig. 7B**) that has been considered to participate in the protein stability (Mocibob & Weygand-Durasevic, 2008).

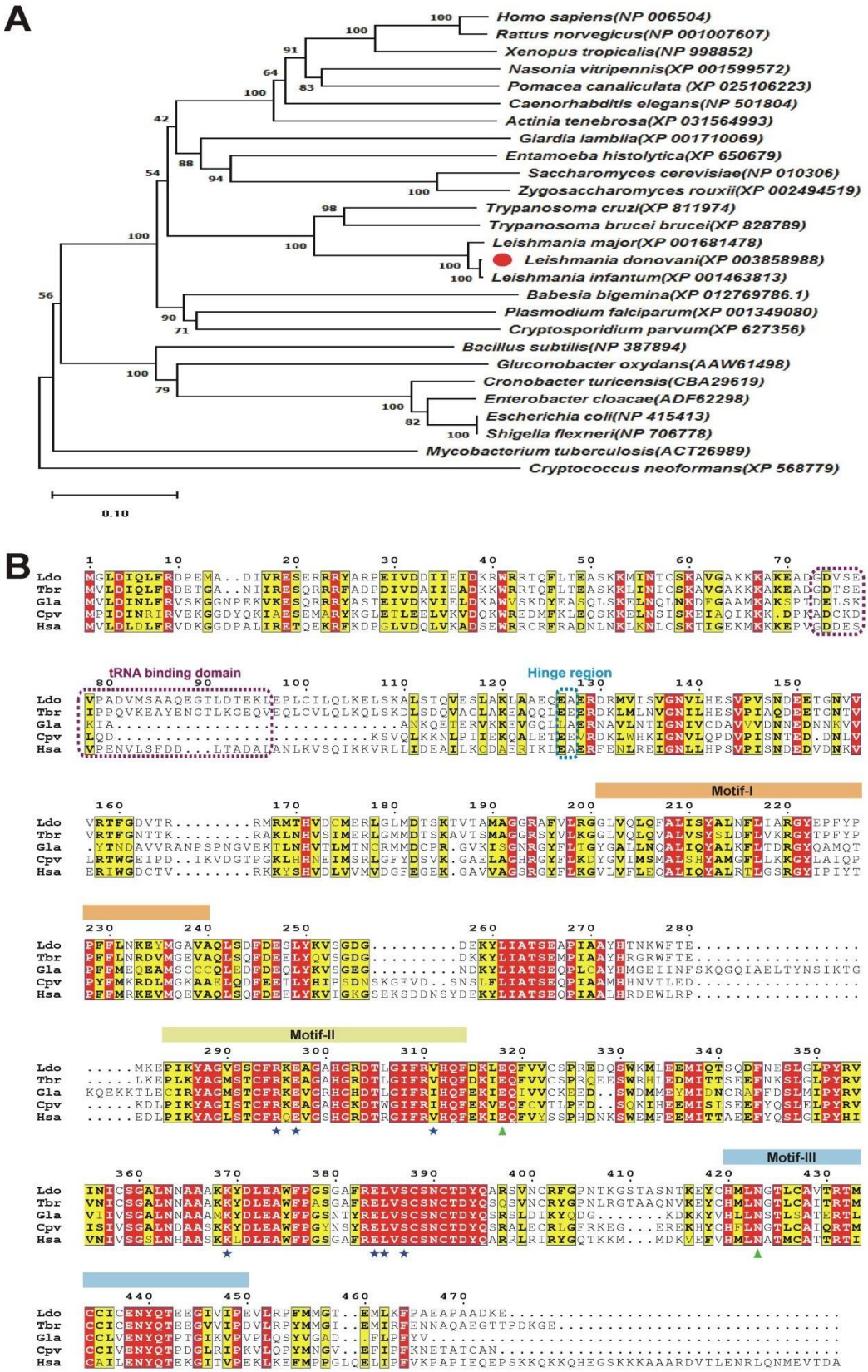

Figure 7: Evolutionary and sequence analysis of *Ld*SerRS. (A) Seryl tRNA synthetase sequences of different organisms were retrieved and the phylogenetic tree was generated by neighbor-joining method. The numbers at the start of each branch correspond to percentage obtained by bootstrap

iterations. (B) Multiple sequence alignment of *Ld*SerRS with its counterpart from different organisms like *T. brucei* (Tbr), *G. lamblia* (Gla), *C. parvum* (Cpv) and *H. sapiens* (Hsa). Green triangle and blue star specify the residues interacting with the substrate (L-Serine) and cofactor (ATP). The tRNA binding domain and hinge region are indicated as dash line box in pink and blue colour, while respective motif-I, II and III are presented in orange, green and blue colour.

Similarly, full-length *Ld*GluRS sequence consists of 594 amino acids with a calculated molecular weight of 67906 Da. The corresponding theoretical pI and instability index of *Ld*GluRS was found to be 8.35 and 33.13, indicating the presence of higher number of positively charged residues and stable nature. The grand average of hydropathicity and aliphatic index were -0.572 and 75.56, respectively, suggesting that *Ld*GluRS is moderately hydrophobic. To understand the evolutionary conservation among various glutamyl tRNA synthetases, a phylogenetic tree was engendered taking GluRS protein sequences of twenty organisms. The assessment of phylogenetic tree revealed that *Ld*GluRS is closely related to other homologs of protozoans including *Trypanosoma brucei*, *T. cruzi* and *Giardia lamblia*. Apicomplexan organisms like *Toxoplasma gondii* and *Cryptosporidium parvum* were found in the neighboring group, whereas prokaryotic GluRSs were located in different clusters with high divergence from *Ld*GluRS. Notably, GluRSs from *Homo sapiens* and *Rattus norvegicus* were observed as next to the apicomplexan cluster showing their divergence from *Ld*GluRS **(Fig. 8A)**. The primary sequence of *Ld*GluRS displayed two domains i.e. N-terminal catalytic domain (48-352 residues) and C-terminal anticodon-binding domain (354-531 residues). The N-terminal catalytic domain possessed two conserved motifs *viz.* HXGX (60-63 residues) and XXSKR (282-286 residues), which participate in interaction with ATP that is a common characteristic of class I tRNA synthetases. Multiple sequence alignment of GluRS has indicated Pro52, Pro53, Glu54, His60, Gly62, His63, Ala66, Thr246, Phe273, Arg275 and Leu276 of *L. donovani* might participate in binding with ATP as observed in crystal structure of its *P. falciparum* homolog. Among ATP interacting residues, mostly catalytic residues were found to be conserved in leishmanial and human GluRS except Phe273 of *Ld*GluRS that is substituted with Tyr423 in its human equivalent **(Fig. 8B)**.

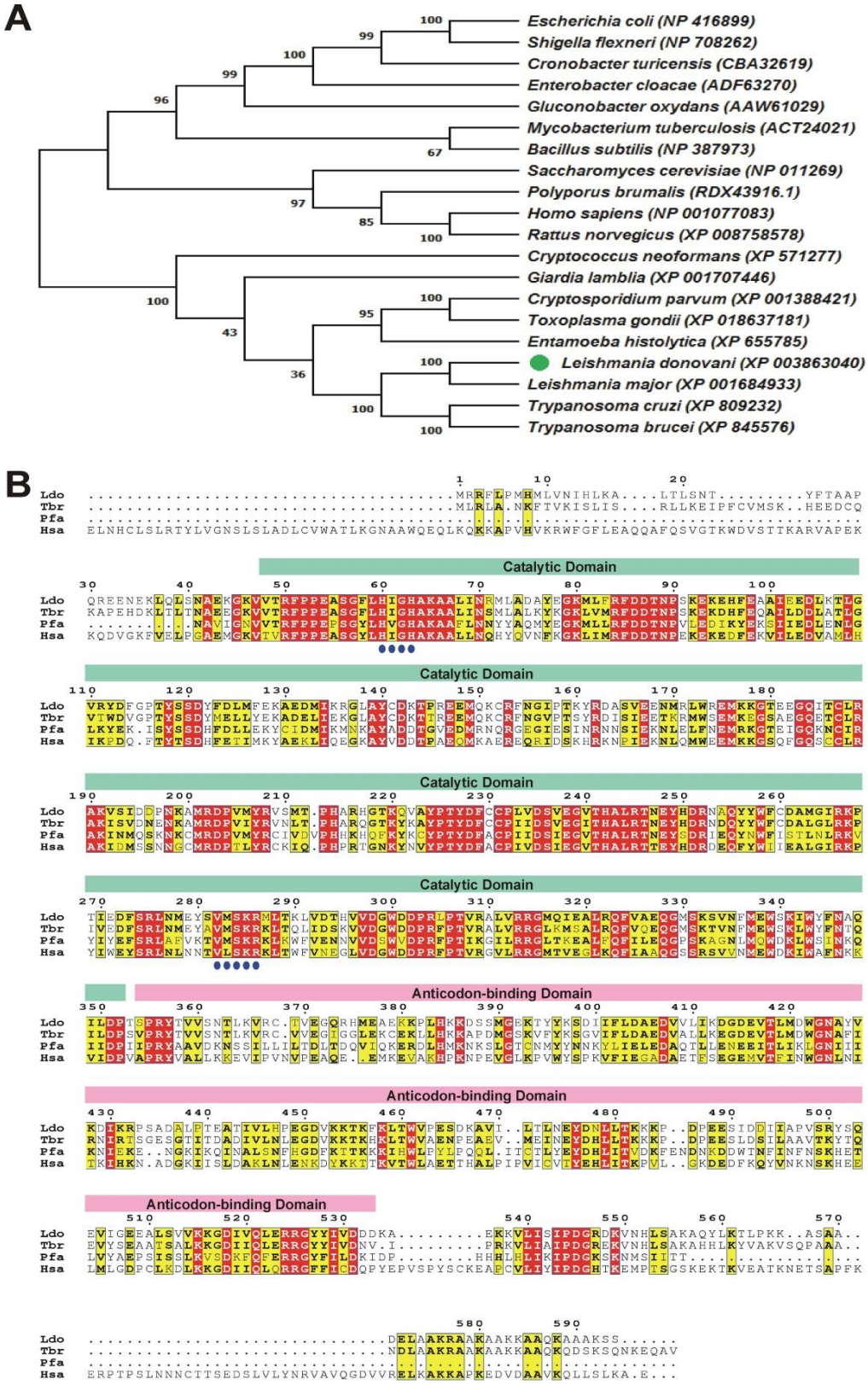

Figure 8: Phylogenetic and sequence analysis of *Ld*GluRS. (A) The protein sequences of glutamyl tRNA synthetase from different organisms were subjected to generation of phylogenetic tree through neighbor-joining method. The percentage generated through bootstrap iterations is denoted as the numbers placed on each branch. (B) Sequence comparison of glutamyl tRNA synthetases from *L.*

donovani (Ldo), *T. bruzi* (Tbr), *P. falciparum* (Pfa) and *H. sapiens* (Hsa). The domains I and II are correspondingly represented in green and pink colour, whereas the residues of HXGX and XXSKR motifs are shown as blue circles.

3.1.2 Cloning of *Ld*SerRS, *Ld*GluRS and site directed mutagenesis

The ORF encoding the full-length *Ld*SerRS was amplified at 58°C of annealing temperature from *L. donovani* genomic DNA. The resulted amplicon was found to be ~1.4 kb on the 1% agarose gel (**Fig. 9A).** Simulatniously, ORF of human SerRS containing 1545 nucleotides was amplified at 63°C of annealing temperature from human cDNA **(Fig. 9C).** The amplified products were ligated by T_4 DNA ligase at 22°C for 2 hrs and clones were confirmed by restriction digestion (**Fig. 9B, 9D**) followed by DNA sequencing. Site directed mutations were generated by PCR amplification of *Ld*SerRS plasmid using the mutated primers and all mutants were verified by DNA sequencing.

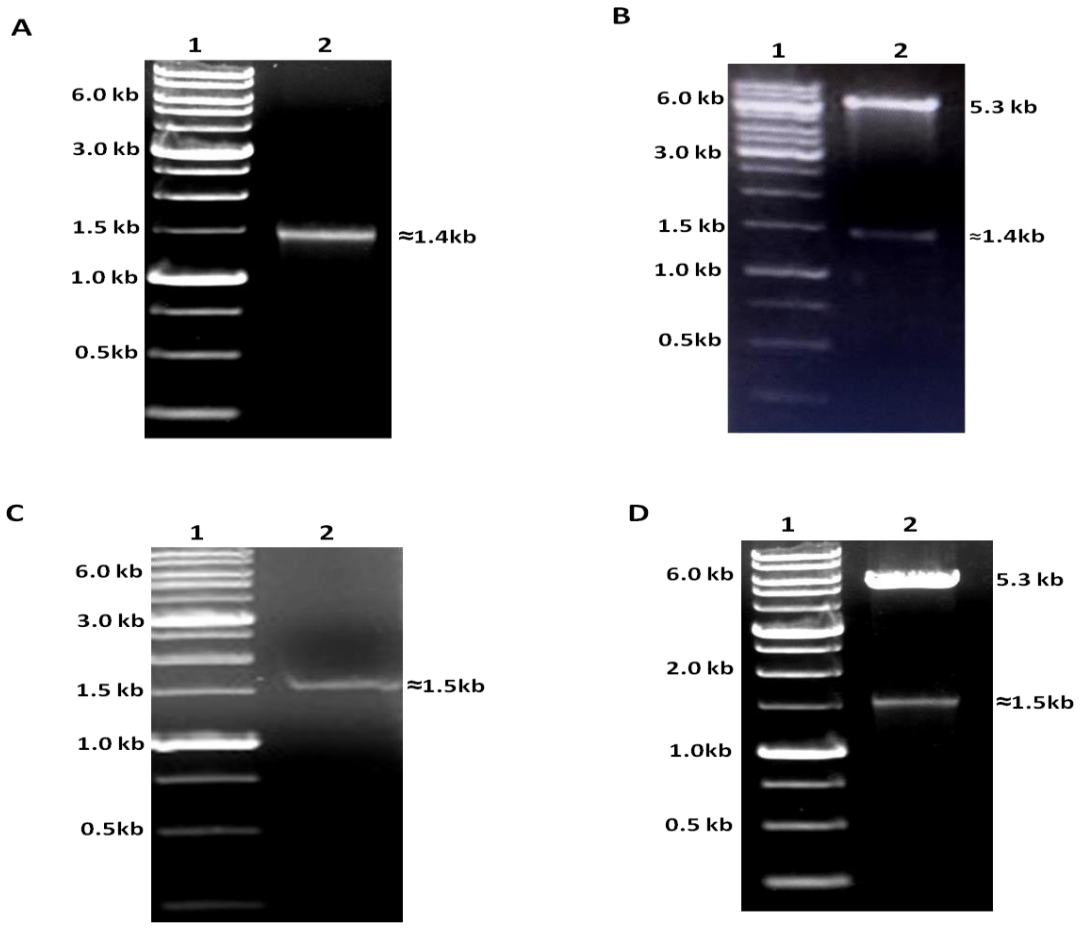

Figure 9: Molecular cloning of *Ld*SerRS and rR*Hs*SeS. (A) Amplification of *Ld*SerRS. Lane 1: 1kb DNA marker mix; Lane 2: amplified SerRS from *L. donovani*. (B) Confirmation of construct by restriction digestion. Lane 1: 1kb DNA marker mix; Lane 2: digestion of *Ld*SerRS:pET28a construct with *BamH*I and *Xho*I. (C) Amplification of *Hs*SerRS. Lane 1: 1kb DNA marker mix; Lane 2:

amplified SerRS fom *Homo sapiens*. (D) Confirmation of construct by restriction digestion. Lane 1: 1kb DNA marker mix; Lane 2: digestion of *Hs*SerRS:pET28a construct with *BamH*I and *Xho*I.

Simultaneously, the best annealing temparature was observed to be 57ºC for the amplification of truncated *Ld*GluRS with the resulted amplicon of ~1.5 kb **(Fig. 10A).** Purified amplicon of *Ld*GluRS was cloned into pET-28a vector and transformed into *E. coli* XL1-Blue competent cells. Plasmid was isolated from positive colonies and then confirmed through restriction digestion (**Fig. 10B**) and DNA sequencing.

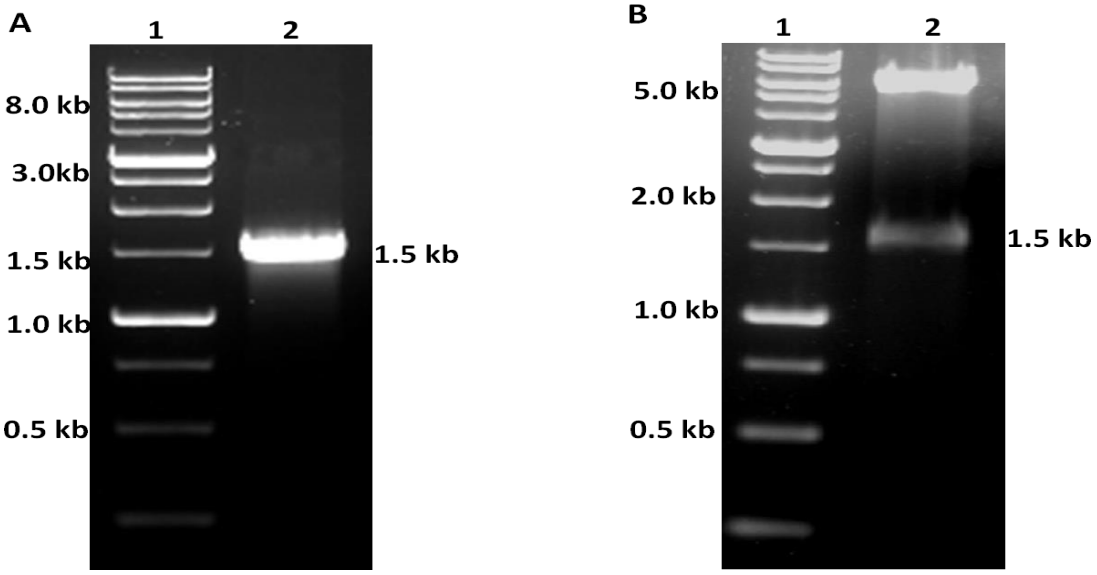

Figure 10: Molecular cloning of GluRS from *L. donovani*. (A) Amplification of *Ld*GluRS. Lane 1: 1kb DNA marker mix; Lane 2: amplified truncated GluRS from *L. donovani*. (B) Confirmation of construct by restriction digestion. Lane 1: 1kb DNA marker mix; Lane 2: digestion of *Ld*GluRS:pET28a construct with *Sac*I and *Xho*I.

3.1.3 Expression and purification of *Ld*SerRS, *Ld*GluRS and their mutants

For expression of proteins, plasmid carrying desired insert was further transformed into bacterial expression cells followed by induction by addition of 0.2 to 1 mM of IPTG. The recombinant *Ld*SerRS, *Hs*SerRS, *Ld*GluRS and mutant proteins were expressed in *E. coli* BL21 (DE3) strain succeeded by their purification from the bacterial cell lysate employing affinity chromatography. The quality of proteins was examined on 10% SDS-PAGE that showed a band corresponding to molecular weight of approximately 56 kDa for native as well as mutant forms of *Ld*SerRS and around 62 kDa for *Hs*SerRS **(Fig. 11A)** with more than 95% purity. Moreover, the purified protein fractions from affinity chromatography were combined and concentrated followed by loading on to gel filtration chromatography column pre-

calibrated with standard protein markers including β-amylase (200.0 kDa), alcohol dehydrogenase (150.0 kDa), bovine serum albumin (66.0 kDa), carbonic anhydrase (29.0 kDa) and cytochrome C (12.4 kDa). *Ld*SerRS was eluted at 76.2 ml as a single predominant peak. A comparison of the partition coefficient with known standard proteins suggested a size of ~112.0 kDa for *Ld*SerRS, indicating its dimeric form in solution **(Fig. 11B).** Protein concentration, estimated on NanoDrop using molar absorption coefficient of 43,860 mol^{-1} cm^{-1} and molecular weight of 56,486 Da, was found to be ~5 mg per liter of culture for *Ld*SerRS.

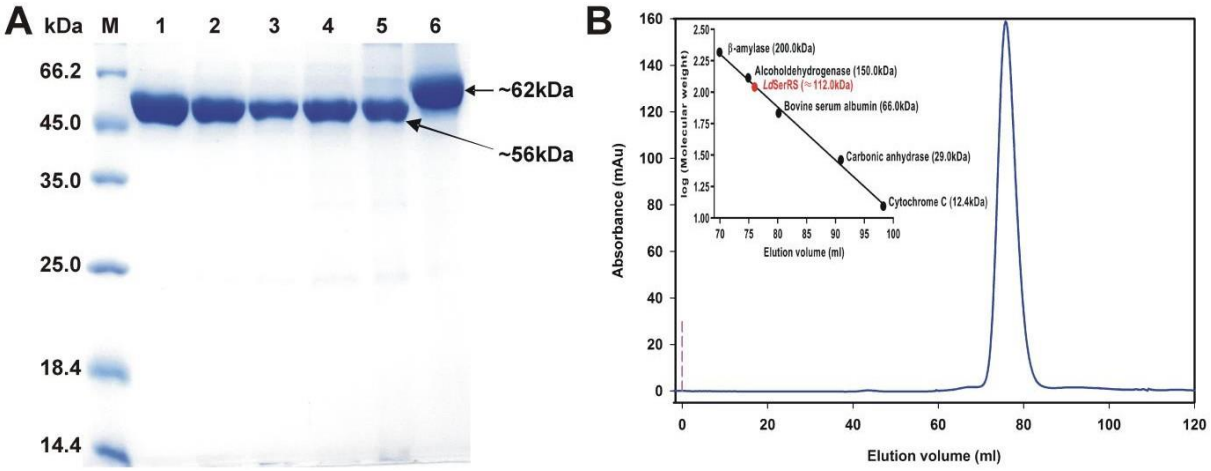

Figure 11: Purification and molecular weight analysis of recombinant *Ld*SerRS. (A) 10 % SDS-PAGE of purified *Ld*SerRS and its mutants along with *Hs*SerRS. Lane M indicates protein marker and Lane 1–5 designate respective native *Ld*SerRS and its mutants R295K, R295A, E297D and E297A, while Lane 6 shows purified *Hs*SerRS. (B) Size exclusion chromatography profile of *Ld*SerRS displaying elution volume at 76.2 ml on Superdex 16/600200 pg column and the corresponding molecular weight was found to be ~112.0 kDa. The inset presents the plot of protein standards including β-amylase (200 kDa), alcohol dehydrogenase (150.0 kDa), bovine serum albumin (66.0 kDa), carbonic anhydrase (29.0 kDa), and cytochrome C (12.4 kDa) along with *Ld*SerRS (red circle).

Simultaneously, The apo *Ld*GluRS and its mutant proteins (H60R and H60A) were purified by Ni-NTA affinity chromatography from induced bacterial cells and analysed on SDS-PAGE that displayed a single band with a molecular weight of around 62 kDa **(Fig. 12A)**. Gel filtration chromatography of *Ld*GluRS showed a single predominant peak with an elution volume of about 86 ml **(Fig. 12B)**. The molecular weight of *Ld*GluRS was enumerated as ~124 kDa by comparing its partition coefficient with that of standard proteins that demonstrates its dimer form in the solution. The estimated protein concentration of *Ld*GluRS using NanoDrop was 2 mg per liter of culture.

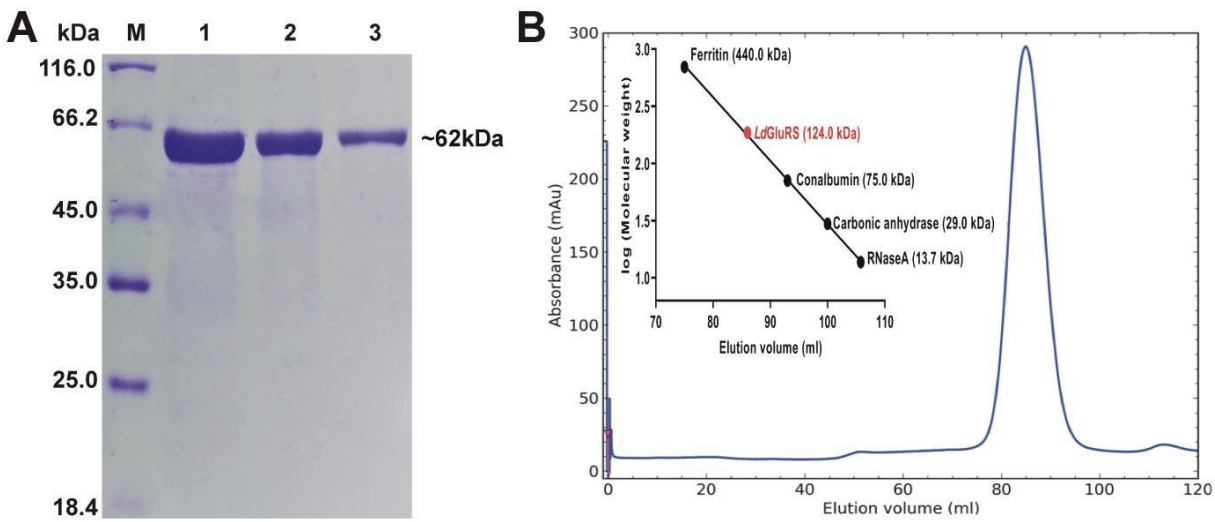

Figure 12: Purification and molecular weight determination of *Ld*GluRS. (A) Purified *Ld*GluRS and its mutants on SDS-PAGE, where lane M designates protein marker and Lanes 1–3 indicate corresponding wild *Ld*GluRS and its mutants H60R and H60A. (B) The profile of gel filtration chromatography on Superdex 16/600 200 pg column exhibits elution volume of *Ld*GluRS at 86.2 ml with the molecular weight of ~124 kDa. The inset displays the plot of protein standards i.e. Ferritin (440.0 kDa), Conalbumin (75.0 kDa), Carbonic anhydrase (29.0 kDa), and RNase A (13.7 kDa) along with *Ld*GluRS (red circle).

3.1.4 Intrinsic fluorescence measurements of *Ld*SerRS and *Ld*GluRS

Fluorescence spectroscopy was used to gain insight into the structure and dynamics nature of the protein molecules, where intrinsic fluorescence predominantly depends on the micro-environment of tryptophan (Trp) and tyrosine (Tyr) residues. Initially, *Ld*SerRS protein possesses four tryptophan residues at positions of 41, 277, 331 and 375. At pH 7.5, intrinsic fluorescence spectra of *Ld*SerRS showed a maximum emission at 337 nm delineating tryptophan residues to be partially exposed to the solvent environment (**Fig. 13A**). The conformational modifications of *Ld*SerRS examined at different pH has shown gradual rise in intensity with increasing pH from 3.5 to 7.5, and drop at basic pH ranging from 8.5 to 9.5 **(Fig. 13B).** Simultaneously, thermal stability of *Ld*SerRS was also analysed in the presence of its substrate/cofactor. The fluorescence spectra of apo *Ld*SerRS and its complexes with ligands (such as L-Ser, ATP and both) measured at various temperatures displayed maximum intensity at 20ºC, which was found to decrease gradually with increase in temperature to 90ºC **(Fig. 13C, 13E, 13G and 13I**). The thermal denaturation curve of *Ld*SerRS was sigmoidal that infers the cooperative unfolding for apo **(Fig. 13D**) and complexes with L-Ser **(Fig. 13F**), ATP **(Fig. 13H**) and both ligands **(Fig. 13J).** Concurrently, the corresponding T_m was observed to be 41.8±0.8, 48.2±0.6, 46.5±0.9 and 45.3±0.2ºC, suggesting an increase in

structural integrity in the presence of ligands. In addition, WESA online server revealed one tryptophan (Try331) to be on the surface of the protein and remaining three (Try41, Try277 and Try375) as buried.

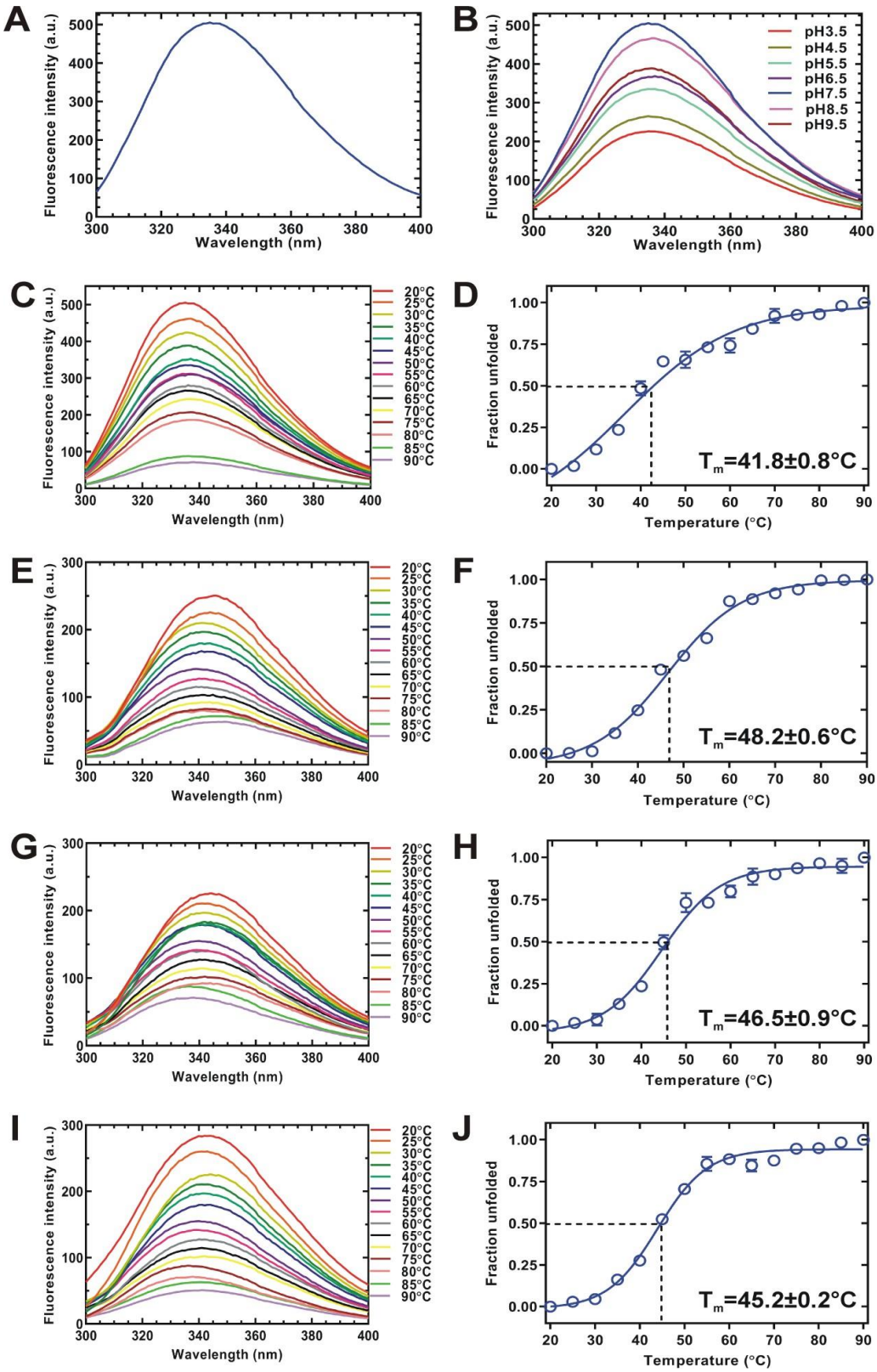

Figure 13: Fluorescence spectra of *Ld*SerRS. (A) Fluorescence emission spectrum of *Ld*SerRS at pH 7.5. (B) Emission spectra of *Ld*SerRS with varying pH from 3.5 to 9.5. Fluorescence spectra with increase in temperature from 20 to 90ºC for *Ld*SerRS (C) and in the presence of L-Ser (E), ATP (G) and L-Ser + ATP (I). The respective thermal denaturation curves are shown in (D), (F), (H) and (J).

Similarly, protein sequence of *Ld*GluRS possesses seven tryptophan residues at 173, 258, 300, 339, 343, 422 and 461 positions. The maximum fluorescence emission of *Ld*GluRS was at 340 nm, indicating that tryptophan residues were partly exposed to the solvent milieu **(Fig. 14A)**. The fluorescence intensity dropped gradually from pH 3.5 to 9.5 **(Fig. 14B)**. Thermal stability studies exhibited decrease in fluorescence intensity for apo *Ld*GluRS and its complexes in the presence of ligands (including L-Glu, ATP, and both) as temperature increased from 20 to 90°C **(Fig. 14C, 14E, 14G and 14I)**. The cooperative unfolding for apo, L-Glu, ATP, and both ligands bound *Ld*GluRS was observed and the respective T_m was found to be 45.2±0.7 **(Fig. 14D)**, 47.4±0.9 **(Fig. 14F)**, 50.3±0.8 **(Fig. 14H)** and 48.3±0.5°C **(Fig. 14J)** that pointed towards enhanced structural stability of protein with ligands.

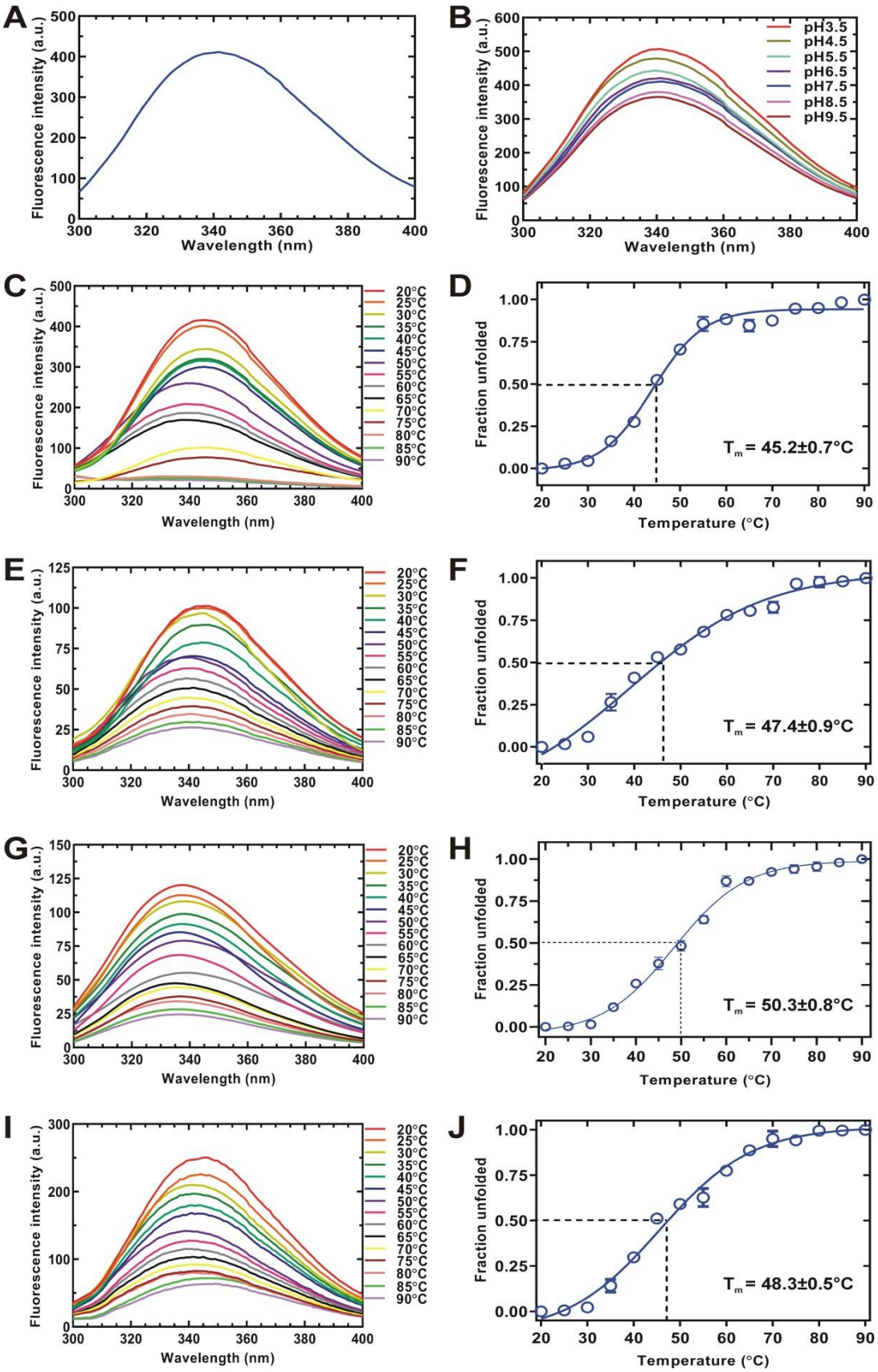

Figure 14: Fluorescence spectra of *Ld*GluRS. (A) Fluorescence emission spectrum of *Ld*GluRS at pH 7.5. (B) Emission spectra of *Ld*GluRS with pH ranging between 3.5 to 9.5. The effect of varying

temperature (20 to 90°C) on fluorescence spectra for *Ld*GluRS (C) and with L-Glu (E), ATP (G) and L-Glu + ATP (I) along with their corresponding thermal denaturation plots (D), (F), (H) and (J).

Furthermore, quenching studies were performed using potassium iodide (KI) and acrylamide that exhibited a gradual decline in fluorescence intensity of *Ld*SerRS when quantity of quenchers increased. At the concentration of 0.5 M of acrylamide and KI, the corresponding fluorescence intensity was reduced by 6.2 and 2.7 times **(Fig. 15A and 15C**). The respective quenching constants of acrylamide and KI, enumerated through the Stern-Volmer plot, were 7.67±0.09 and 3.47±0.07 M^{-1} (**Fig. 15B and 15D**) that delineate towards higher impact of acrylamide as quencher and most of the tryptophan residues were buried in the hydrophobic region. Simultaneously, unfolding studies of *Ld*SerRS were carried out using guanidium hydrochloride (GdHCl) and urea. The stability of *Ld*SerRS was observed to remain unaffected up to 2 and 1.2 M followed by complete denaturation at 7 and 4 M of urea and GdHCl, respectively, which suggests that GdHCl is more effective denaturant for leishmanial SerRS as compared to urea. Further, the data of fraction unfolded vs. denaturant concentrations were normalized and fitted into a two-state equation, where it depicted three phases viz. folded, transition and unfolded states. The free energies (ΔG) for *Ld*SerRS in the presence of urea and GdHCl were calculated to 2.6±0.03 and 1.9±0.1 M^{-1}, while corresponding mid transition concentration (C_m) were 3.8±0.01 and 2.02±0.04 M^{-1} (**Fig. 15E–F)**.

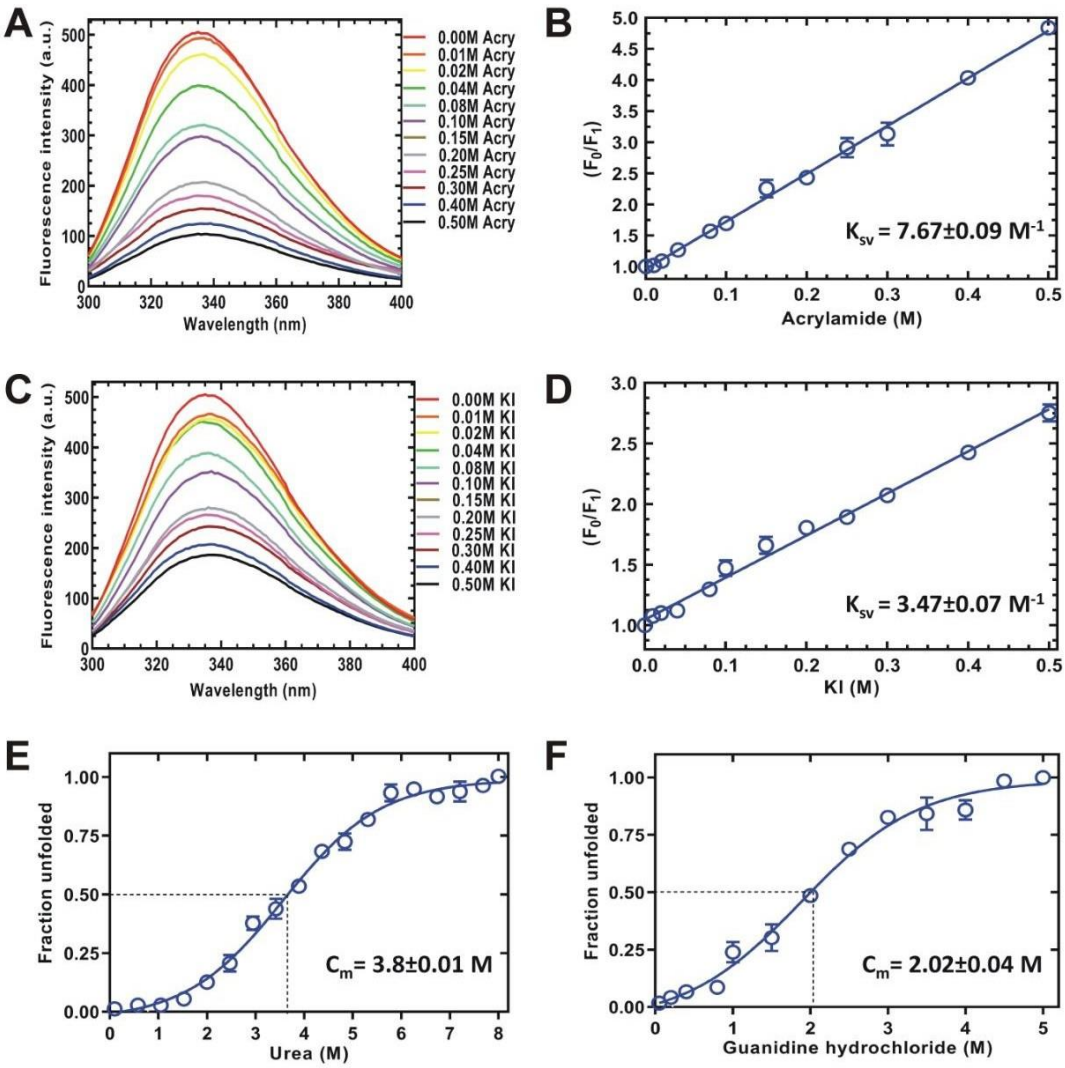

Figure 15: Fluorescence quenching and chemical denaturation studies of *Ld*SerRS. Intrinsic fluorescence spectra of *Ld*SerRS with increasing concentrations of quenchers i.e. acrylamide (A) and potassium iodide (C). Stern-Volmer plots of *Ld*SerRS in the presence of acrylamide (B) and potassium iodide (D). Denaturation plots of *Ld*SerRS with various conc. of urea (E) and guanidine hydrochloride (F).

Similarly, WESA server predicted two tryptophan residues (Trp173 and Trp343) to be positioned on the surface of *Ld*GluRS and the remaining five (Trp258, Trp300, Trp339, Trp422 and Trp461) in a hydrophobic environment. Quenching studies with acrylamide and potassium iodide (KI) showed intensity of the emission spectra gradually declined with increasing quencher concentrations. The intrinsic fluorescence intensity decreased by 4.2 and 2.8 times at elevated amounts of acrylamide and potassium iodide i.e. 0.5 M **(Fig. 16A, 16C)**. Stern-Volmer plot revealed corresponding quenching constant of acrylamide and KI to be 6.64±0.04 and 3.61±0.06 M^{-1} **(Fig. 16B, 16D)**, implying that acrylamide has a more

significant effect in quenching as mostly tryptophan residues are located in the hydrophobic pocket. The chemical stability analysis delineated that *Ld*GluRS had negligible effect with 2.5 and 1.5 M of urea and GdHCl, respectively, whereas complete denaturation was observed with 8 and 5 M corresponding concentrations. Subsequently, the fraction unfolded vs. denaturant concentration plot was fit into a two-state equation that illustrates three different stages viz. folded, transition and unfolded. The individual free energy (ΔG) of *Ld*GluRS with urea and GdHCl was 2.3±0.03 and 1.83±0.04 M^{-1}, while the respective mid-transition concentrations (C_m) were 3.8±0.03 and 2.18±0.06 M **(Fig. 16E–F)**. Fluorescence binding studies of *Ld*GluRS with L-Glu, ATP and sodium salicylate showed a concentration-dependent reduction in the fluorescence intensity (**Fig. 17A, 17C, 17E)** advocating towards the binding of protein and ligands. The corresponding binding constants (K_b) of ATP, L-Glu and salicylate for *Ld*GluRS were calculated to be 4.37 x 10^{-4}, 1.96 x 10^{-4} and 3.61 x 10^{-4} M^{-1} **(Fig. 17B, 17D, 17F)**.

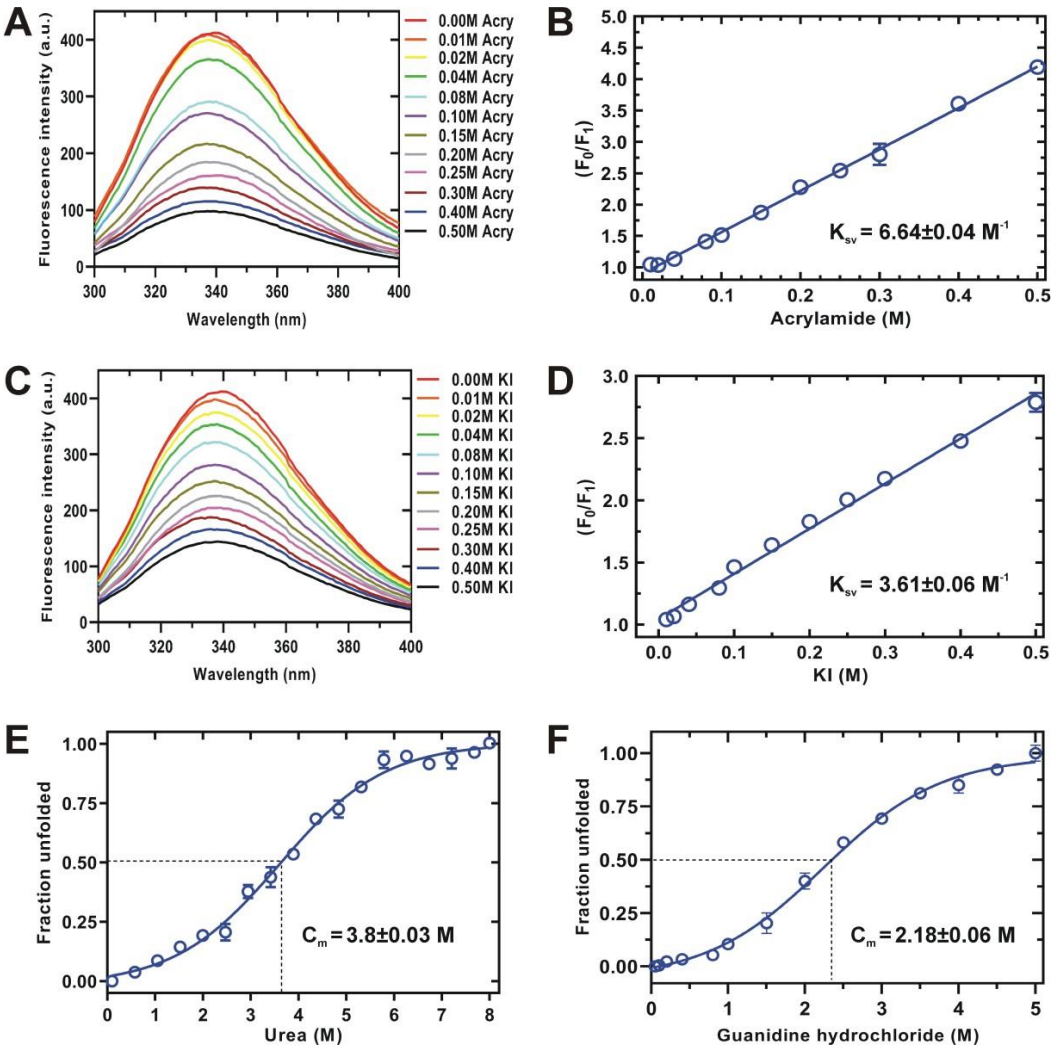

Figure 16: Quenching and chemical denaturation analysis of *Ld*GluRS. Intrinsic fluorescence spectra of *Ld*GluRS in the presence of acrylamide (A) and potassium iodide (C). Stern-Volmer plots of *Ld*GluRS with acrylamide (B) and potassium iodide (D). Denaturation graphs of *Ld*GluRS with urea (E) and guanidine hydrochloride (F).

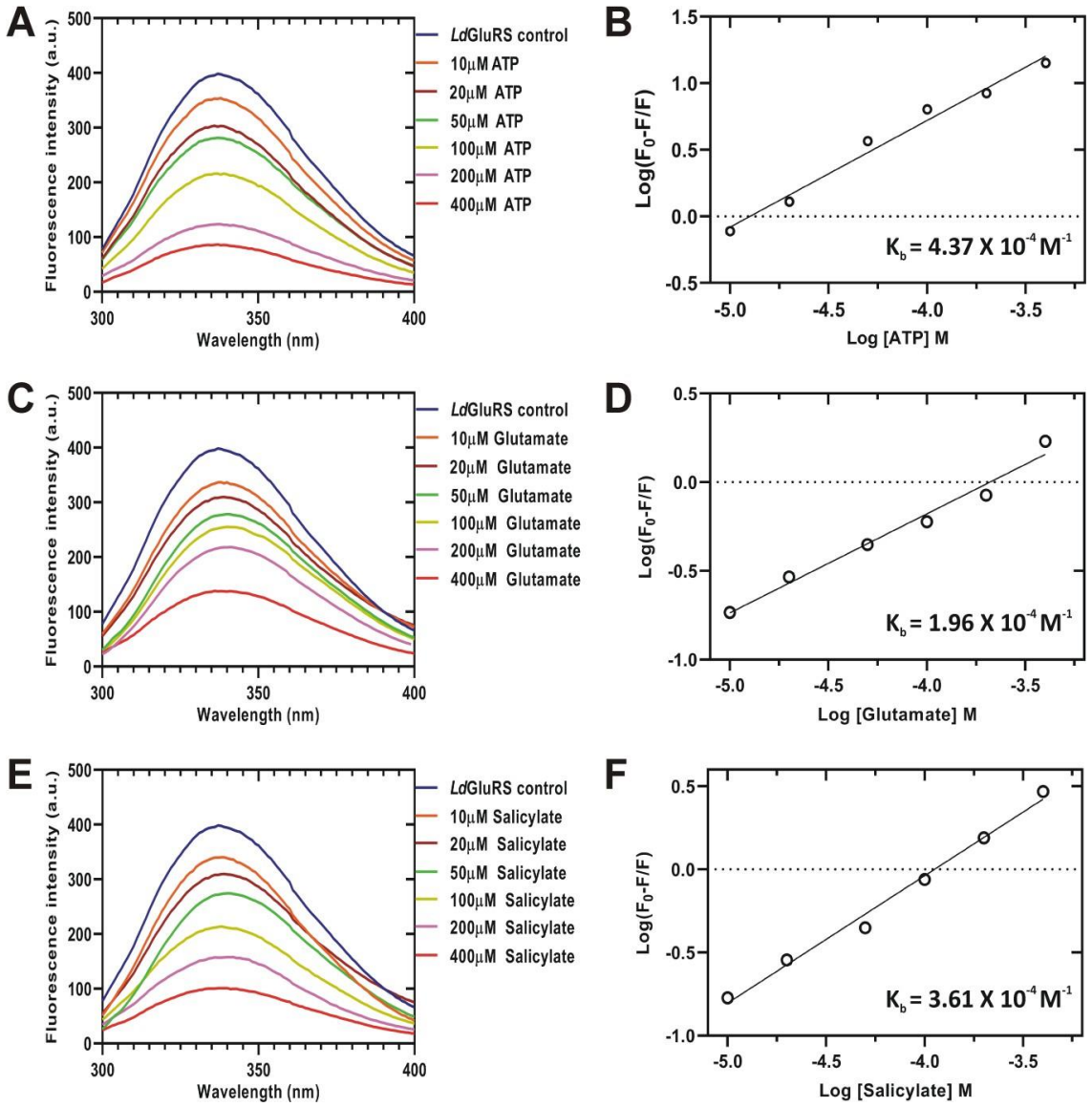

Figure 17: Binding of *Ld*GluRS with ATP, L-glutamate, and salicylate. Intrinsic fluorescence emission spectra demonstrating reduction in the intensity of *Ld*GluRS with increasing concentrations of ATP (A), L-glutamate (C), and salicylate (E). Modified Stern-Volmer plots of *Ld*GluRS with ATP (B), L-glutamate (D), and salicylate (F).

3.2 Discussion

Aminoacyl tRNA synthetases (aaRSs) are a class of enzymes that are involved in the esterification of amino acid on to their cognate tRNA and play a significant role in various cellular processes **[76].** The aaRSs have been presented as an attractive candidate for the design and development of new antimicrobials **[133]**. Earlier studies have suggested tRNA synthetase as a therapeutic target against several eukaryotic pathogens such as *P. falciparum* **[134]**, *L. donovani* **[135]**, *Loa loa* and *Schistosoma mansomi* **[136**]. Since inhibition of tRNA aminoacylation has been considered as a promising antimicrobial strategy **[137, 138**]**,** we have cloned, expressed and purified seryl and glutamyl tRNA synthetases of *L. donovani*. The evolutionary study depicted that *Ld*SerRS and *Ld*GluRS are closely related to other trypanosomatid species and have presented high divergence from their human counterpart. Sequence analysis delineated *Ld*SerRS to possess three domains and its catalytic residues were mostly conserved among the orthologs of SerRSs. Simultaneously, *Ld*GluRS possesses similar domain organization as reported in other glutamyl tRNA synthetases **[134]** with the majority of its catalytic residues remaining unchanged except a few alterations in the residues of ATP binding pocket. Purified *Ld*SerRS existed as a homodimer, which is the characteristic feature of class II aaRS. SerRSs from *E. coli* **[139]**, *H. sapiens* **[103]**, and *S. cerevisiae* **[98**] were also reported to be dimer. Similarly, purified *Ld*GluRS is found as a homodimer in solution that is consistent to the previous report from wheat GluRS **[140]**. This oligomeric arrangement is in contrast to the monomeric form of *Bacillus subtilis* GluRS [**141**] and multienzyme complexes of GluRSs from mammalian cells **[117]**. The outcome of fluorescence quenching delineated more effect of acrylamide on *Ld*SerRS and *Ld*GluRS than potassium iodide that portrays acrylamide as a neutral molecule interacting with surface as well as buried tryptophan residues, while KI being a charged molecule can quench tryptophan residues present only on the surface and does not penetrate the core of the protein. Other leishmanial proteins like AspRS **[96]** and 6PGDH **[142]** had also displayed the position of Trp residues majorly in the core of the protein structure. Urea and guanidine hydrochloride (GdHCl) are commonly used denaturants to evaluate the conformational stability of protein in the folded (native) and unfolded (denatured) states **[143]**. *Ld*SerRS and *Ld*GluRS were highly sensitive to guanidine hydrochloride (GdHCl) and moderately stable in the presence of urea, which could be due to the strong ionic strength of GdHCl that reduces the electrostatic interactions in the proteins **[144]**. Similar to *Ld*SerRS and *Ld*GluRS, other leishmanial enzymes such as RPE **[145]** and 6PGDH **[142]** have also been reported as moderately stable towards urea.

Chapter-II

4. Enzyme kinetics and inhibition studies of recombinant proteins

4.1 Result

4.1.1 Aminoacylation assay of *Ld*SerRS and *Ld*GluRS:

Aminoacylation reaction occurs in two steps, wherein SerRS hydrolyzes firstly ATP to activate L-serine by forming a seryl-adenylate intermediate and discharging inorganic pyrophosphate (PPi) as a by-product. In the second step, the inorganic pyrophosphatase (PPase) enzyme is coupled to the aminoacylation reaction for exchange of PPi to inorganic phosphate (Pi). Addition of malachite green reagent to the reaction leads to a change in colour from yellow to green, which can be detected and quantitatively measured at wavelength of 620 nm to estimate the relative activity of the recombinant protein. To quantify the inorganic phosphate (Pi) in this reaction, a standard phosphate graph was plotted taking concentrations of phosphate on X-axis and optical density value on Y-axis **(Fig. 18A).** An aminoacylation assay was conducted in presence and absence of PPase and recombinant enzyme, wherein about 10% relative activity was detected in the absence of *Ld*SerRS and almost no relative activity was observed in absence of both of the enzymes **(Fig. 18B).** The enzymatic activity of recombinant protein has gradually increased from pH 3.5 to 7.5, reached to maximum at pH 7.5, and drastically decreased at pH 8.5 and 9.5 (**Fig. 18C**). The sharp decline in the activity of *Ld*SerRS could be due to whitish precipitation observed during reaction with alkaline pH buffer. To investigate the optimum temperature for *Ld*SerRS activity, the reaction was carried out at the temperature ranging from 10 to 90ºC. Enzyme exhibited the highest activity at 30ºC, which reduced to about 50% at 40ºC and appeared as negligible at 90ºC **(Fig. 18D).** Simultaneously, it was also observed that SerRS activity is increased in the presence of various divalent metals and showed maximum activity in the presence of Mg^{2+}. The respective activity of *Ld*SerRS has been reduced to 30%, 32%, 40%, 80%, 80% and 85% when magnesium was replaced with Zn^{2+}, Mn^{2+}, Ca^{2+}, Cu^{2+}, Co^{2+} and Fe^{2+} (**Fig. 18E**). Notably, the relative activity of *Ld*SerRS was found to be maximum with 15 mM of magnesium ions followed by gradual decrease upto 40 mM **(Fig. 18F).** Similarly, *Ld*SerRS had shown the maximum activity in the presence of potassium ions among the various monovalent cations, which was dropped correspondingly 40% and 60% with Li^{+} and Cs^{+} in comparison to that of K^{+} ions **(Fig. 18G)**. Interestingly, the highest activity was observed with 30 mM of potassium ions with a sharp decline from 35 to 45 mM of the same **(Fig. 18H).**

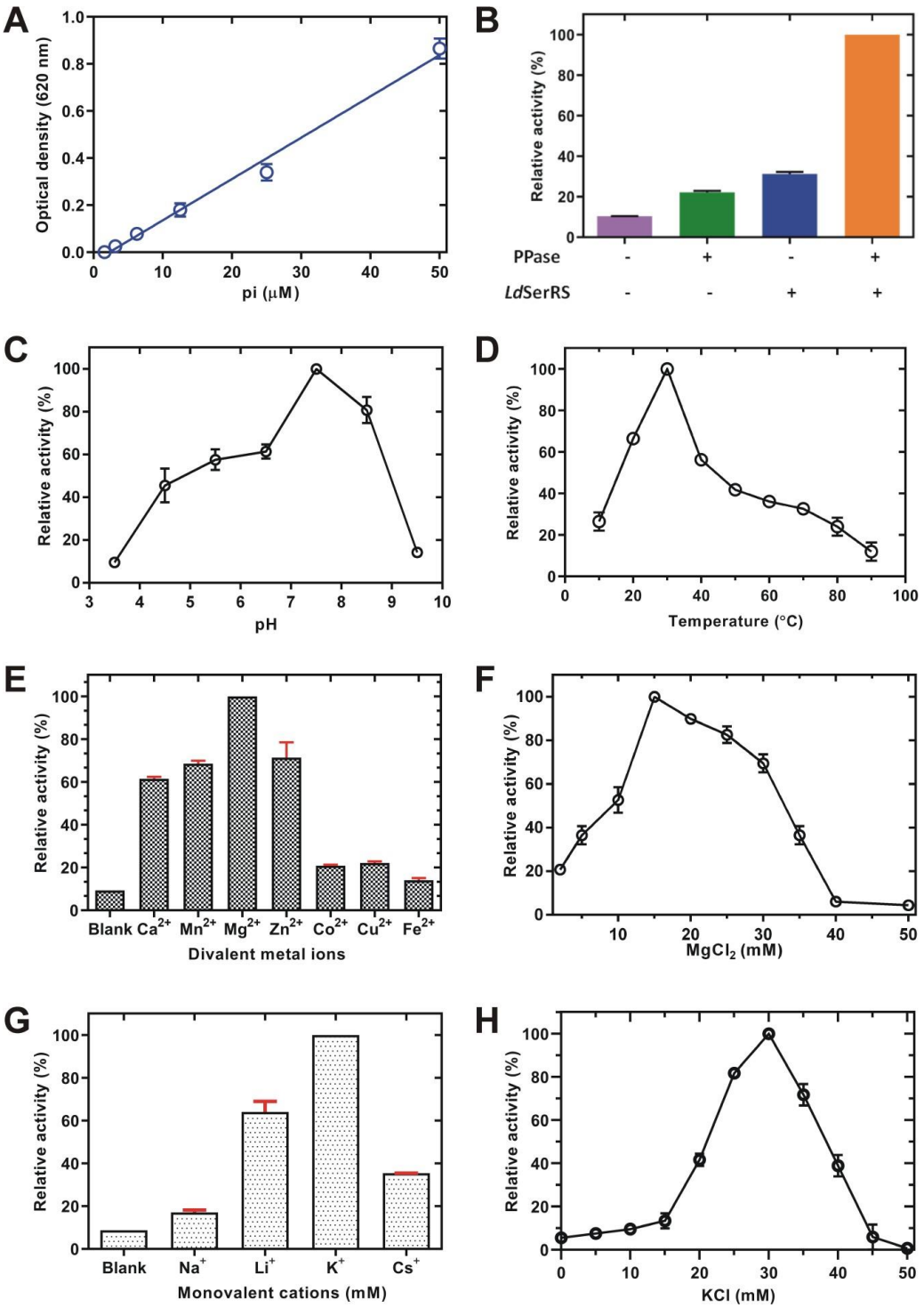

Figure 18: Aminoacylation assays of *Ld*SerRS. (A) Standard inorganic phosphate plot from 0 to 50 μM. (B) Plot of relative activity with/without *Ld*SerRS and PPase. Effect of pH (C) and temperature (D) on the enzymatic activity of *Ld*SerRS. Enzymatic activity of *Ld*SerRS in the presence of various divalent (E) and monovalent (G) ions. Concentration based activity of *Ld*SerRS with $MgCl_2$ (F) and KCl (H) from 0 to 50 mM.

Similarly, a standard phosphate graph was prepared by varying concentration of phosphate on X-axis and absorbance at 620 nm on Y-axis **(Fig. 19A)** to determine the inorganic phosphate (Pi) released during the process. The aminoacylation assay exhibited 10% relative activity without PPase and *Ld*GluRS, whereas only PPase and *Ld*GluRS displayed corresponding activity of 20 and 25% in comparison to the presence of both of the enzymes **(Fig. 19B)**. At different pH, the enzymatic activity was increased from pH 3.5 to pH 7.5 and then sharply declined at pH 8.5 and 9.5 **(Fig. 19C)**. Temperature based assay of *Ld*GluRS revealed maximum activity at 40ºC, while further increase in temperature reduced the activity by 60% at 50ºC after which there was a progressive decline from 60ºC to 90ºC **(Fig. 19D)**. Additionally, the presence of several divalent metals (Ca^{2+}, Mn^{2+}, Mg^{2+}, Zn^{2+}, Co^{2+}, Cu^{2+} and Fe^{2+}) enhanced activity of *Ld*GluRS, where Mg^{2+} ion showed the maximum activity. The substitution of Mg^{2+} ion by Zn^{2+}, Ca^{2+}, Mn^{2+}, Co^{2+}, Cu^{2+}, and Fe^{2+} ions lowered the activity by 80%, 72%, 35%, 55%, 75%, and 92%, respectively **(Fig. 19E)**. The relative activity of *Ld*GluRS was steadily increased from 0 to 25 mM of Mg^{2+} ions, reached to highest at 30 mM and then it gradually decreased up to 50 mM **(Fig. 19F)**. Among the monovalent ions tested, *Ld*GluRS activity was highest with potassium ions, while decrease in activity by 35%, 70% and 80% was evident corresponding to Li^{+}, Cs^{+} and Na^{+} as compared to K^{+} ions **(Fig. 19G)**. The maximum activity was at 40 mM of K^{+} ions followed by a rapid fall from 45 to 50 mM of KCl **(Fig. 19H)**.

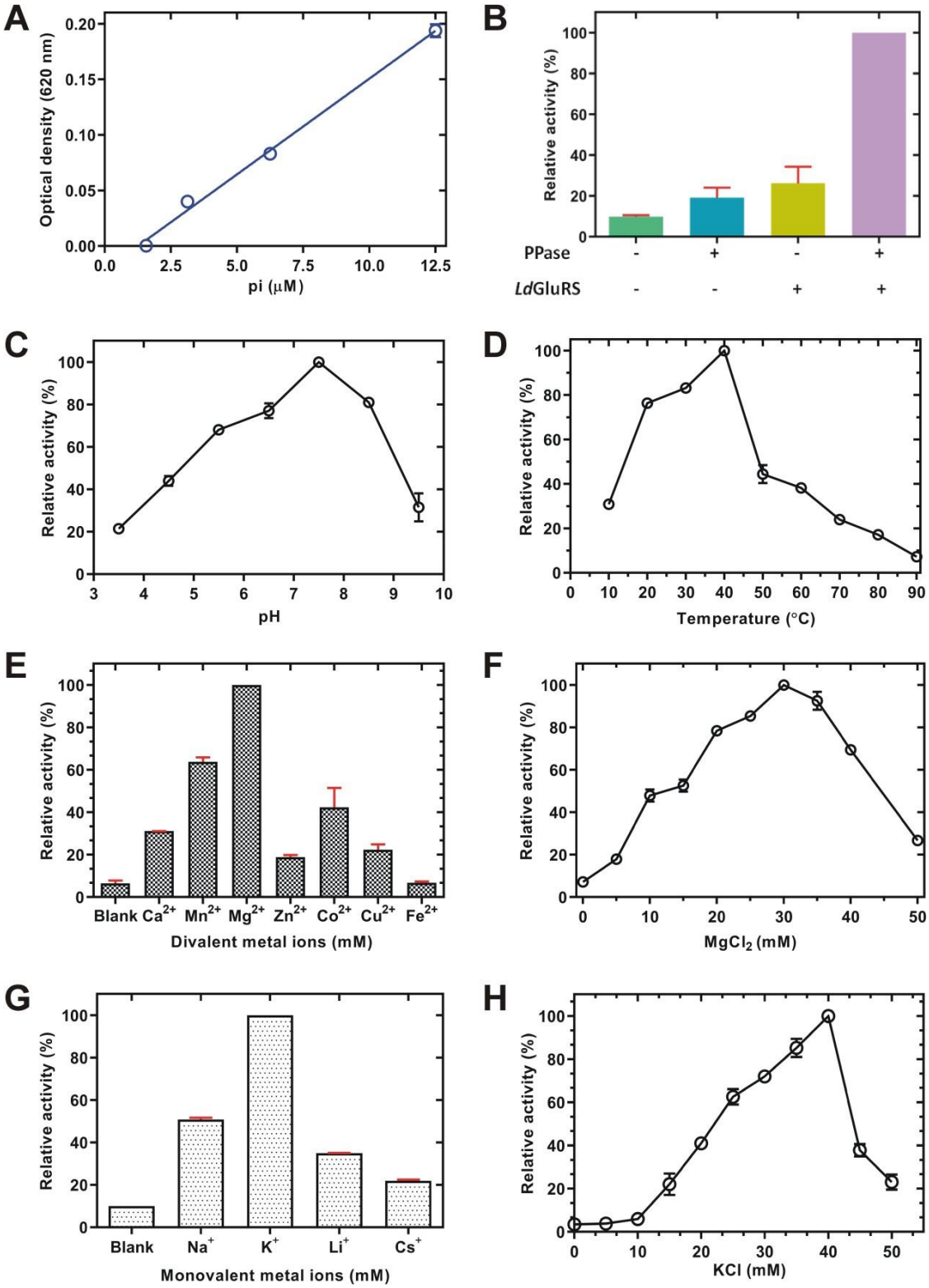

Figure 19: Enzymatic activity of *Ld*GluRS. (A) A standard graph of inorganic phosphate from 0 to 12.5 μM. (B) Plots of relative activity in the presence and absence of *Ld*GluRS and PPase. The aminoacylation activity of *Ld*GluRS at different pH (C) and temperature (D). Effect of different divalent (E) and monovalent (G) ions on enzymatic activity of *Ld*GluRS. The activity of *Ld*GluRS with various concentrations of $MgCl_2$ (F) and KCl (H).

4.1.2 Kinetic parameters of *Ld*SerRS, *Ld*GluRS and mutant proteins

The kinetic parameters of *Ld*SerRS demonstrated binding affinity (K_m) of 8.32±0.01 and 0.04±0.004 mM for L-Ser and ATP, respectively **(Fig 20A-B, Table 2**), which delineate that the affinity of *Ld*SerRS towards L-Ser is quite low when compared to that of ATP. The turnover number (k_{cat}) of the enzyme for the substrate was two-fold higher than that of the cofactor. The catalytic efficiency (k_{cat}/K_m) of *Ld*SerRS for the cofactor (ATP) was calculated to be 175 times more than that of substrate (L-Ser). Moreover, R295 and E297 were mutated with alanine and similar charge residues to understand the role of these residues during interaction with ATP. Notably, significant variations in affinities of R295K and R295A mutants were detected towards cofactor with corresponding K_m values of 0.145±0.017 and 0.239±0.04 mM as compared to that of native enzyme (0.04±0.004 mM). Additionally, E297D and E297A mutants showed corresponding upsurge of 4 and 5 folds in K_m values, presenting a substantial reduction in the affinity for cofactor (ATP) as compared to that of native protein **(Fig. 20C**). The k_{cat} values of R295K and R295A mutants exhibited 3.5 fold reductions from that of native *Ld*SerRS, while E297D and E297A revealed a fall of approximately 3 fold in k_{cat} values (**Fig. 20D).** Concomitantly, k_{cat}/K_m for ATP was found to diminish by approximately 10 times in the case of R295K and 16 times for R295A mutant, whereas k_{cat}/K_m values for E297D and E297A mutants had shown 8.7 and 14.5 fold decrease from that of native protein. The catalytic efficiency reduced drastically for both mutants indicating that these two charged amino acids are involved in binding with cofactor and definitely essential for enzyme.

Table 2: Kinetic parameters of *Ld*SerRS and its mutants for substrate and cofactor

Enzyme	**Substrate/ Co-factor**	**K_m (mM)**	**V_{max} (µM min^{-1})**	**k_{cat} (min^{-1})**	**k_{cat} / K_m (mM $^{-1}$min^{-1})**
*Ld*SerRS (WT)	Serine	8.32±0.01	0.72±0.02	0.14	0.017
	ATP	0.04±0.03	0.3 ± 0.01	0.068	1.7
R295A	ATP	0.239±0.04	0.136±0.01	0.027	0.11
R295K	ATP	0.145±0.01	0.116+0.06	0.023	0.16
E297A	ATP	0.203±0.03	0.127±0.008	0.025	0.12
E297D	ATP	0.158±0.06	0.183±0.02	0.033	0.208

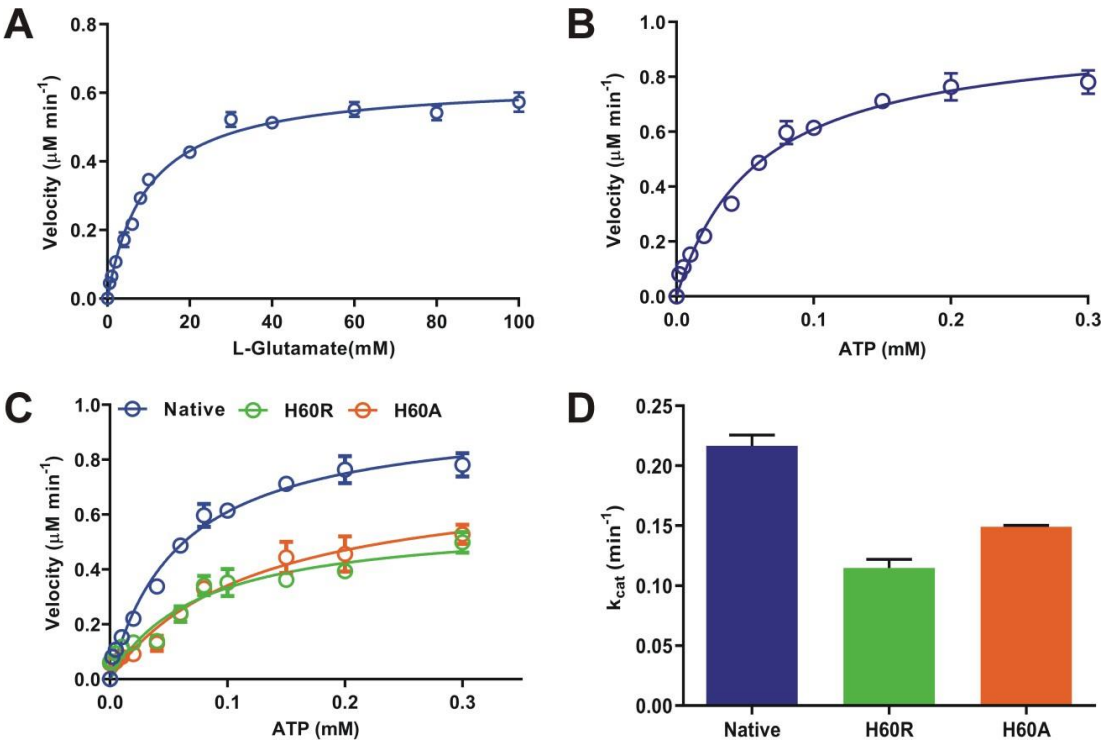

Figure 20: Enzyme kinetic studies of *Ld*SerRS. (A-B) Enzyme kinetic plots of *Ld*SerRS with substrate L-Ser (0–50 mM) and cofactor ATP (0–0.3 mM). (C) Kinetic analysis of *Ld*SerRS and its mutants with respect to cofactor ATP. (D) Comparison of k_{cat} value for *Ld*SerRS and its mutants.

Kinetic parameters of *Ld*GluRS exhibited that its affinity for substrate (L-glutamate) is 158 times lesser in comparison to the cofactor (ATP). The turnover number (k_{cat}) for the cofactor (ATP) was 1.7 times higher than substrate, while the catalytic efficiency (k_{cat}/K_m) of *Ld*GluRS for ATP is 240 times greater than that of L-glutamate **(Fig. 21A-B)**. The mutation of H60 to arginine and alanine was executed to understand the role of histidine in interaction of *Ld*GluRS with cofactor. Considerable differences were observed in the binding affinity values of cofactor (ATP) towards the native *Ld*GluRS (0.06±0.01 mM), mutants H60R (0.08±0.02 mM) and H60A (0.11±0.03 mM) **(Fig. 21C)**. Comparison of k_{cat} values of H60R and H60A mutants with native *Ld*GluRS have shown 1.9 and 1.4 fold decline, respectively **(Fig. 21D)**. In addition, the corresponding k_{cat}/K_m values of H60R and H60A mutants for ATP reduced by 2.1 and 2.4 fold when compared to the wild type **(Table 3)**.

Table 3: Kinetic parameters of *Ld*GluRS and its mutants for substrate and cofactor

Enzyme	Substrate/ Cofactor	K_m (mM)	V_{max} (µM min^{-1})	K_{cat} (min^{-1})	K_{cat} /K_m ($mM^{-1}min^{-1}$)
*Ld*GluRS (WT)	L-Glutamate	9.5 ± 0.5	0.63 ± 0.0	0.12	0.01
	ATP	0.06 ± 0.01	1.01 ± 0.03	0.21	3.12
H60R	ATP	0.08 ± 0.02	0.58 ± 0.08	0.11	1.45
R295A	ATP	0.11±0.03	0.75 ± 0.08	0.15	1.33

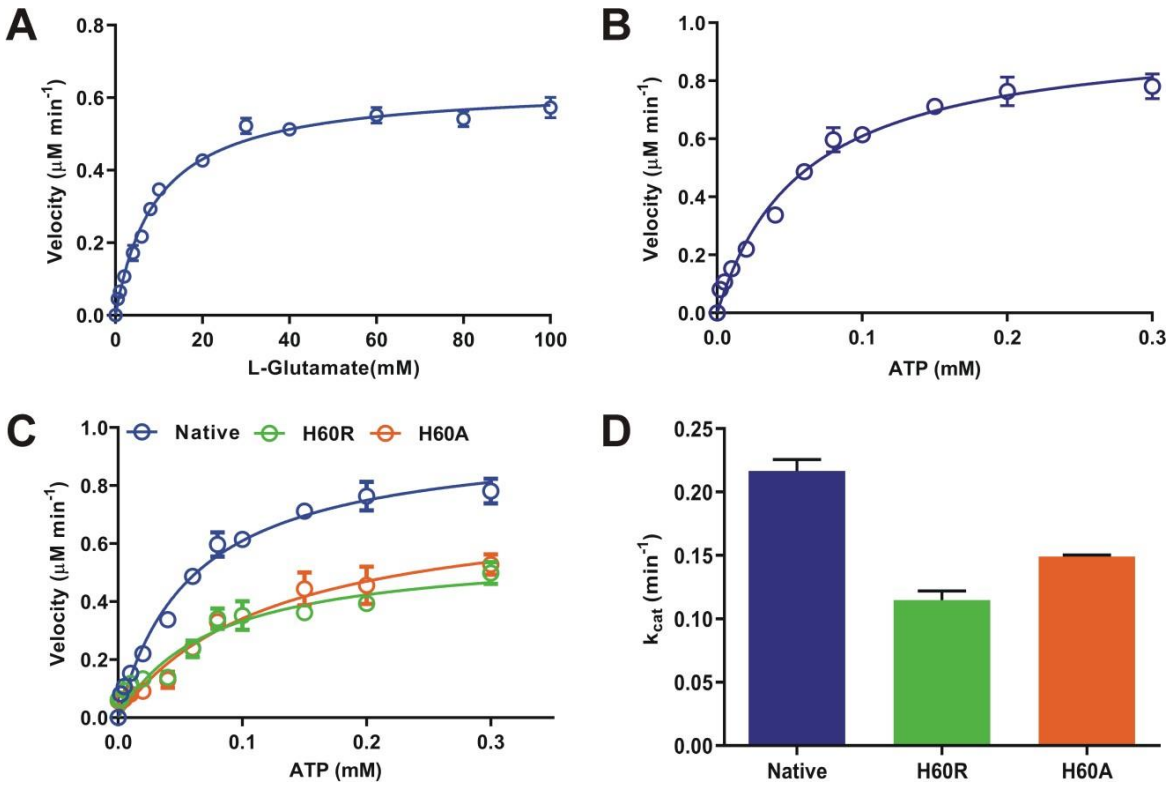

Figure 21: Enzyme kinetics of *Ld*GluRS. The activity of *Ld*GluRS with varying concentrations of L-Glu (0–50 mM) (A) and ATP (0–0.3 mM) (B). (C) Kinetic study for native and mutant forms of *Ld*GluRS with ATP. (D) Comparative analysis of k_{cat} values for native and mutants of *Ld*GluRS.

4.1.3 Inhibition of *Ld*SerRS by ureidosulfocoumarin derivatives

Inhibition studies of *Ld*SerRS and *Hs*SerRS were performed using synthesized ureidosulfocoumarin derivatives to find out a specific inhibitor against leishmanial enzyme. Out of all the compounds tested, only three (Comp 5l, 5q and 5r) have exhibited higher potency towards *Ld*SerRS than *Hs*SerRS **(Table 4**). The corresponding IC_{50} values of Comp 5l, 5q and 5r against *Ld*SerRS were 4.28±0.1, 10.92±0.3 and 16.45±0.1 µM, while it was

91.18±0.01, 77.61±0.01 and 75.36±0.01 μM for *Hs*SerRS **(Fig. 22A-C).** These observations demonstrated that Comp 5l, 5q and 5r inhibit *Ld*SerRS by 21.3, 7.1 and 4.5 fold than its human counterpart.

Table 4: IC_{50} values of synthesized compounds for *Ld*SerRS and *Hs*SerRS

S. No.	Compounds	*Ld*SerRS IC_{50} μM	*Hs*SerRS IC_{50} μM
1	Comp 5a	23.61±0.28	26.15±0.08
2	Comp 5b	35.86±1.23	44.65±0.03
3	Comp 5c	19.84±0.42	37.10±0.06
4	Comp 5d	27.654±0.15	40.26±0.02
5	Comp 5e	48.256±1.31	57.65±0.09
6	Comp 5f	72.05±0.98	80.35±0.05
7	Comp 5g	84.53±0.46	60.45±0.02
8	Comp 5h	41.36±0.31	15.68±0.01
9	Comp 5i	16.07±0.01	22.92±0.03
10	Comp 5j	53.25±1.33	68.68±0.02
11	Comp 5k	61.25±0.93	85.15±0.05
12	Comp 5l	4.28±0.1	91.18±0.01
13	Comp 5m	48.256±1.55	90.65±0.04
14	Comp 5n	72.05±2.33	106.53±0.01
15	Comp 5o	39.56±1.56	123.56±0.08
16	Comp 5p	43.25±0.23	110.56±0.04
17	Comp 5q	10.92±0.03	77.61±0.01
18	Comp 5r	16.4±0.01	75.36±0.01
19	Comp 5s	65.32±0.63	98.25±0.07
20	Comp 5t	69.53±1.24	130.56±0.09
21	Comp 5u	86.32±1.45	82.6±0.1
22	Comp 5v	78.56±0.95	58.98±0.2
23	Comp 5w	54.35±0.68	118.36±0.06
24	Comp 5x	97.65±0.89	168.52±0.07
25	Comp 5y	68.65±1.36	145.65±0.04
26	Comp 5z	71.85±1.65	110±0.02

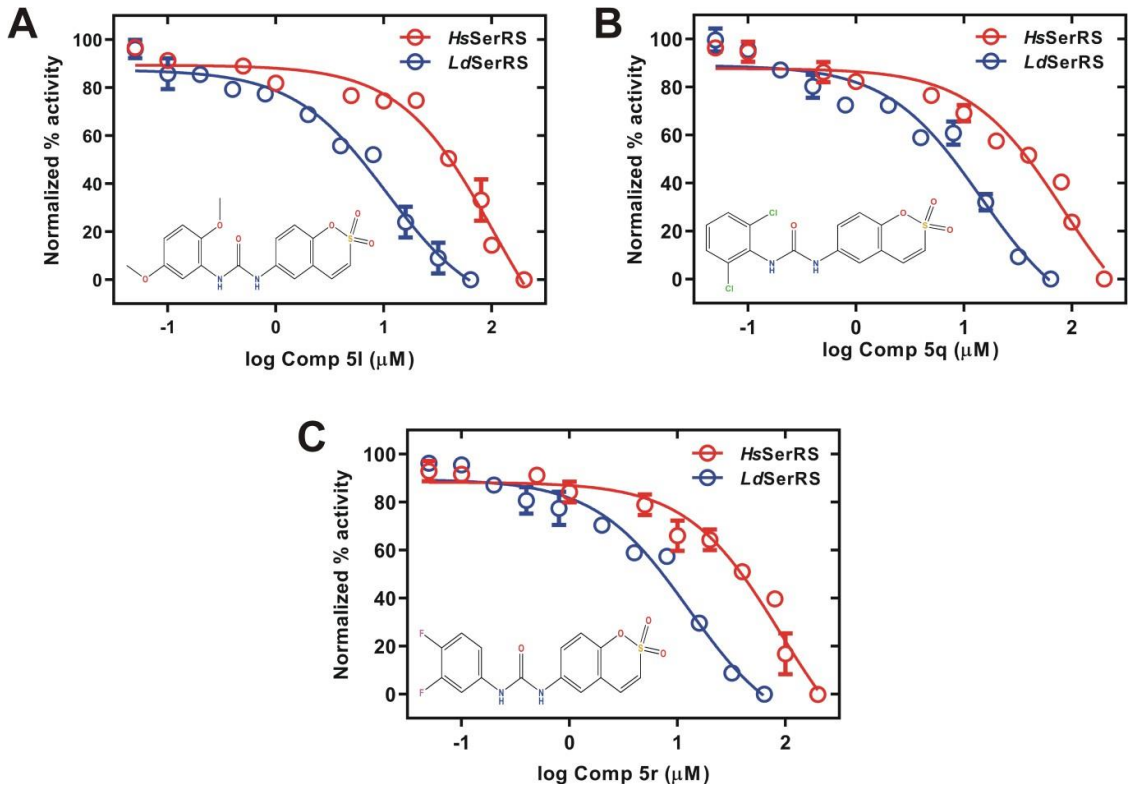

Figure 22: Inhibition assays of leishmanial and human SerRSs. Comparative inhibition of *Ld*SerRS and *Hs*SerRS with increasing concentration of synthesized molecules Comp 5l (A), 5q (B) and 5r (C).

In addition, binding studies with the Comp 5l illustrated a concentration (0 to 200 µM) based decrease in the fluorescence intensity of *Ld*SerRS **(Fig. 23A**) and *Hs*SerRS **(Fig. 23C)** suggesting towards the interaction of the inhibitor with the purified proteins. The respective binding constant (K_b) of Comp 5l for *Ld*SerRS and *Hs*SerRS were computed as 6.16×10^{-4} **(Fig. 23B)** and 3.13×10^{-4} M^{-1} **(Fig. 23D**), while the number of binding sites was found to be one for both leishmanial and human SerRS.

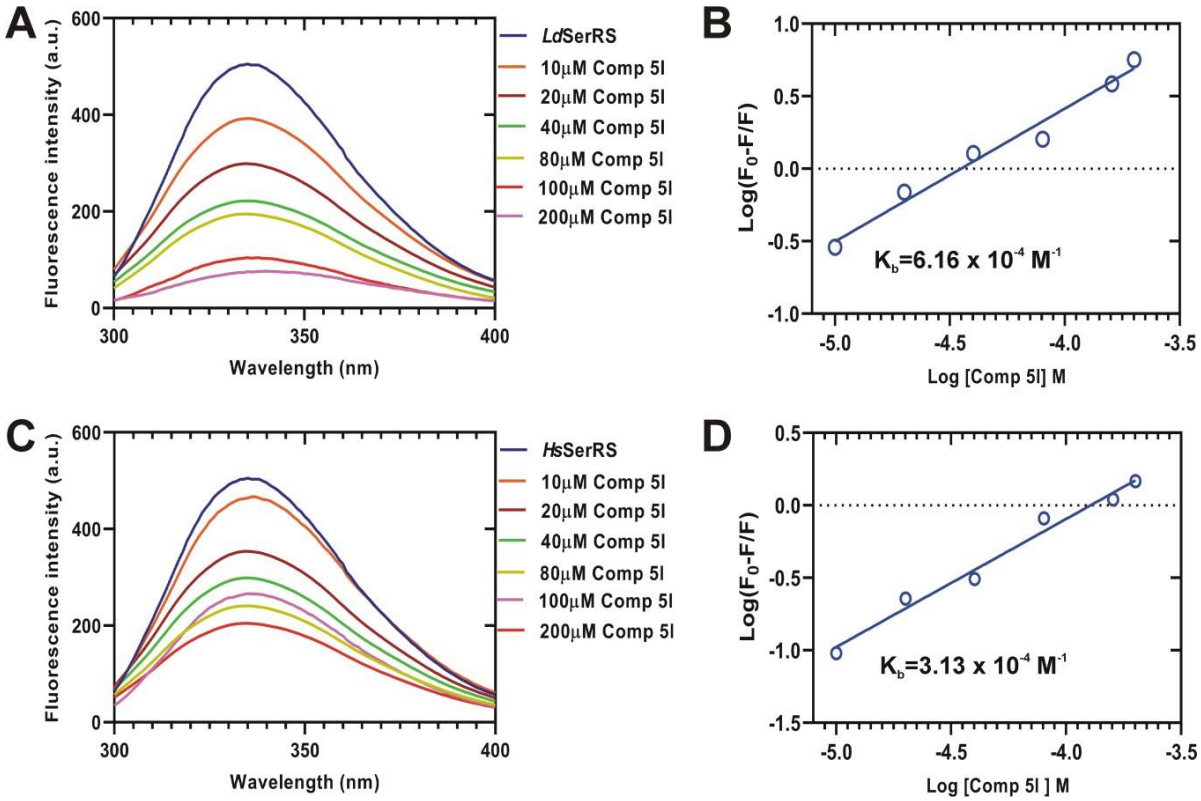

Figure 23: Binding of *Ld*SerRS and *Hs*SerRS with lead molecule. Intrinsic fluorescence emission spectra displaying decrease in fluorescence intensity of *Ld*SerRS (A) and *Hs*SerRS (C) with increasing concentrations of Comp 5l. Modified Stern-Volmer plots of *Ld*SerRS (B) and *Hs*SerRS (D) with Comp 5l.

Inhibition kinetics conducted with these compounds illustrated that mode of inhibition of Comp 5l is competitive with respect to cofactor ATP as there was no change in V_{max} with an increase in K_m **(Fig. 24A),** whereas Comp 5q and 5r were found to be uncompetitive with decrease in both V_{max} and K_m **(Fig. 24C, 6E).** The inhibition constant (K_i) of Comp 5l, 5q and 5r for *Ld*SerRS was computed as 3.2±0.04 **(Fig. 24B),** 31.9±0.02 **(Fig. 24D)** and 19.1±0.04 μM **(Fig. 24F),** respectively.

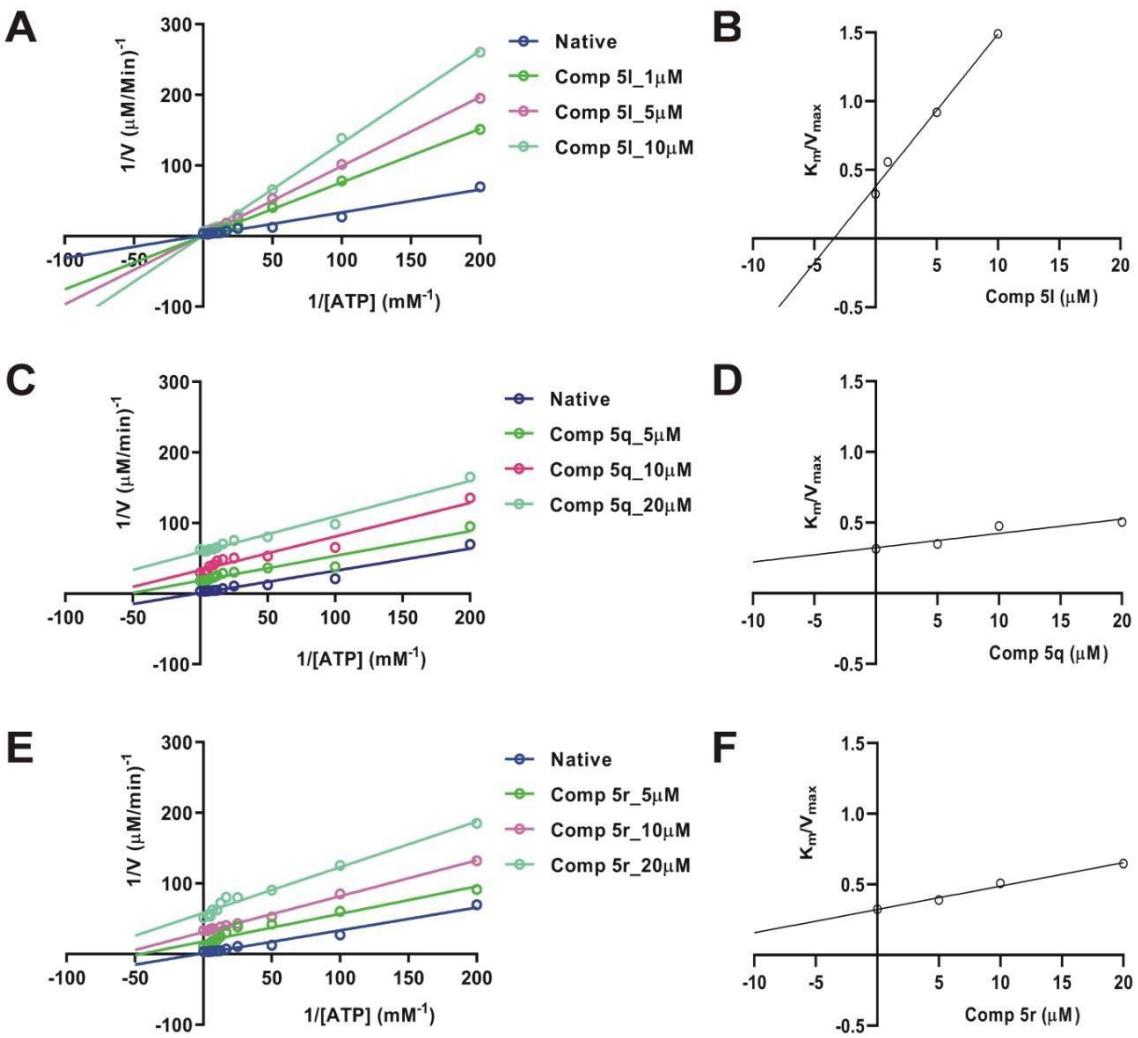

Figure 24: Inhibition kinetics of *Ld*SerRS with hit compounds. Double reciprocal plot of *Ld*SerRS with identified hit compounds exhibiting competitive mode of inhibition with Comp 5l (A) and uncompetitive inhibition in the presence of Comp 5q (C) and 5r (E). Inhibitory constant (K_i) plots of Comp 5l (B), 5q (D) and 5r (F) towards *Ld*SerRS.

The corresponding IC_{50} of Comp 5l towards mutants R295K, R295A, E297D and E297A was enumerated to be 18.23±0.1, 14.61±0.2, 25.65±0.3 and 28.96±0.1 μM, which were higher in comparison to that of native *Ld*SerRS (4.28±0.1 μM). Subsequently, inhibition kinetics using Comp 5l performed against mutant proteins of *Ld*SerRS depicted mode of inhibition to be non-competitive for R295K, R295A, E297D **(Fig. 25A, 25C and 25E**) and un-competitive for E297A **(Fig. 25G)** with respect to ATP. Subsequently, the respective K_i of Comp 5l against mutants R295K, R295A, E297D and E297A (**Fig. 25B, 25D, 25F and 25H**) was found to be 5.4±0.08, 6.4±0.09, 4.8±0.06 and 11.2±0.04 μM. The change in the mode of inhibition and an increase in K_i value after the mutation established that residues R295 and E297 play a crucial

role in the binding of hit compound (Comp 5l) and are also part of the cofactor binding pocket.

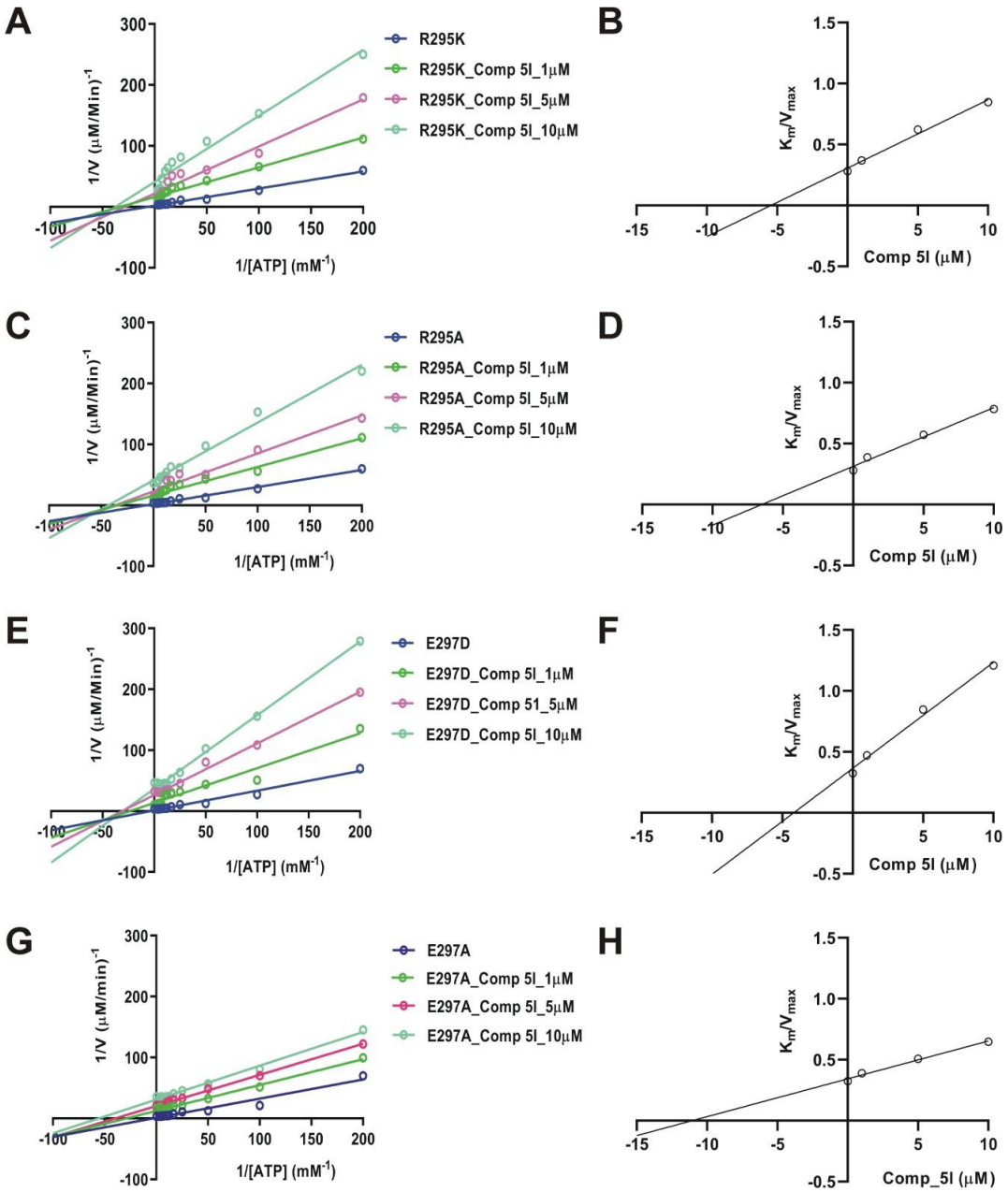

Figure 25: Inhibition kinetics of *Ld*SerRS mutants. Lineweaver–Burk plots demonstrating non-competitive mode of inhibition for R295K (A), R295A (C) and E297D (E) with Comp 5l, while E297A illustrates uncompetitive mode (G). Determination of K_i for Comp 5l towards R295K (B), R295A (D), E297D (F) and E297A (H) mutants.

Further, Comp 5l was found to possess the druglikeness as it follow the Lipinski's rule including corresponding molecular weight, Log P and Log S of 376.38 Da, 2.75 and -3.44

(Table 5). Simultaneously, it also exhibited very low toxicity against murine macrophages RAW264.7 cells during MTT assay.

Table 5: SwissADME properties of identified compound (Comp 5l)

Compound	M. W. (g/mol)	Log P	Log S	Pharmacokinetics	Druglikeness	Cytotoxicity (µM)
Comp 5l	376.38	2.75	-3.44	High	Yes	197±3.5

4.1.4 Inhibition studies of *Ld*GluRS

The half maximal inhibition concentration (IC_{50}) of salicylate and pCMB against *Ld*GluRS were found to be 236.7±0.24 **(Fig. 26A)** and 208.2±0.18 µM **(Fig. 26B)**, suggesting that pCMB inhibits activity of protein by 1.17 fold more than the salicylate. Inhibition kinetics with salicylate demonstrated the mode of inhibition as competitive and non-competitive in regard to its substrate (L-Glu) **(Fig. 27A)** and cofactor (ATP) **(Fig. 27C)**. Similarly, pCMB showed the modality to be uncompetitive towards L-Glu **(Fig. 27E)** and non-competitive for ATP **(Fig. 27G)**. The inhibition constant (K_i) of salicylate for substrate and cofactor were deduced to be 0.19±0.05 and 0.26±0.06 mM, respectively **(Fig. 27B, D)**. While the corresponding K_i for pCMB was estimated to be 0.21±0.09 and 0.19±0.06 mM towards substrate and cofactor **(Fig. 27F, H)**. The respective IC_{50} of salicylate with H60R and H60A mutants were computed to be 175.3±1.12 and 187.5±0.45, while corresponding values were 171±0.35 and 197±0.65 mM for pCMB. Notably, both mutant proteins have shown lesser IC_{50} values in comparison to the wild *Ld*GluRS.

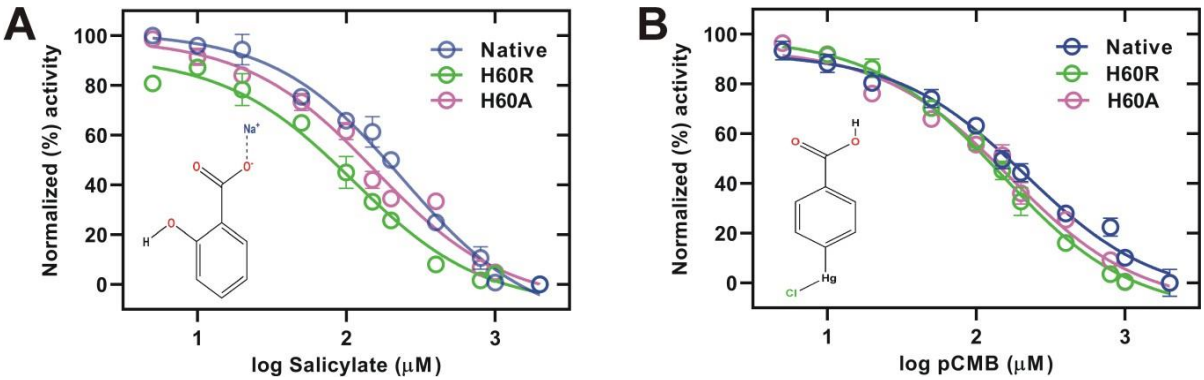

Figure 26: Inhibition studies of *Ld*GluRS. Comparative inhibition analysis of *Ld*GluRS and its mutants with the increasing concentration of salicylate (A) and pCMB (B).

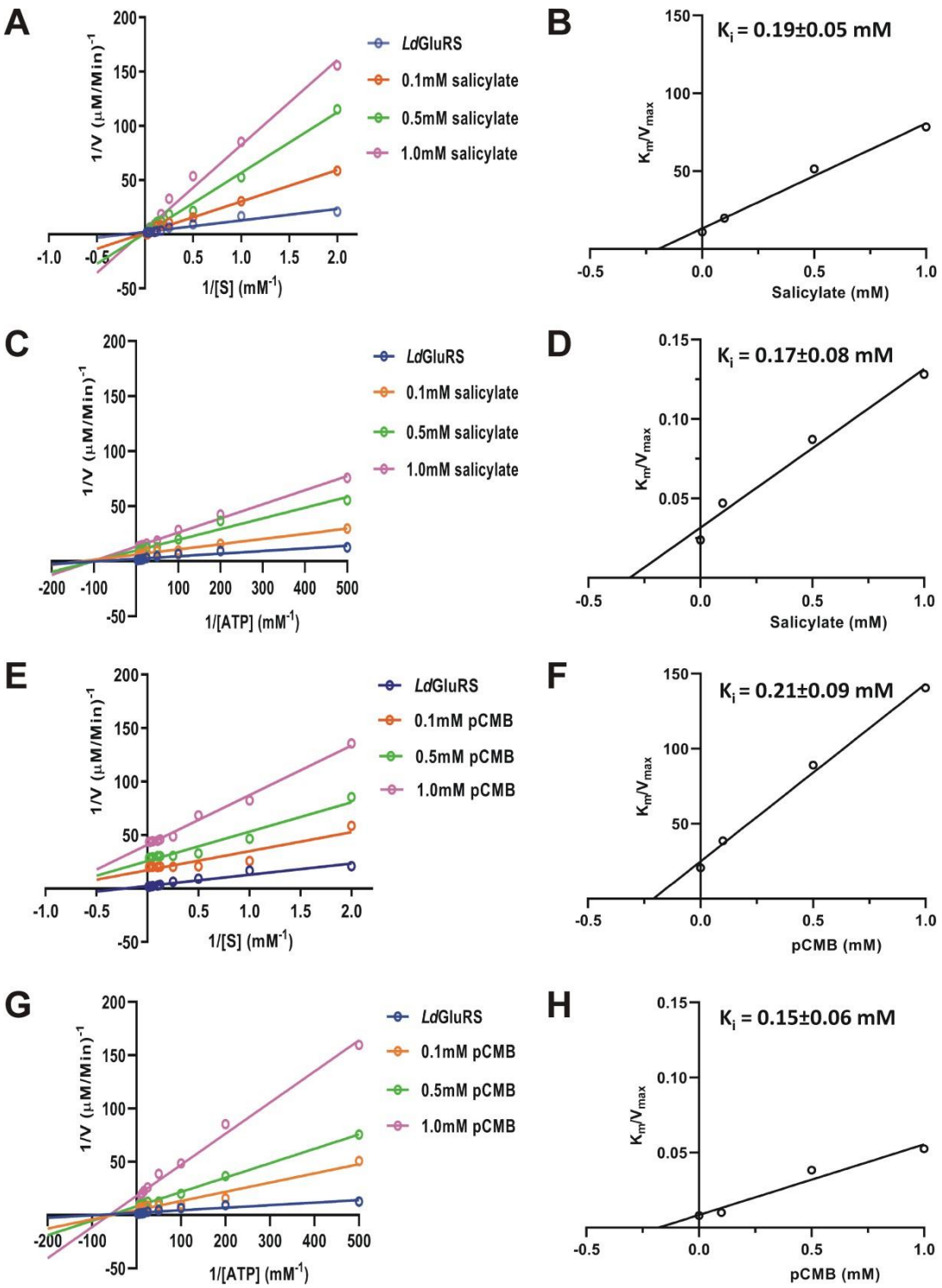

Figure 27: Inhibition kinetics of *Ld*GluRS with salicylate and pCMB. Double reciprocal plot of *Ld*GluRS displaying salicylate as competitive inhibitor for substrate (A) and non-competitive towards ATP (C), whereas pCMB delineates respective uncompetitive and non-competitive mode of inhibition towards L-Glu (E) and ATP (G). Plots of Inhibitory constant (K_i) for salicylate (B and D) and pCMB (F and H) for *Ld*GluRS.

Additionally, salicylate obeyed Lipinski's rule and exhibited drug-likeness with respective molecular weight, log P and log S of 137.11 g/mol, 1.13 and -2.49 **(Table 6)**. Moreover, it did not depict cell toxicity towards murine macrophages at the high concentration i.e. 14.7±1.4 mM.

Table 6: SwissADME properties and cell toxicity of salicylate

Compound	**M. W. (g/mol)**	**Log P**	**Log S**	**Pharmacokinetics**	**Druglikeness**	**Cytotoxicity (mM)**
Salicylate	137.11	1.13	-2.49	High	Yes	14.7 ± 1.4

4.2 Discussion

The enzymatic activity of *Ld*SerRS and *Ld*GluRS were highest near physiological pH and temperature, which is in correlation with their counterparts of *E. coli* **[146, 147]** that presents the maximum activity close to the physiological conditions. Seryl and glutamyl tRNA synthetases are known as divalent metal-dependent enzymes and both proteins showed maximum activity when Mg^{2+} is present in reaction mixture. Magnesium has a role in the stable positioning of cofactor ATP through strengthening the electropositivity of α-phosphate, which has also been reported for aspartyl-tRNA synthetase from *S. cerevisiae* **[148].** The activity of *Ld*SerRS and *Ld*GluRS has been found to be higher with K^+ ion in comparison to Na^+ ion, which could be due to the formation of more ionic interactions by K^+ than Na^+ that might help in stabilization of protein structure. Similarly, isoleucine tRNA synthetase from baker's yeast had also shown the enhancement in its activity with potassium ions **[149]**. Interestingly, higher amount of metal ions (Mg^{2+} and K^+) showed inhibition of both proteins activity that corresponds to earlier report of isoleucine tRNA synthetase from *E. coli* **[150]** and baker's yeast **[149]**. The binding affinity of *Ld*SerRS for ATP was comparable to that of *S. cerevisiae* SerRS **[98]**, while it was lesser than SerRS of *E. coli* **[151]**. Similarly, *Ld*GluRS has presented a stronger affinity for ATP than L-glutamate that is similar to glutamyl tRNA synthetases from *P. falciparum* **[152]** and *M. tuberculosis* **[153],** while the reverse pattern of preference has been reported for *E. coli* GluRS **[154]**. The substitution of alanine at position R295 and E297of *Ld*SerRS and H60 of *Ld*GluRS had deleterious impact on the steady state kinetics parameters with respect to ATP, suggesting the role of charged residues for ATP binding in two purified enzymes. Yeast seryl-tRNA synthetase had also unravelled the importance of charged residues in the cofactor binding [**98**].

Several heterocyclic molecules are explored as inhibitors against various tRNA synthetases such as prolyl tRNA synthetase of C. *albicans* **[155]**, methionyl tRNA synthetase of *Staphylococcus aureus* **[156]**, aspartyl and seryl tRNA synthetases of *E. coli* **[110]**. In our study, most of the ureidosulfocoumarin compounds had specificity towards *Ld*SerRS than *Hs*SerRS due to the different interactions formed with the 6 carbon ring that is linked to the coumarin moiety via urea and this ring interacts distinctly to *Ld*SerRS when compared to *Hs*SerRS. Comp 5l, 5q and 5r had high inhibitory effect towards *Ld*SerRS due to presence of corresponding oxygen, chlorine and fluorine for interaction with 6th carbon. Also, pivotal amino acid alterations have been observed within 6Å of the ATP binding site of leishmanial SerRS and its human counterpart as *Ld*SerRS comprised Ala267, Asp315, Leu317, and Tyr370, while human equivalent possessed Gln274, Glu322, Ile324 and Leu377 at

corresponding position. Similar aspect has also been reported recently for 6-phosphogluconate dehydrogenase of *L. donovani*, where two antibiotics (cefuroxime and gentamicin) exhibited more inhibition towards the parasitic protein as compared to its human equivalent **[142]**. Another study also displayed quinoline-carbaldehyde inhibitors (HQ14 and HQ15) showing higher inhibition towards *L. donovani* methionine aminopeptidase 1 than its human counterpart due to differences near the catalytic site **[157]**. Additionally, all mutant forms of *Ld*SerRS displayed less inhibition by Comp 5l depicting towards the importance of Arg295 and Glu297 residues which are also involved in ATP binding that is conserved throughout the prokaryotic and eukaryotic parasites. Moreover, *in vitro* implementation of amino acids into the protein of rat costal cartilage was demonstrated to be inhibited by salicylate at large concentrations (10–15 mM) **[158]**. Notably, salicylate is known to demonstrate a straightforward competitive inhibition with respect to the amino acid, and the most susceptible aaRSs are those that introduce histidine, aspartate, and glutamate **[159]**. The enzymatic activity of *Ld*GluRS is competitively inhibited by salicylate at very low concentration that is also evident from earlier report which has depicted the competitive inhibition of GluRS in regard to substrate and non-competitive for ATP **[159]**. As observed in purified GluRS from rat liver **[160]**, pCMB also inhibited *Ld*GluRS and showed more potency than salicylate but it was not competitive towards either L-Glu or ATP.

Chapter-III

5. Structural characterization of leishmanial seryl and glutamyl tRNA synthetases

5.1 Result

5.1.1 Secondary structural analysis of *Ld*SerRS and *Ld*GluRS

Secondary structural content of native and mutant forms of *Ld*SerRS was determined by CD spectroscopy. The Far-UV CD spectra of *Ld*SerRS exhibited negative peaks at 222 and 208 nm and a positive peak at 195 nm, demonstrating adequate secondary structural elements **(Fig. 28A).** Subsequently, analysis of data with DichroWeb server suggested α-helical content as 38% and β-sheet of 18% at pH 7.5. Simultaneously, the mutants R295K, R295A, E297D and E297A also showed spectrum similar to that of wild type with 36%, 41%, 38% and 37% α-helices and 17%, 16%, 18% and 17% β-sheets, respectively **(Fig. 28B, Table 7**) that explicitly display no significant deviation in secondary structure after mutation. Additionally, there were negligible changes in the secondary structure content in the presence of ligands (such as ATP, L-Ser or both) for *Ld*SerRS (**Fig. 28C, Table 8**). Likewise, mutant proteins R295K, R295A, E297D and E297A had also not shown major deviation in the CD spectra with the ligands, highlighting no alterations in the secondary structural elements.

Table 7: Secondary structural contents of wild and mutant type of *Ld*SerRS

Protein	**α-helices**	**β-sheets**	**Coils**
*Ld*SerRS (WT)	38	18	44
R295K mutant	36	17	47
R295A mutant	41	16	43
E297D mutant	38	18	44
E297A mutant	37	17	46

Table 8: Secondary structural contents of *Ld*SerRS in the presence of ligands

Protein	**α-helices**	**β-sheets**	**Coils**
*Ld*SerRS (Apo)	38	18	44
*Ld*SerRS-Serine	33	19	48
*Ld*SerRS-ATP	36	17	47
*Ld*SerRS-Ser-ATP	32	16	52

Further, secondary structure of *Ld*SerRS had shown changes in α-helix and β-sheet contents with pH varying from 3.5 to 9.5. The maximum structural integrity was observed at pH 8.5, while there was loss in α-helical content at acidic condition **(Fig. 28D, Table 9**). The thermal denaturation curve of *Ld*SerRS depicted a folded state up to 38ºC followed by transition stage

between 42 to 50ºC, while the unfolding state was detected from 50 to 90ºC (**Fig. 28E**). The melting temperature (T_m) for native *Ld*SerRS was found to be 41.8±0.2ºC, whereas it was 42.3±0.9, 45.1±0.8, 46.4±0.6 and 41.5±0.3ºC for R295K, R295A, E297D and E297A mutants, respectively **(Fig. 28F).** Simultaneously, alterations in secondary structure of native *Ld*SerRS in the presence of urea showed gradual decrease in ellipticity upon increasing concentration of denaturant from 1 to 8 M (**Fig. 28G).** The normalized denaturant curve of *Ld*SerRS exhibited corresponding folded, transition and unfolded regions at 0-1, 1-5 and 5-8 M concentrations of urea with the transition mid-concentration of urea (C_m) as 2.6±0.3 M **(Fig. 28H**), indicating moderate tolerance towards urea.

Table 9: Secondary structural contents of *Ld*SerRS with varying pH

Secondary structure	**pH 3.5**	**pH 4.5**	**pH 5.5**	**pH 6.5**	**pH 7.5**	**pH 8.5**	**pH 9.5**
α-helices	22	26	27	30	38	42	36
β-sheets	21	20	18	15	18	22	15
Random coils	57	54	55	55	44	36	49

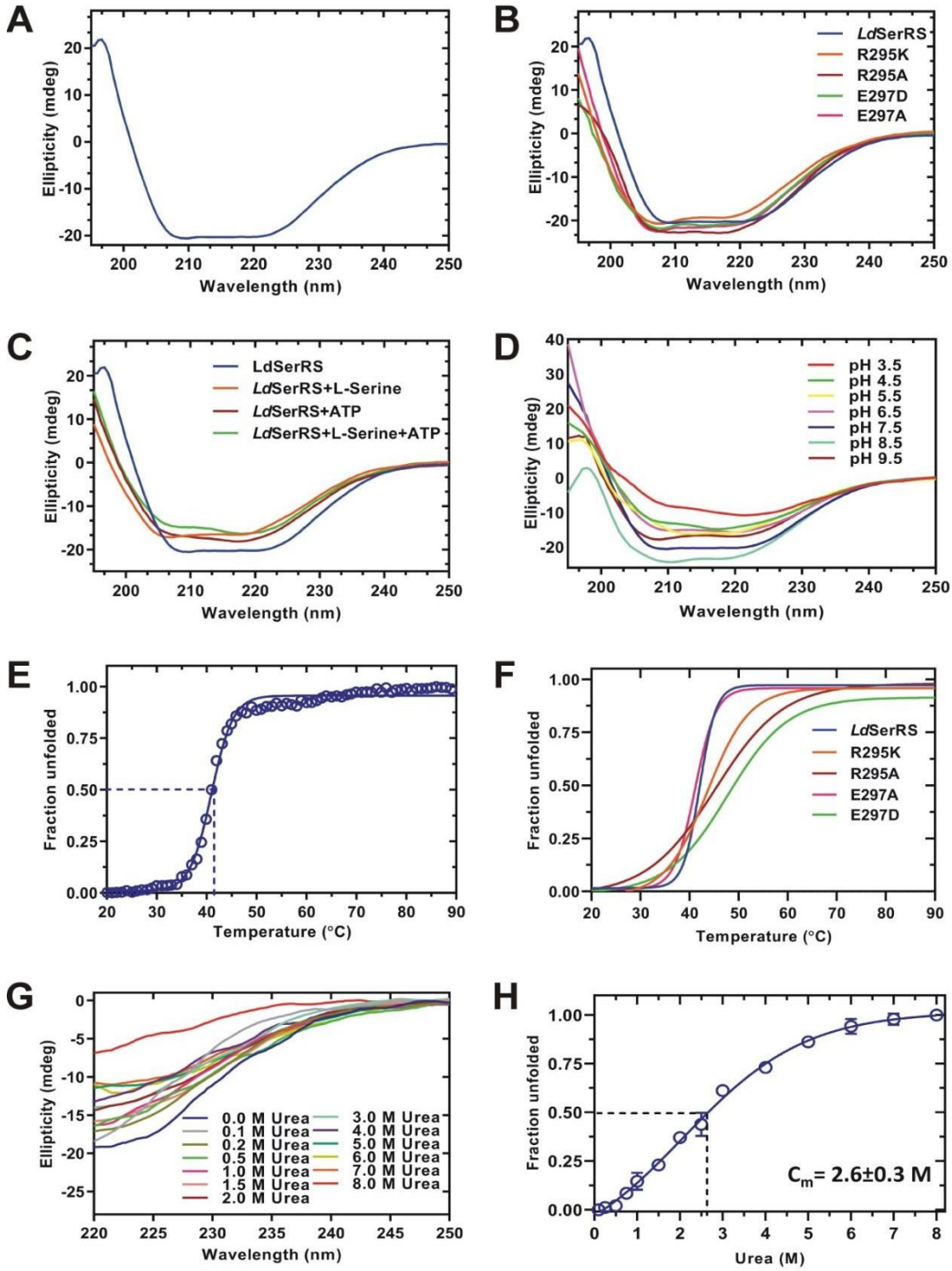

Figure 28: Secondary structure analysis of *Ld*SerRS. (A) CD spectra of purified *Ld*SerRS from 250-195 nm in 10 mM HEPES pH 7.5. (B) Comparison of far-UV CD spectra of *Ld*SerRS and its mutants (R295K, R295A, E297D and E297A). (C) Secondary structure spectra of *Ld*SerRS in the presence of ligands (L-Ser, ATP and L-Ser+ATP). (D) Effect of pH on the CD spectra of *Ld*SerRS. (E-F) Normalized thermal stability graph of *Ld*SerRS and its mutants (R295K, R295A, E297D and E297A). (G) Far-UV CD spectrum of *Ld*SerRS with urea from 0-8 M. (H) Plot of urea concentration versus fraction unfolded showing C_m with respect to urea.

The secondary structural elements of *Ld*GluRS in its native and mutant forms were deduced by CD spectroscopy. A positive peak at 195 nm and two negative peaks positioning at 222 and 208 nm were visible in the far-UV CD spectra of *Ld*GluRS, indicating that it possesses adequate secondary structural content **(Fig. 29A)**. Afterward, data analysis using the DichroWeb server indicated the α-helical content as 43%, β-sheets as 12% and the random coil as 45% at pH 7.5. In addition, the spectra of the mutants H60R and H60A were also comparable to that of the wild type with corresponding 44% and 42% α-helices along with 12% β-sheets for each mutant that clearly demonstrated negligible variations in the secondary structural features in mutated forms **(Fig. 29B, Table 10)**. Moreover, there were unnoticeable differences in the secondary structure elements of native *Ld*GluRS along with ligands (such as ATP, L-glutamate, or both) **(Fig. 29C, Table 11)**. The CD spectra of the mutant proteins (H60R and H60A) also did not exhibit significant alteration with the ligands. Besides that, modification in the components of α- helices and β-sheets in the secondary structure of *Ld*GluRS was observed with pH ranging from 3.5 to 9.5. The optimum structural integrity was seen at pH 7.5, while an acidic condition (pH 3.5 to 6.5) contributed in loss of α-helical content **(Fig. 29D, Table 12)**. Thermal denaturation curve revealed properly folded protein up to 39ºC followed by a transition stage between 42 and 50ºC and finally unfolding condition between 50ºC and 90ºC **(Fig. 29E)**. Notably, native *Ld*GluRS has a melting temperature (T_m) of 44±0.3ºC **(Fig. 29F)**, whereas corresponding T_m for mutants H60R and H60A was 41±0.1 and 40±0.6ºC. Furthermore, deviations in the secondary structure of native *Ld*GluRS with denaturant represented a steady loss of ellipticity as the amount of the urea was increased from 1 to 8 M **(Fig. 29G)**. The normalised denaturant curve of *Ld*GluRS showed folded, transition, and unfolded areas at 0-1, 1-5, and 5-8 M of urea concentration, respectively, with the mid-transition concentration (C_m) of urea as 2.81±0.07 M demonstrating a mild tolerance of the protein to urea **(Fig. 29H)**.

Table 10: Secondary structural elements of wild and mutant type of *Ld*GluRS

Protein	α-helices	β-sheets	Coils
*Ld*GluRS (WT)	43	12	45
H60R	44	12	47
H60A	42	12	43

Table 11: Secondary structure contents of *Ld*GluRS and its mutants in the presence of ligands

Protein	**L-glutamate**			**ATP**			**L-glutamate + ATP**		
	α	β	Coil	α	β	Coil	α	β	Coil
***Ld*GluRS**	45	11	44	44	12	44	40	14	46
H60R	43	11	46	43	12	45	39	14	47
H60A	42	12	46	42	12	46	40	15	45

Table 12: Secondary structural contents of *Ld*GluRS with varying pH

Secondary structure	**pH 3.5**	**pH 4.5**	**pH 5.5**	**pH 6.5**	**pH 7.5**	**pH 8.5**	**pH 9.5**
α-helices	20	28	25	30	43	36	34
β-sheets	28	26	24	18	12	18	15
Random coils	52	46	51	52	45	46	51

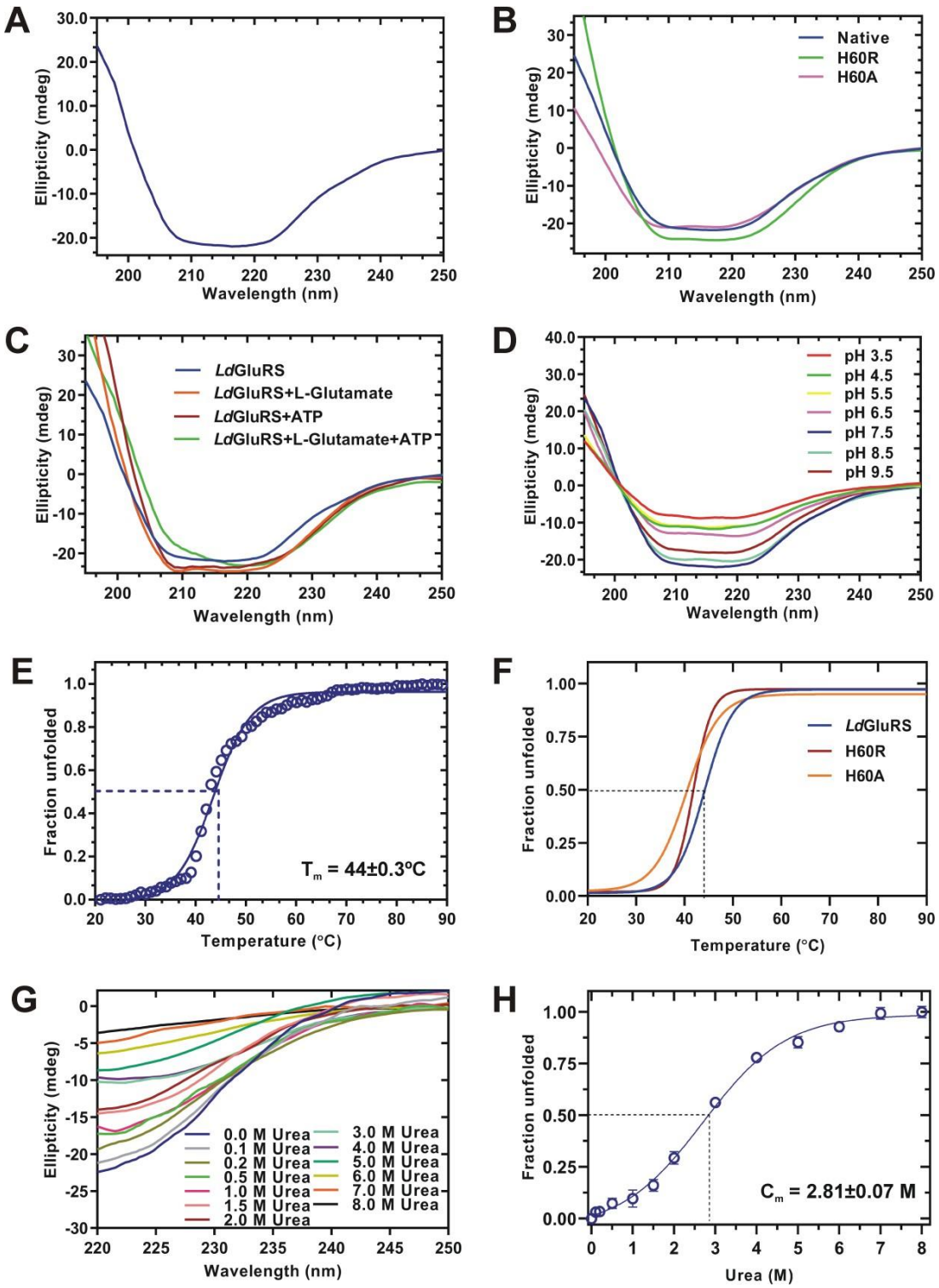

Figure 29: Analysis of secondary structure of *Ld*GluRS. (A) Far-UV CD spectrum of purified *Ld*GluRS from 250 to 195 nm at pH 7.5. (B) Secondary structural spectra of *Ld*GluRS and its mutants (H60R and H60A). (C) CD spectra of *Ld*GluRS with L-glutamate, ATP and L-glutamate + ATP. (D-E) CD spectra of *Ld*GluRS with varying pH and temperature. (F) Comparative plots of thermal stability for *Ld*GluRS and its mutants (H60R and H60A). (G) CD spectra of *Ld*GluRS in presence of different conc. of urea and (H) the enumeration of mid-transition concentration (C_m) of urea.

5.1.2 Structure of *Ld*SerRS and its complexes

The modelled *Ld*SerRS structure analysed by Ramachandran plot deciphered 93.4% of residues in most favoured, 6.3% residues in additional allowed, 0.2% residues in generously allowed and no residues in disallowed region. The ERRAT value of the final structure was observed to be 98.2 that indicate the appropriately organized non-bonded atomic coordination in *Ld*SerRS structure. Additionally, Verify3D server displayed 94.73% agreeableness between its primary sequences (1D) and atomic model (3D) with an average 3D-1D score of ≥ 0.2. Three-dimensional structure of *Ld*SerRS is organized into two domains i.e. N-terminal coiled-coil tRNA binding domain (1-135 residues) and C-terminal globular catalytic core domain (136-474 residues) (**Fig. 30A**). The N-terminal domain comprises six α-helices wherein α3 and α6 form coiled-coil that is involved in the recognition of the cognate tRNA. While, the catalytic core domain (CCD) consists of 12 α-helices and 12 β-sheets and its architecture aligned with a conserved antiparallel β-sheet that are surrounded with α-helices to form the active site, which is a common characteristic feature found in all class II aaRSs. The motifs-II and III are situated in this domain possessing critical residues that interact with substrate and cofactor.

The molecular docking studies revealed that binding affinity of cofactor (ATP, -8.4 kcal/mol) towards *Ld*SerRS was higher than that of substrate (L-Ser, -5.2 kcal/mol), which has also been seen in the *in vitro* kinetic studies performed by us. Further, separate binding pockets were observed for substrate and cofactor that are situated adjacent to each other. The molecular interaction analysis of L-Ser with *Ld*SerRS had shown that it forms four polar contacts with Glu316, Glu318, Asn423 and Thr425 **(Fig. 30B**) and two hydrophobic interactions with Ser387 and Gly424 (**Fig. 31A**). The epsilon oxygen (-OE2) of Glu316, Glu318 and gamma oxygen (-OG1) of Thr425 formed hydrogen bonds with gamma oxygen (-OG) of L-serine, similarly delta oxygen of Asn423 interacted with nitrogen atom of substrate. The *Ld*SerRS-ATP complex displayed hydrogen bonds along with hydrophobic linkages between cofactor and residues of the protein. Among these interacting residues, Arg295, Glu297, Phe309, Arg310, and Phe314 were present in the motif-II, while Val311, Lys316, Lys369, Glu284, Leu385, Val386 and Ser387 were located between motif-II and III, and the residues Thr425, Ala428, Thr430 and Arg431 were from motif-III. Further analysis illustrated that -NH1 of Arg295 interacts with -O5 of alpha and -O3A of beta phosphate of ATP, whereas -OE1 of Glu297 forms H-bond with N6 of adenine ring portion of ATP. Likewise, nitrogen (-N) and oxygen (-O) of Val311 correspondingly interacted with N1 and N6 of adenine ring, while zeta nitrogen (-NZ) of Lys369 formed hydrogen bonds with O2G and O1G of gamma phosphate

(**Fig. 30C**). Notably, Glu284, Leu385, Val386, Ser387, Phe309, Arg310, Phe314, Lys316, Thr425, Ala428, Thr430 and Arg431 exhibited hydrophobic interactions with cofactor (**Fig. 31B).**

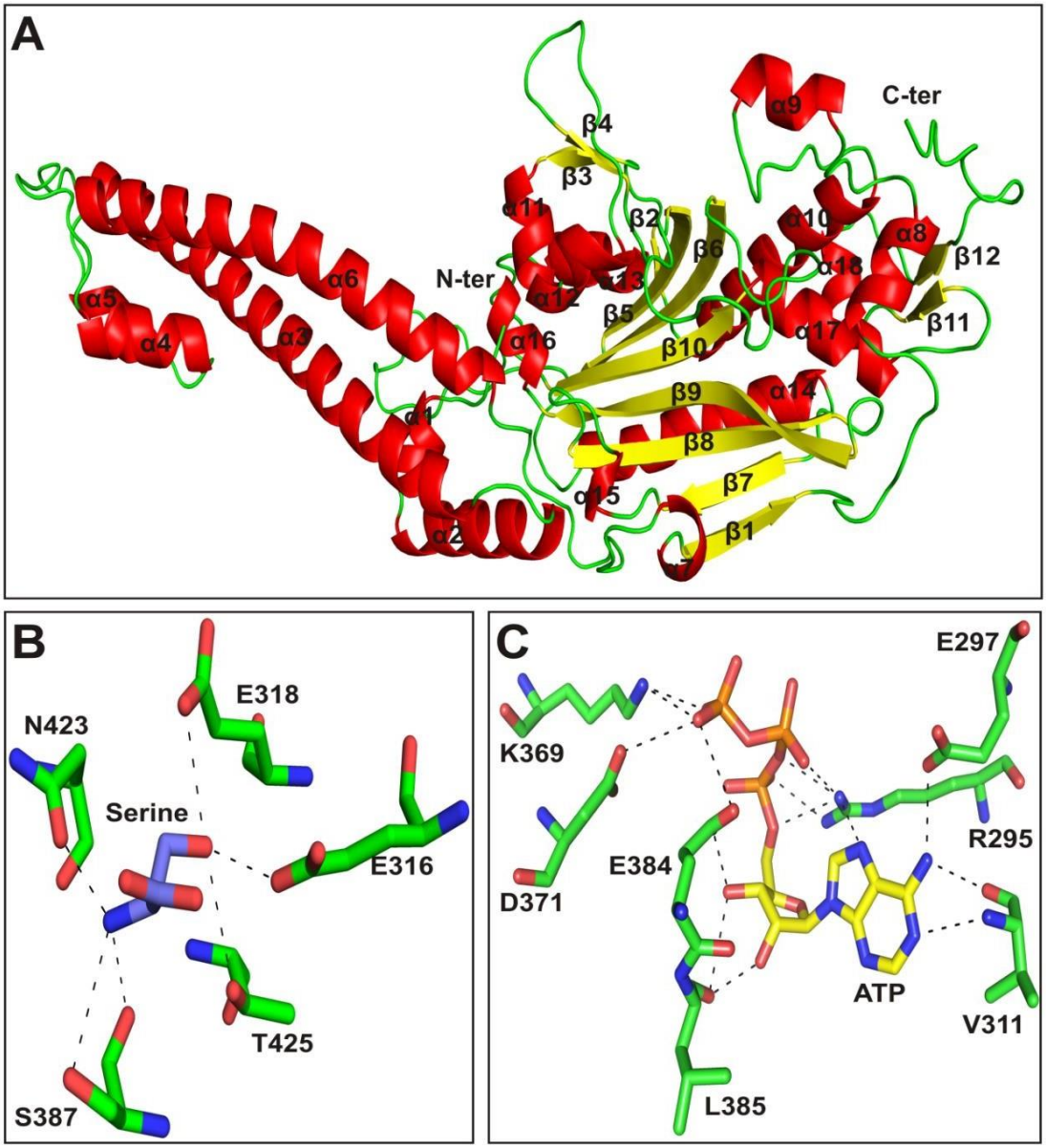

Figure 30: Three-dimensional structure of *Ld*SerRS. (A) Three-dimensional structure of *Ld*SerRS is presented in cartoon form and the secondary structural elements α-helices, β-strands and random coils are represented in red, yellow and green colour, respectively. AutoDock Vina was used to generate the docked complexes of *Ld*SerRS with substrate L-Ser (B) and cofactor ATP (C). Residues interacting with the ligands are displayed as sticks, while polar contacts are shown as dash lines.

In silico docking studies of ureidosulfocoumarin Comp 5l with *Ld*SerRS and *Hs*SerRS unravelled its binding affinity as -7.3 and -6.2 kcal/mol, respectively. The binding affinity of ATP and Comp 5l towards *Ld*SerRS was found to be higher than the substrate. Comp 5l was

positioned at the ATP binding site and interaction analysis showed that –NH1 of Arg295 form hydrogen bond with urea carboxylic group of coumarin moiety, and zeta nitrogen atom (-NZ) of Lys369 interact with oxygen at the C2 positions of the six carbon ring side of Comp 5l. Similarly, nitrogen (-N) of Val311 and epsilon nitrogen of Arg431 formed H-bonds with sulphur containing oxygen of Comp 5l. Further, Glu266, Glu297, Phe309, Arg310, Phe314, Glu384, Ser387 and Ala428 showed hydrophobic interaction with Comp 5l (**Fig. 31C).** Simultaneously, in *Hs*SerRS-Comp 5l complex, Arg295, Glu384, Ser387, and Thr430 were involved via the formation of H-bonds with inhibitor. The –NH2 of Arg295 was connected through hydrogen bond with oxygen at C5 side chain ring of Comp 5l. While, gamma oxygen (-OG) of Ser387 interacted with C2 side chain oxygen of Comp 5l and epsilon oxygen (-OE2) of Glu384 connected to Comp 5l through two H-bonds with two nitrogen atoms of urea moiety of Comp 5l. Glu266, Ile308, Phe309, Arg310, Val311, Phe314, Lys369, Leu385, Ala428 and Arg431 participated in hydrophobic interactions with Comp 5l (**Fig. 31D**).

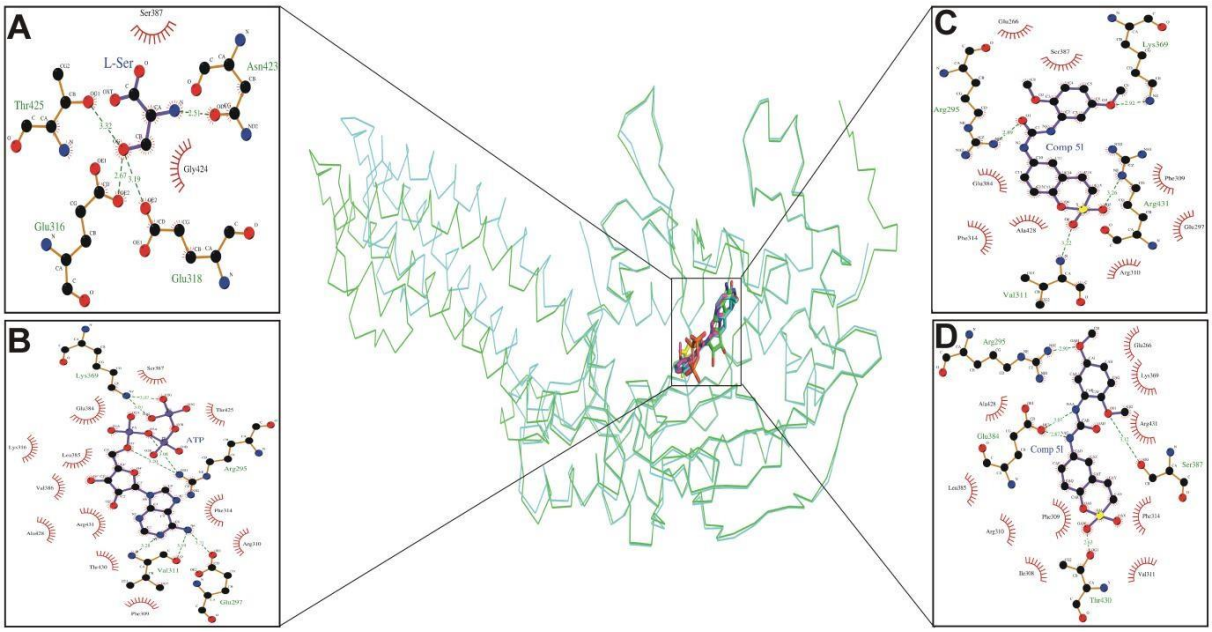

Figure 31: Interaction analysis of ligands bound *Ld*SerRS and *Hs*SerRS: The ligands bound *Ld*SerRS and *Hs*SerRS were superimposed and represented in ribbon form with green and cyan, respectively. The ligands such as L-Ser, ATP and Comp 5l docked with *Ld*SerRS are colored yellow, green and pink, respectively, while Comp 5l bound with *Hs*SerRS is shown in blue. The hydrogen bonds and hydrophobic interactions are presented through LigPlots for *Ld*SerRS bound with L-Ser (A), ATP (B) and Comp 5l (C) as well as *Hs*SerRS- Comp 5l (D).

5.1.3 *Ld*GluRS structure and its complexes

Due to presence of more than 38 and 48 residues in the disordered region corresponding to N and C-terminus of *Ld*GluRS, BLASTp search was unable to find the suitable structural template for these portions. Hence, the three-dimensional structure of truncated *Ld*GluRS (39-546 amino acids) was generated using template (PDB ID: 7WAI) that had 45.28% sequence identity and 86% query coverage with an e-value of $1e^{-148}$. The Ramachandran plot of modelled structure revealed that 92.3% of the residues were in the most favourable, 6.6% in additional allowed, 0.9% in generously allowed, and one residue (Asp495) in disallowed regions. The refinement using ModLoop had fixed the outlier residue and then no residue was in disallowed region **(Fig. 32B)**. The global quality of refined structure, evaluated using ProSA-web server, depicted Z-score as -9.46 advocating for a native protein structure of more than 500 residues towards x-ray crystallography **(Fig. 32C)**. Similarly, the local quality assessment of refined structure depicted average energy for majority of the amino acids of *Ld*GluRS fall below 0, whilst local regions scoring above 1 mostly belongs to the part of loops in *Ld*GluRS structure **(Fig. 32D)**. On superimposition with the template, energy minimized structure had shown a RMSD of 0.436 Å and presented all characteristic features of class-I tRNA synthetases i.e. N-terminal catalytic domain (CD) and C-terminal anticodon binding domain (ABD). The catalytic domain (48-352) folded predominantly into α/β structure possessing Rossmann fold with five parallel β-sheets surrounded by α-helices from both sides. The active site possessed residues responsible for binding with L-glutamate and ATP including the conserved ATP-binding motifs *viz.* HIGH (His60-Ile61-Gly62-His63) and VMSKR (Val282-Met283-Ser284-Lys285-Arg286). The C-terminal of *Ld*GluRS consisted anticodon binding domain (354-531) that participates in formation of proximal and distant β-sheet bundles **(Fig. 32A)**.

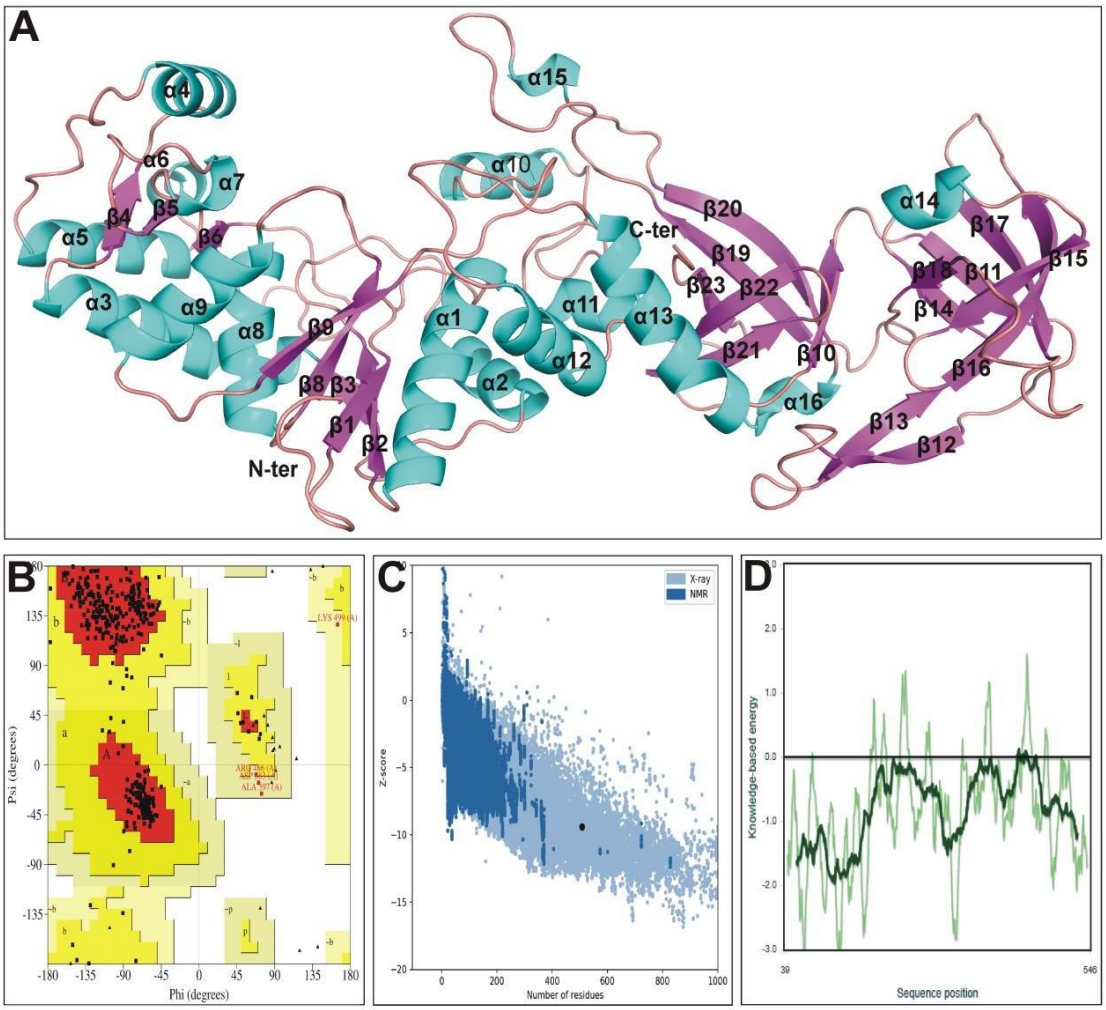

Figure 32: Structure of *Ld*GluRS and its validation. (A) Modelled three-dimensional structure of *Ld*GluRS after refinement, wherein alpha helices, beta strands and coils are labelled and correspondingly shown in cyan, pink and red colour. (B) Ramachandran plot, (C) ProSA overall model quality, and (D) ProSA local model quality of refined *Ld*GluRS structure.

The outcome of molecular docking implied that the binding affinity of cofactor (ATP, -5.3 kcal/mol) for *Ld*GluRS was more than that of the substrate (L-glutamate, -4.2 kcal/mol), which was also found in our kinetic investigations. Additionally, the interacting pockets for cofactor and substrate were observed to be adjacent to each other **(Fig. 33A)**. The complex of *Ld*GluRS-ATP presented nine hydrophobic interactions between ATP and Pro52, Pro53, His60, Gly62, Ala66, Arg245, Thr246, Phe273, and Arg275, whereas three hydrogen bonds with Glu54, His63 and Leu276. Subsequent analysis indicated that the nitrogen (-N) atom of Glu54 and the nitrogen (-NE2) of His63 form hydrogen bond with ATP at oxygen atom (-O1A) of alpha phosphate. Likewise, the oxygen (-O) atom of Leu276 formed a bond with the nitrogen (-N6) atom of adenine ring adenine ring of ATP **(Fig. 33B)**. *Ld*GluRS-substrate

docked structure revealed that L-Glu has nine interactions in which it formed hydrogen bonds with Arg50, Tyr227 and Arg252, while it made hydrophobic interactions with Pro52, Asp86, Cys231, Leu244, Arg245 and Thr246. Further, the hydrogen bond interactions divulged that the nitrogen (-NH2) atom of Arg50 and hydroxyl group (-OH) of Tyr227 interacted with oxygen (-OXT) of L-Glu, while nitrogen (-NH1) of Arg252 bonded to oxygen (-OE2) of L-Glu **(Fig. 33C)**. Similarly, *Ld*GluRS-salicylate complex has shown seven hydrophobic interactions in which Pro52, Asp86, Tyr227, Cys231, Leu244, Arg245 and Thr246 formed bonding with inhibitor, whereas the nitrogen (-NH2) atom of Arg50 made hydrogen bond with the oxygen (-O3) of salicylate **(Fig. 33D)**.

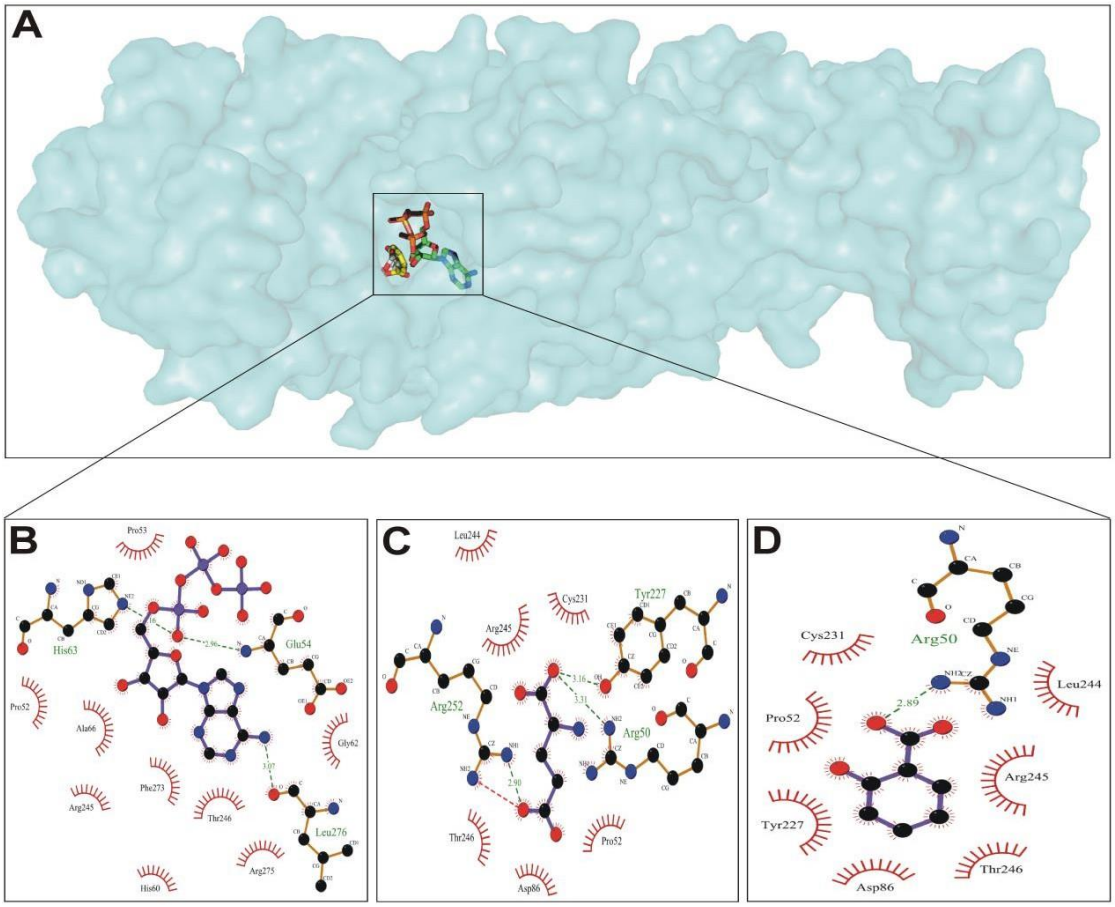

Figure 33: Molecular docking of *Ld*GluRS with ligands. (A) Docking of *Ld*GluRS was conducted with various ligands through AutoDock Vina, where substrate and cofactor binding sites are adjacent to each other. The protein is presented as cyan colored surface view, while cofactor, substrate and inhibitor are represented as green, white and yellow colored sticks, respectively. The hydrophobic and hydrogen interactions are exhibited using LigPlots for ATP (B), L-Glu (C) and salicylate (D) bound *Ld*GluRS.

5.1.4 Structural stability of proteins and their complexes

Molecular dynamics simulation (MDS) was run for apo *Ld*SerRS and its complexes with substrate, cofactor and inhibitor (Comp 5l) to evaluate the structural stability, flexibility and compactness of the systems. The RMSD of backbone was analysed throughout the MD run for apo and complex forms of *Ld*SerRS, which showed higher deviations in the initial duration from 0-40 ns after that it was steady for the rest of the time period advocating for stabilization of the systems. The RMSD profiles of apo as well as its ligand forms showed similar graphs during the simulation delineating a comparable stability in the presence of ligands **(Fig. 34A).** The Rg was plotted for backbone atoms with respect to time for all the systems that demonstrate the compactness of each system. From the duration 70 to 100 ns, the compactness of *Ld*SerRS was found to be high in the presence of ligands (ATP and Comp 5l) when compared to its apo system illustrating increase in compactness in the presence of these ligands (**Fig. 34B).** The RMSF profiles were evaluated to know the residue specific fluctuations during the progression of the simulation. Residues from motif-II (284-314) and motif-III (420-450) that play a major role in the ligand binding showed less fluctuations suggesting constrain in flexibility of residues due to the formation of bonds. However, higher fluctuations were observed at the residues (70-73 and 455-474) which are not involved in the interactions with the ligands (**Fig. 34C**).

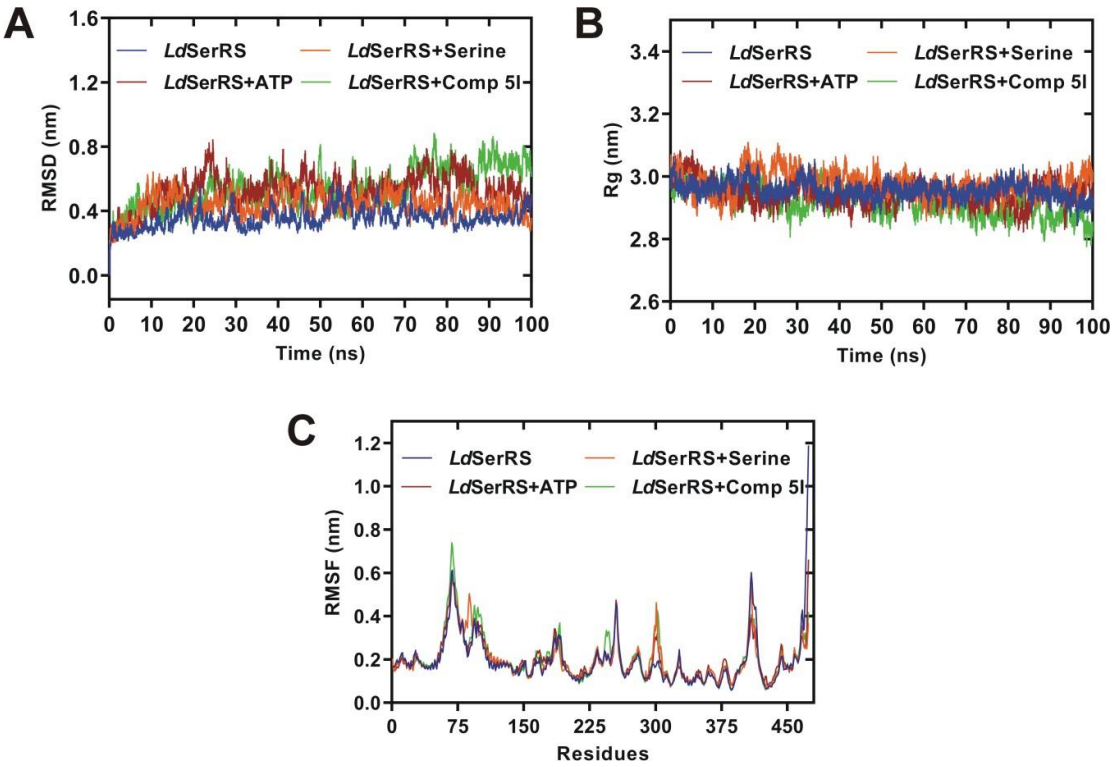

Figure 34: Molecular dynamic simulations of *Ld*SerRS and its complexes. Comparison of RMSD (A), Rg (B) and RMSF (C) of apo *Ld*SerRS and its complexes with substrate (L-Ser), cofactor (ATP) and inhibitor (Comp 5l).

MDS studies of four systems (*Ld*GluRS, *Ld*GluRS+ATP, *Ld*GluRS+L-Glu and *Ld*GluRS+salicylate) were performed for 50 ns to assess the stability, compactness and flexibility of the protein with/without ligands. The RMSD plots had shown deviation between 0-0.34 for *Ld*GluRS, while its complex forms with ATP, L-Glu and salicylate had deviations in the range of 0-0.28, 0-0.34 and 0-0.31 nm, respectively. The apo and its complex systems of ATP and salicylate had divergences from 0 to 15 ns afterwards steadiness was attained for the remaining period of MD run. The average RMSD for apo as well as complexes with ATP, L-Glu and salicylate was enumerated to be 0.31, 0.29, 0.31 and 0.30, respectively, suggesting minor increase in protein stability with ATP and salicylate as compared to its apo form **(Fig. 35A)**. However, the complex structure with L-Glu showed stability comparable to the apo form. The initial Rg value of all systems started at approximately 3.09 nm and reached around 3.2 nm at the end of simulation with an increase of about 0.11 nm. The respective computed average Rg for *Ld*GluRS, *Ld*GluRS+ATP, *Ld*GluRS+L-Glu and *Ld*GluRS+salicylate were 3.23, 3.21, 3.15 and 3.21 nm, illustrating that overall compactness of protein increased slightly with all the ligands **(Fig. 35B)**. The corresponding average RMSF values were calculated to be 0.15, 0.14, 0.15 and 0.13 nm, for apo and its complex forms (ATP, L-Glu and salicylate). The minor reduction in fluctuations was observed for systems with ATP and salicylate, while equal fluctuations were found in the presence of L-Glu. Interestingly, higher fluctuations were detected in the residues at N-terminus as well as those are not participating in the interactions with ligands **(Fig. 35C)**. In particular, most of the residues binding with substrate and inhibitor *viz*. Arg50, Asp86, Tyr227, Cys231, Arg245, Thr246 and Arg252 displayed lesser fluctuations in comparison to apo *Ld*GluRS supporting the interactions observed during molecular docking studies **(Fig 35D)**.

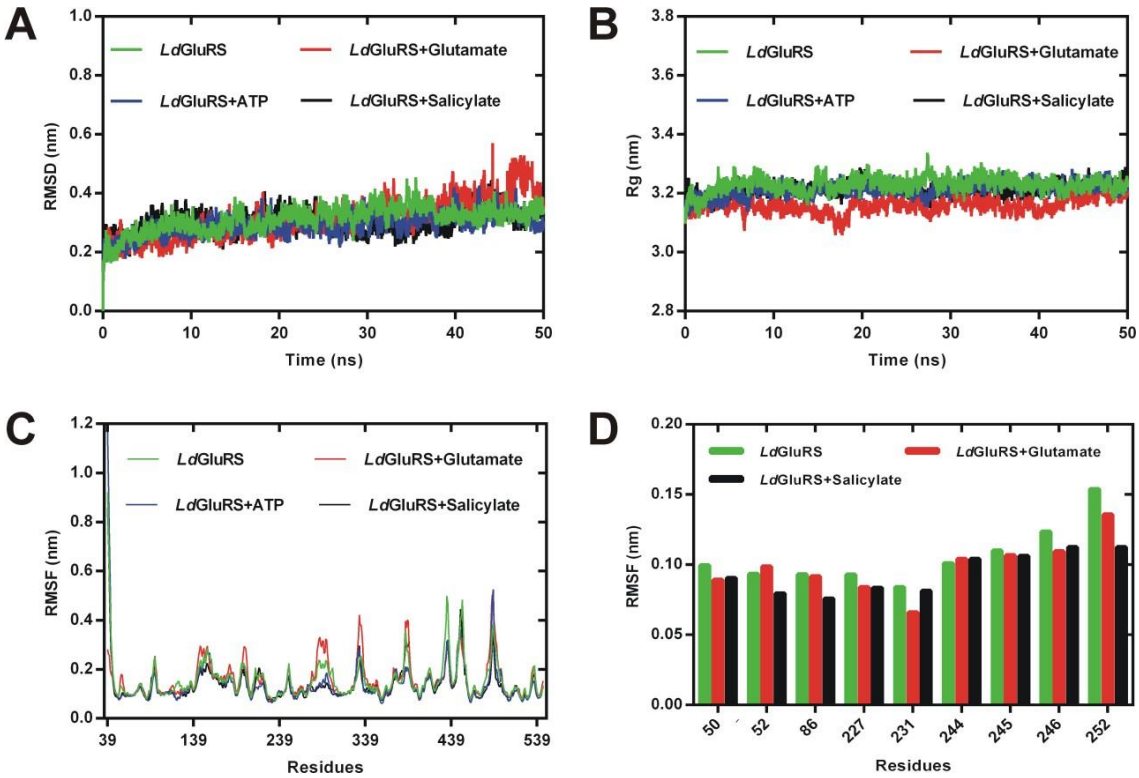

Figure 35: MDS studies of apo *Ld*GluRS and its complexes. Comparative analysis of RMSD (A), Rg (B) and RMSF (C) of apo, substrate (L-glutamate), cofactor (ATP) and inhibitor (salicylate) bound *Ld*GluRS. Comparison of RMSF for residues of substrate binding pocket for apo *Ld*GluRS and its complexes with L-Glu and salicylate during simulations (D).

5.2 Discussion

Secondary structural elements of *Ld*SerRS and *Ld*GluRS had shown higher α-helical content than the β-sheets, which are in correlation with their respective homolog from *T. brucei* [PDB ID: 3LSS] and *Mycobacterium tuberculosis* [PDB ID: 2JA2]. Likewise, mutants of both enzymes had not revealed any major changes in secondary structure. Similar effects of mutations have also been observed in PepT of *L. donovani*, where mutations did not show much impact on its secondary structural features **[161**]. The secondary structure of both proteins has changed at the extreme pH and started unfolding above the optimum temperature required for the activity that that is consistent to our enzymatic analysis. The thermal unfolding pattern of both proteins was comparable to other proteins including leishmanial ribulose 5-phosphate 3 epimerase **[145]** and PP2C **[162]** as well as *Thermus thermophilus* glutaminyl tRNA synthetase **[163]** showing discrete native and denatured states. Denaturation analysis of both aaRSs had shown loss of secondary structural content, which could be due to the exposure of more binding sites to denaturant upon unfolding of protein with increasing concentrations of urea **[164]**.

The three-dimensional structure of *Ld*SerRS demonstrated atypical topological features similar to crystal structure of *T. thermophilus* **[101]**, *E. coli* **[102]**, and *H. sapiens* **[103]** SerRSs. Further, the docking studies revealed that mostly interactions of *Ld*SerRS with substrate and cofactor are confined within the motifs-II and III residues. It is in corroboration of co-crystal structure of *H. sapiens* SerRS with substrate and cofactor that had binding pockets adjacent to each other between motifs-II and III **[103] [18]**. Similarly, the three-dimensional structure of *Ld*GluRS displayed common topological characteristics that have been reported in other glutamyl tRNA synthetases including *P. falciparum* GluRS **[134**]. Additionally, interaction analysis exhibited residues of *Ld*GluRS binding with substrate and cofactor are from domain-I with their binding pockets located adjacent to each other. It corroborates to the co-crystal structure of substrate and cofactor bound GluRSs of *Borrelia burgdorferi* **[165**] and *P. falciparum* **[166]**, which exhibited binding pockets to be close to each other in domain-I. Remarkably, binding affinities enumerated through docking analysis suggested illustrated *Ld*GluRS to present higher affinity for the cofactor than the substrate that is in correlation with *in vitro* kinetic studies performed by us. Concurrently, Comp 5l was found as placed into the ATP binding pocket of *Ld*SerRS with the coumarin moiety superimposing on the ribose ring of the ATP. Similar finding was reported in the cladosporin bound crystal structure of lysyl tRNA synthetase of *P. falciparum* wherein isocoumarin group of cladosporin was oriented equivalent to the ribose ring of ATP **[109]**. Molecular dynamic

simulations have shown stable profiles of RMSD, Rg and RMSF in the presence of ligands during MDS validating the obtained docking result to be more close to the *in vivo* system. However, exploration of more compounds followed by *in vitro* and *in vivo* studies would help to develop specific inhibitors against leishmanial parasite.

6. Summary

The essentiality of aaRSs for parasitic survival in other protozoans and substantial evolutionary deviations from their human counterparts indicates these enzymes could be assessed as a potential drug target in leishmanial parasites. Hence, recombinant *Ld*SerRS and *Ld*GluRS were purified to homogeneity and found to be existed as a homodimer in solution, which is in accordance to their homologs from various parasites. Both leishmanial enzymes had characteristic features of their respective classes of aminoacyl tRNA synthetase with conserved binding residues for the substrate and cofactor. Comparable of other aaRSs, both proteins possessed primarily α-helical content in their secondary structure with tryptophan residues positioned majorly in the hydrophobic environment. In corroboration to the earlier reports, monovalent and divalent metal ions were required for the aminoacylation reaction. Enzyme kinetics and docking studies had presented that the affinity of cofactor was greater than that of the substrate. Moreover, ureidosulfocoumarin derivative (Comp 5l) was more specific towards *Ld*SerRS in comparison to *Hs*SerRS and its modality of inhibition was competitive with respect to cofactor. Similarly, the enzymatic activity was inhibited at very low concentration of salicylate with competitive mode of inhibition towards substrate. Mutation analysis revealed significance of charged residues for the cofactor binding, which has been proven by thermal stability, kinetics and structural studies. Computational analysis showed the positioning of Comp 5l at the cofactor binding pocket of *Ld*SerRS, whereas salicylate bound into substrate binding pocket of *Ld*GluRS. Furthermore, molecular dynamics simulation studies deciphered more stable complex forms of both proteins with ligands as compared to the apo one. Our study provides critical insights on the molecular basis of inhibition of leishmanial SerRS and GluRS as well as its structural characteristics that could be useful to screen more structure-based compounds to treat leishmaniasis.

7. References

1. Ivens AC, Peacock CS, Worthey EA, et al. The genome of the kinetoplastid parasite, *Leishmania major*. *Science*. 2005; 309 (5733):436-442. doi:10.1126/science.1112680
2. Alvar J, Yactayo S, Bern C. Leishmaniasis and poverty. *Trends Parasitol*. 2006; 22(12):552-557. doi:10.1016/j.pt.2006.09.004
3. Pasha F, Saleem S, Nazir T, Tariq J, Qureshi K. Visceral Leishmaniasis (Kala-Azar): A Triumph Against a Trickster Disease. *Cureus*. 2022; 14(6):e25698. doi:10.7759/cureus.25698
4. Russell A. The Natural History of Aleppo, and Parts Adjacent. London: A. Millar; 1756. p. 262–6
5. Ross MR. Further notes on leishman's bodies. *Br. Med. J*. 1903; 2:1401
6. Akhoundi M, Kuhls K, Cannet A, et al. A Historical overview of the classification, evolution, and dispersion of *Leishmania* parasites and sandflies [published correction appears in PLoS Negl Trop Dis. 2016; 10(6): e0004770]. *PLoS Negl Trop Dis*. 2016; 10(3): e0004349. doi:10.1371/journal.pntd.0004349
7. Klatt S, Simpson L, Maslov DA, Konthur Z. *Leishmania tarentolae*: Taxonomic classification and its application as a promising biotechnological expression host. *PLoS Negl Trop Dis*. 2019; 13(7):e0007424. doi:10.1371/journal.pntd.0007424
8. Ready PD. Biology of phlebotomine sand flies as vectors of disease agents. *Annu Rev Entomol*. 2013; 58:227-250. doi:10.1146/annurev-ento-120811-153557
9. de Vries HJ, Reedijk SH, Schallig HD. Cutaneous leishmaniasis: recent developments in diagnosis and management. *Am J Clin Dermatol*. 2015; 16(2):99-109. doi:10.1007/s40257-015-0114-z
10. Kashif M, Manna PP, Akhter Y, Alaidarous M, Rub A. Screening of novel inhibitors against *Leishmania donovani* calcium ion channel to fight leishmaniasis. *Infect Disord Drug Targets*. 2017; 17(2):120-129. doi:10.2174/1871526516666161230124513
11. Dorlo TP, Huitema AD, Beijnen JH, de Vries PJ. Optimal dosing of miltefosine in children and adults with visceral leishmaniasis. *Antimicrob Agents Chemother*. 2012; 56(7):3864-3872. doi:10.1128/AAC.00292-12
12. Balasegaram M, Ritmeijer K, Lima MA, et al. Liposomal amphotericin B as a treatment for human leishmaniasis. *Expert Opin Emerg Drugs*. 2012; 17(4):493-510. doi:10.1517/14728214.2012.748036
13. Chowdhury R, Kumar V, Mondal D, Das ML, Das P, Dash AP, Kroeger A. Implication of vector characteristics of Phlebotomus argentipes in the kala-azar elimination

programme in the Indian sub-continent. *Pathog Glob Health*. 2016;110(3):87-96. doi:10.1080/20477724.2016.1180775

14. Ashford RW. Leishmaniasis reservoirs and their significance in control. *Clin Dermatol*. 1996; 14(5):523-532. doi:10.1016/0738-081x(96)00041-7
15. Cardo LJ. Leishmania: risk to the blood supply. *Transfusion*. 2006; 46(9):1641-1645. doi:10.1111/j.1537-2995.2006.00941.x
16. Blanco VM, Cossio A, Martinez JD, Saravia NG. Clinical and epidemiologic profile of cutaneous leishmaniasis in Colombian children: considerations for local treatment. *Am J Trop Med Hyg*. 2013; 89(2):359-364. doi:10.4269/ajtmh.12-0784
17. Desjeux P. Leishmaniasis: current situation and new perspectives. *Comp Immunol Microbiol Infect Dis*. 2004; 27(5):305-318. doi:10.1016/j.cimid.2004.03.004
18. Singh S. New developments in diagnosis of leishmaniasis. *Indian J Med Res*. 2006; 123(3):311-330
19. Torres-Guerrero E, Quintanilla-Cedillo MR, Ruiz-Esmenjaud J, Arenas R. Leishmaniasis: a review. F1000Res. 2017; 6:750. doi: 10.12688/f1000research.11120
20. Oliveira CC, Lacerda HG, Martins DR, et al. Changing epidemiology of American cutaneous leishmaniasis (ACL) in Brazil: a disease of the urban-rural interface. *Acta Trop*. 2004; 90(2):155-162. doi:10.1016/j.actatropica.2003.11.011
21. Bravo F, Sanchez MR. New and re-emerging cutaneous infectious diseases in Latin America and other geographic areas. *Dermatol Clin*. 2003; 21(4):655-viii. doi:10.1016/s0733-8635(03)00090-1
22. Alvar J, Vélez ID, Bern C, et al. Leishmaniasis worldwide and global estimates of its incidence. *PLoS One*. 2012; 7(5):e35671. doi:10.1371/journal.pone.0035671
23. Singh OP, Hasker E, Boelaert M, Sundar S. Elimination of visceral leishmaniasis on the Indian subcontinent. *Lancet Infect Dis*. 2016;16(12):e304-e309. doi:10.1016/S1473-3099(16)30140-2
24. Wetzel H, Luger D. *In vitro* feeding in the rearing of tsetse flies (Glossina m. morsitans and G.p. palpalis, Diptera: Glossinidae). *Tropenmed Parasitol*. 1978;29(2):239-251
25. Rijal S, Koirala S, Van der Stuyft P, Boelaert M. The economic burden of visceral leishmaniasis for households in Nepal. *Trans R Soc Trop Med Hyg*. 2006;100(9):838-841. doi:10.1016/j.trstmh.2005.09.017
26. Addy M, Nandy A. Ten years of kala-azar in west Bengal, Part I. Did post-kala- azar dermal leishmaniasis initiate the outbreak in 24-Parganas?.*Bull World Health Organ*. 1992; 70(3):341-346

27. Mathur P, Samantaray JC, Vajpayee M, Samanta P. Visceral leishmaniasis/human immunodeficiency virus co-infection in India: the focus of two epidemics. *J Med Microbiol*. 2006; 55(Pt 7):919-922. doi:10.1099/jmm.0.46574
28. Burza S, Mahajan R, Sanz MG, et al. HIV and visceral leishmaniasis coinfection in Bihar, India: an underrecognized and underdiagnosed threat against elimination. *Clin Infect Dis*. 2014; 59(4):552-555. doi:10.1093/cid/ciu333
29. Maroli M, Feliciangeli MD, Bichaud L, Charrel RN, Gradoni L. Phlebotomine sandflies and the spreading of leishmaniases and other diseases of public health concern. *Med Vet Entomol*. 2013;27(2):123-147. doi:10.1111/j.1365-2915.2012.01034.x
30. Davies CR, Kaye P, Croft SL, Sundar S. Leishmaniasis: new approaches to disease control. *BMJ*. 2003; 326(7385):377-382. doi:10.1136/bmj.326.7385.377
31. Steverding D. The history of leishmaniasis. *Parasit Vectors*. 2017; 10(1):82. doi:10.1186/s13071-017-2028-5
32. Herwaldt BL. Leishmaniasis. *Lancet*. 1999; 354(9185):1191-1199. doi:10.1016/S0140-6736(98)10178-2
33. Pulvertaft RJ, Hoyle GF. Stages in the life-cycle of *Leishmania donovani*. *Trans R Soc Trop Med Hyg*. 1960; 54:191-196. doi:10.1016/0035-9203(60)90057-2
34. Bates PA. Leishmania sand fly interaction: progress and challenges. *Curr Opin Microbiol*. 2008; 11(4):340-344. doi:10.1016/j.mib.2008.06.003
35. Hommel M. Visceral leishmaniasis: biology of the parasite. *J Infect*. 1999; 39(2):101-111. doi:10.1016/s0163-4453(99)90000-2
36. Launois P, Tacchini-Cottier F, Parra-Lopez C, Louis JA. Cytokines in parasitic diseases: the example of cutaneous leishmaniasis. *Int Rev Immunol*. 1998; 17(1-4):157-180. doi:10.3109/0883018980908449
37. Solbach W, Laskay T. The host response to Leishmania infection. *Adv Immunol*. 2000; 74:275-317. doi:10.1016/s0065-2776(08)60912-8
38. Launois P, Tacchini-Cottier F, Parra-Lopez C, Louis JA. Cytokines in parasitic diseases: the example of cutaneous leishmaniasis. *Int Rev Immunol*. 1998; 17(1-4):157-180. doi:10.3109/08830189809084491
39. Lehane MJ. Peritrophic matrix structure and function. *Annu Rev Entomol*. 1997; 42:525-550. doi:10.1146/annurev.ento.42.1.525
40. Zilberstein D, Shapira M. The role of pH and temperature in the development of *Leishmania* parasites. *Annu Rev Microbiol*. 1994; 48:449-470. doi:10.1146/annurev.mi.48.100194.002313

41. Gontijo NF, Almeida-Silva S, Costa FF, Mares-Guia ML, Williams P, Melo MN. Lutzomyia longipalpis: pH in the gut, digestive glycosidases, and some speculations upon *Leishmania* development. *Exp Parasitol*. 1998; 90(3):212-219. doi:10.1006/expr.1998.4336
42. Pace D. Leishmaniasis. *J Infect*. 2014; 69 Suppl 1:S10-S18. doi:10.1016/j.jinf.2014.07.016
43. Zhang WW, Matlashewski G. Characterization of the A2-A2rel gene cluster in *Leishmania donovani*: involvement of A2 in visceralization during infection. *Mol Microbiol*. 2001; 39(4):935-948. doi:10.1046/j.1365-2958.2001.02286.x
44. Engwerda CR, Ato M, Kaye PM. Macrophages, pathology and parasite persistence in experimental visceral leishmaniasis. *Trends Parasitol*. 2004;20(11):524-530. doi:10.1016/j.pt.2004.08.009
45. De Trez C, Magez S, Akira S, Ryffel B, Carlier Y, Muraille E. iNOS-producing inflammatory dendritic cells constitute the major infected cell type during the chronic *Leishmania major* infection phase of C57BL/6 resistant mice. *PLoS Pathog*. 2009; 5(6):e1000494. doi:10.1371/journal.ppat.1000494
46. Stenger S, Donhauser N, Thüring H, Röllinghoff M, Bogdan C. Reactivation of latent leishmaniasis by inhibition of inducible nitric oxide synthase. *J Exp Med*. 1996;183(4):1501-1514. doi:10.1084/jem.183.4.1501
47. Braga AS, Toledo Junior AC, Rabello A. Factors of poor prognosis of visceral leishmaniasis among children under 12 years of age. A retrospective monocentric study in Belo Horizonte, State of Minas Gerais, Brazil, 2001-2005. *Rev Soc Bras Med Trop*. 2013; 46(1):55-59. doi:10.1590/0037-868216432013
48. Ashkan MM, Rahim KM. Visceral leishmanisis in paediatrics: a study of 367 cases in southwest Iran. *Trop Doct*. 2008; 38(3):186-188. doi:10.1258/td.2007.070259
49. Grech V, Mizzi J, Mangion M, Vella C. Visceral leishmaniasis in Malta--an 18 year paediatric, population based study. *Arch Dis Child*. 2000; 82(5):381-385. doi:10.1136/adc.82.5.381
50. Ahmed MA, Suleman SM, Kordofani AA, Mustafa MD. Outbreak of visceral leishmaniasis in the western bank of the White Nile--Sudan, report and clinical study. *East Afr Med J*. 1988; 65(12):824-828
51. Ejara ED, Lynen L, Boelaert M, Van Griensven J. Challenges in HIV and visceral Leishmania co-infection: future research directions. *Trop Med Int Health*. 2010; 15(10):1266-1267. doi:10.1111/j.1365-3156.2010.02612.x

52. Burza S, Mahajan R, Sanz MG, et al. HIV and visceral leishmaniasis coinfection in Bihar, India: an underrecognized and underdiagnosed threat against elimination. *Clin Infect Dis*. 2014; 59(4):552-555. doi:10.1093/cid/ciu333
53. Zijlstra EE, el-Hassan AM. Leishmaniasis in Sudan. Visceral leishmaniasis. *Trans R Soc Trop Med Hyg*. 2001; 95(1):27-58. doi:10.1016/s0035-9203(01)90218-4
54. Ramesh V, Ramam M, Singh R, Salotra P. Hypopigmented post-kala-azar dermal leishmaniasis. *Int J Dermatol*. 2008;47(4):414-416. doi:10.1111/j.1365-4632.2008.03621.x
55. Desjeux P, Ghosh RS, Dhalaria P, Strub-Wourgaft N, Zijlstra EE. Report of the Post Kala-azar Dermal Leishmaniasis (PKDL) Consortium Meeting, New Delhi, India, 27-29 June 2012. *Parasit Vectors*. 2013; 6:196. doi:10.1186/1756-3305-6-196
56. Dorlo TP, Huitema AD, Beijnen JH, de Vries PJ. Optimal dosing of miltefosine in children and adults with visceral leishmaniasis. *Antimicrob Agents Chemother*. 2012; 56(7):3864-3872. doi:10.1128/AAC.00292-12
57. Kimutai R, Musa AM, Njoroge S, et al. Safety and Effectiveness of Sodium Stibogluconate and Paromomycin Combination for the Treatment of Visceral Leishmaniasis in Eastern Africa: Results from a Pharmacovigilance Programme. *Clin Drug Investig*. 2017; 37(3):259-272. doi:10.1007/s40261-016-0481-0
58. Balasegaram M, Ritmeijer K, Lima MA, et al. Liposomal amphotericin B as a treatment for human leishmaniasis. *Expert Opin Emerg Drugs*. 2012; 17(4):493-510. doi:10.1517/14728214.2012.748036
59. WHO, Leishmaniasis. Geneva: *World Health Organization*. 2010
60. Palade GE. A small particulate component of the cytoplasm. *J Biophys Biochem Cytol*. 1955; 1(1):59-68. doi:10.1083/jcb.1.1.59
61. Dever TE, Kinzy TG, Pavitt GD. Mechanism and regulation of protein synthesis in *Saccharomyces cerevisiae*. Genetics. 2016; 203(1):65-107. doi: 10.1534/genetics.115.186221
62. Khan S, Vihinen M. Spectrum of disease-causing mutations in protein secondary structures. *BMC Struct Biol*. 2007; 7:56. doi:10.1186/1472-6807-7-56
63. Pham JS, Dawson KL, Jackson KE, et al. Aminoacyl-tRNA synthetases as drug targets in eukaryotic parasites. *Int J Parasitol Drugs Drug Resist*. 2013; 4(1):1-13. doi:10.1016/j.ijpddr.2013.10.001

64. Kim S, Lee SW, Choi EC, Choi SY. Aminoacyl-tRNA synthetases and their inhibitors as a novel family of antibiotics. *Appl Microbiol Biotechnol*. 2003; 61(4):278-288. doi:10.1007/s00253-003-1243-5

65. Ochsner UA, Sun X, Jarvis T, Critchley I, Janjic N. Aminoacyl-tRNA synthetases: essential and still promising targets for new anti-infective agents. *Expert Opin Investig Drugs*. 2007; 16(5):573-593. doi:10.1517/13543784.16.5.573

66. Chaubey S, Kumar A, Singh D, Habib S. The apicoplast of *Plasmodium falciparum* is translationally active. *Mol Microbiol*. 2005; 56(1):81-89. doi:10.1111/j.1365-2958.2005.04538.x

67. Pino P, Aeby E, Foth BJ, et al. Mitochondrial translation in absence of local tRNA aminoacylation and methionyl tRNA Met formylation in Apicomplexa. *Mol Microbiol*. 2010; 76(3):706-718. doi:10.1111/j.1365-2958.2010.07128

68. Vondenhoff GH, Van Aerschot A. Aminoacyl-tRNA synthetase inhibitors as potential antibiotics. *Eur J Med Chem*. 2011; 46(11):5227-5236. doi:10.1016/j.ejmech.2011.08.049

69. Gadakh B, Van Aerschot A. Aminoacyl-tRNA synthetase inhibitors as antimicrobial agents: a patent review from 2006 till present. *Expert Opin Ther Pat*. 2012; 22(12):1453-1465. doi:10.1517/13543776.2012.732571

70. Arnez JG, Moras D. Structural and functional considerations of the aminoacylation reaction. *Trends Biochem Sci*. 1997; 22(6):211-216. doi:10.1016/s0968-0004(97)01052-9

71. Eriani G, Delarue M, Poch O, Gangloff J, Moras D. Partition of tRNA synthetases into two classes based on mutually exclusive sets of sequence motifs. *Nature*. 1990; 347(6289):203-206. doi:10.1038/347203a0

72. Rubio Gomez MA, Ibba M. Aminoacyl-tRNA synthetases. RNA. 2020; 26(8):910-936. doi: 10.1261/rna.071720.119

73. Cusack S. Sequence, structure and evolutionary relationships between class 2 aminoacyl-tRNA synthetases: an update. *Biochimie*. 1993; 75(12):1077-1081. doi:10.1016/0300-9084(93)90006-e

74. Ruff M, Krishnaswamy S, Boeglin M, et al. Class II aminoacyl transfer RNA synthetases: crystal structure of yeast aspartyl-tRNA synthetase complexed with tRNA(Asp). *Science*. 1991; 252(5013):1682-1689. doi:10.1126/science.2047877

75. Ribas de Pouplana L, Schimmel P. Two classes of tRNA synthetases suggested by sterically compatible dockings on tRNA acceptor stem. *Cell*. 2001; 104(2):191-193. doi:10.1016/s0092-8674(01)00204-5

76. Smirnova EV, Lakunina VA, Tarassov I, Krasheninnikov IA, Kamenski PA. Noncanonical functions of aminoacyl-tRNA synthetases. *Biochemistry (Mosc)*. 2012; 77(1):15-25. doi:10.1134/S0006297912010026

77. Nie A, Sun B, Fu Z, Yu D. Roles of aminoacyl-tRNA synthetases in immune regulation and immune diseases. *Cell Death Dis*. 2019; 10(12):901. doi:10.1038/s41419-019-2145-5

78. Ivens AC, Peacock CS, Worthey EA, et al. The genome of the kinetoplastid parasite, *Leishmania major*. *Science*. 2005; 309(5733):436-442. doi:10.1126/science.1112680

79. Berriman M, Ghedin E, Hertz-Fowler C, et al. The genome of the African trypanosome *Trypanosoma brucei*. *Science*. 2005; 309(5733):416-422. doi:10.1126/science.1112642

80. Merritt EA, Arakaki TL, Gillespie JR, et al. Crystal structures of trypanosomal histidyl-tRNA synthetase illuminate differences between eukaryotic and prokaryotic homologs. *J Mol Biol*. 2010; 397(2):481-494. doi:10.1016/j.jmb.2010.01.051

81. Istvan ES, Dharia NV, Bopp SE, Gluzman I, Winzeler EA, Goldberg DE. Validation of isoleucine utilization targets in *Plasmodium falciparum*. *Proc Natl Acad Sci U S A*. 2011; 108(4):1627-1632. doi:10.1073/pnas.1011560108

82. Gonzalez-y-Merchand JA, Colston MJ, Cox RA. Effects of growth conditions on expression of mycobacterial murA and tyrS genes and contributions of their transcripts to precursor rRNA synthesis. *J Bacteriol*. 1999; 181(15):4617-4627. doi:10.1128/JB.181.15.4617-4627.1999

83. Silvian LF, Wang J, Steitz TA. Insights into editing from an ile-tRNA synthetase structure with tRNAile and mupirocin. *Science*. 1999; 285(5430):1074-1077

84. Nakama T, Nureki O, Yokoyama S. Structural basis for the recognition of isoleucyl-adenylate and an antibiotic, mupirocin, by isoleucyl-tRNA synthetase. *J Biol Chem*. 2001; 276(50):47387-47393. doi:10.1074/jbc.M109089200

85. Vondenhoff GH, Van Aerschot A. Aminoacyl-tRNA synthetase inhibitors as potential antibiotics. *Eur J Med Chem*. 2011; 46(11):5227-5236. doi:10.1016/j.ejmech.2011.08.049

86. Tanaka K, Tamaki M, Watanabe S. Effect of furanomycin on the synthesis of isoleucyl-tRNA. *Biochim Biophys Acta*. 1969; 195(1):244-245. doi:10.1016/0005-2787(69)90621-2

87. Konrad I, Röschenthaler R. Inhibition of phenylalanine tRNA synthetase from *Bacillus subtilis* by ochratoxin A. *FEBS Lett*. 1977;83(2):341-347. doi:10.1016/0014-5793(77)81037-5

88. Nasim F, Qureshi IA. Aminoacyl tRNA Synthetases: Implications of Structural Biology in Drug Development against Trypanosomatid Parasites. *ACS Omega*. 2023; 8(17):14884-14899. doi:10.1021/acsomega.3c00826

89. Jakubowski H, Goldman E. Editing of errors in selection of amino acids for protein synthesis. *Microbiol Rev*. 1992; 56(3):412-429. doi:10.1128/mr.56.3.412-429.1992

90. Lee JW, Beebe K, Nangle LA, et al. Editing-defective tRNA synthetase causes protein misfolding and neurodegeneration. *Nature*. 2006; 443(7107):50-55. doi:10.1038/nature05096

91. Zhou Z, Sun B, Nie A, Yu D, Bian M. Roles of Aminoacyl-tRNA Synthetases in Cancer. *Front Cell Dev Biol*. 2020; 8:599765. doi:10.3389/fcell.2020.599765

92. Woese CR, Olsen GJ, Ibba M, Söll D. Aminoacyl-tRNA synthetases, the genetic code, and the evolutionary process. *Microbiol Mol Biol Rev*. 2000; 64(1):202-236. doi:10.1128/MMBR.64.1.202-236.2000

93. Baron C, Sturchler C, Wu XQ, Gross HJ, Krol A, Böck A. Eukaryotic selenocysteine inserting tRNA species support selenoprotein synthesis in *Escherichia coli*. *Nucleic Acids Res*. 1994; 22(12):2228-2233. doi:10.1093/nar/22.12.2228

94. Schmidt RL, Simonović M. Synthesis and decoding of selenocysteine and human health. *Croat Med J*. 2012; 53(6):535-550. doi:10.3325/cmj.2012.53.535

95. Khan S, Garg A, Camacho N, et al. Structural analysis of malaria-parasite lysyl-tRNA synthetase provides a platform for drug development. *Acta Crystallogr D Biol Crystallogr*. 2013; 69(1):785-795. doi:10.1107/S0907444913001923

96. Panigrahi GC, Qureshi R, Jakkula P, Kumar KA, Khan N, Qureshi IA. Leishmanial aspartyl-tRNA synthetase: Biochemical, biophysical and structural insights. *Int J Biol Macromol*. 2020; 165(1)2869-2885. doi:10.1016/j.ijbiomac.2020.10.140

97. Biou V, Yaremchuk A, Tukalo M, Cusack S. The 2.9 A crystal structure of *T. thermophilus* seryl-tRNA synthetase complexed with tRNA(Ser). *Science*. 1994; 263(5152):1404-1410. doi:10.1126/science.8128220

98. Lenhard B, Filipić S, Landeka I, Skrtić I, Söll D, Weygand-Durasević I. Defining the active site of yeast seryl-tRNA synthetase. Mutations in motif 2 loop residues affect tRNA-dependent amino acid recognition. *J Biol Chem*. 1997; 272(2):1136-1141. doi:10.1074/jbc.272.2.1136

99. Lenhard B, Praetorius-Ibba M, Filipic S, Söll D, Weygand-Durasevic I. C-terminal truncation of yeast SerRS is toxic for *Saccharomyces cerevisiae* due to altered mechanism of substrate recognition. *FEBS Lett*. 1998; 439(3):235-240. doi:10.1016/s0014-5793(98)01376-3
100. Kisselev LL, Wolfson AD. Aminoacyl-tRNA synthetases from higher eukaryotes. *Prog Nucleic Acid Res Mol Biol*. 1994; 48:83-142. doi:10.1016/s0079-6603(08)60854-5
101. Biou V, Yaremchuk A, Tukalo M, Cusack S. The 2.9 A crystal structure of *T. thermophilus* seryl-tRNA synthetase complexed with tRNA(Ser). *Science*. 1994; 263(5152):1404-1410. doi:10.1126/science.8128220
102. Cusack S, Berthet-Colominas C, Härtlein M, Nassar N, Leberman R. A second class of synthetase structure revealed by X-ray analysis of *Escherichia coli* seryl-tRNA synthetase at 2.5 A. *Nature*. 1990; 347(6290):249-255. doi:10.1038/347249a0
103. Xu X, Shi Y, Yang XL. Crystal structure of human Seryl-tRNA synthetase and Ser-SA complex reveals a molecular lever specific to higher eukaryotes. *Structure*. 2013; 21(11):2078-2086. doi:10.1016/j.str.2013.08.021
104. Belrhali H, Yaremchuk A, Tukalo M, et al. Crystal structures at 2.5 angstrom resolution of seryl-tRNA synthetase complexed with two analogs of seryl adenylate. *Science*. 1994; 263(5152):1432-1436. doi:10.1126/science.8128224
105. El-Sayed AK, Hothersall J, Cooper SM, Stephens E, Simpson TJ, Thomas CM. Characterization of the mupirocin biosynthesis gene cluster from *Pseudomonas fluorescens* NCIMB 10586. *Chem Biol*. 2003; 10(5):419-430. doi:10.1016/s1074-5521(03)00091-7
106. Zeng Y, Roy H, Patil PB, Ibba M, Chen S. Characterization of two seryl-tRNA synthetases in albomycin-producing *Streptomyces sp*. strain ATCC 700974. *Antimicrob Agents Chemother*. 2009; 53(11):4619-4627. doi:10.1128/AAC.00782-09
107. Jacyno JM, Harwood JS, Cutler HG, Lee MK. Isocladosporin, a biologically active isomer of cladosporin from *Cladosporium cladosporioides*. *J Nat Prod*. 1993; 56(8):1397-1401. doi:10.1021/np50098a023
108. Cattel L, Grove JF, Shaw D. New metabolic products of *Aspergillus flavus*. 3. Biosynthesis of asperentin. *J Chem Soc Perkin 1*. 1973; 21:2626-2629. doi:10.1039/p19730002626
109. Khan S, Sharma A, Belrhali H, Yogavel M, Sharma A. Structural basis of malaria parasite lysyl-tRNA synthetase inhibition by cladosporin. *J Struct Funct Genomics*. 2014; 15(2):63-71. doi:10.1007/s10969-014-9182-1

110. Pang L, Nautiyal M, De Graef S, et al. Structural Insights into the Binding of Natural Pyrimidine-Based Inhibitors of Class II Aminoacyl-tRNA Synthetases. *ACS Chem Biol*. 2020; 15(2):407-415. doi:10.1021/acschembio.9b00887
111. Ito T, Kiyasu N, Matsunaga R, Takahashi S, Yokoyama S. Structure of nondiscriminating glutamyl-tRNA synthetase from *Thermotoga maritima*. *Acta Crystallogr D Biol Crystallogr*. 2010; 66(Pt 7):813-820. doi:10.1107/S0907444910019086
112. Schulze JO, Masoumi A, Nickel D, et al. Crystal structure of a non-discriminating glutamyl-tRNA synthetase. *J Mol Biol*. 2006; 361(5):888-897. doi:10.1016/j.jmb.2006.06.054
113. Baick JW, Yoon JH, Namgoong S, et al. Growth inhibition of *Escherichia coli* during heterologous expression of *Bacillus subtilis* glutamyl-tRNA synthetase that catalyzes the formation of mischarged glutamyl-tRNA1 Gln. *J Microbiol*. 2004; 42(2):111-116
114. Sheppard K, Yuan J, Hohn MJ, Jester B, Devine KM, Söll D. From one amino acid to another: tRNA-dependent amino acid biosynthesis. *Nucleic Acids Res*. 2008; 36(6):1813-1825. doi:10.1093/nar/gkn015
115. Sekine S, Nureki O, Dubois DY, et al. ATP binding by glutamyl-tRNA synthetase is switched to the productive mode by tRNA binding. *EMBO J*. 2003; 22(3):676-688. doi:10.1093/emboj/cdg053
116. Nureki O, Vassylyev DG, Katayanagi K, et al. Architectures of class-defining and specific domains of glutamyl-tRNA synthetase [published correction appears in *Science* 1995; 267(5206):1958-1965. doi:10.1126/science.7701318
117. Cerini C, Semeriva M, Gratecos D. Evolution of the aminoacyl-tRNA synthetase family and the organization of the *Drosophila* glutamyl-prolyl-tRNA synthetase gene. Intron/exon structure of the gene, control of expression of the two mRNAs, selective advantage of the multienzyme complex. *Eur J Biochem*. 1997; 244(1):176-185. doi:10.1111/j.1432-1033.1997.00176.x
118. Kaiser E, Hu B, Becher S, et al. The human EPRS locus (formerly the QARS locus): a gene encoding a class I and a class II aminoacyl-tRNA synthetase. *Genomics*. 1994; 19(2):280-290. doi:10.1006/geno.1994.1059
119. Beale SI. Biosynthesis of the Tetrapyrrole Pigment Precursor, delta-Aminolevulinic Acid, from Glutamate. *Plant Physiol*. 1990; 93(4):1273-1279. doi:10.1104/pp.93.4.1273

120. Kalidas S, Cestari I, Monnerat S, et al. Genetic validation of aminoacyl-tRNA synthetases as drug targets in *Trypanosoma brucei*. *Eukaryot Cell*. 2014; 13(4):504-516. doi:10.1128/EC.00017-14
121. Mailu BM, Ramasamay G, Mudeppa DG, et al. A nondiscriminating glutamyl-tRNA synthetase in the *plasmodium* apicoplast: the first enzyme in an indirect aminoacylation pathway. *J Biol Chem*. 2013; 288(45):32539-32552. doi:10.1074/jbc.M113.507467
122. Singh P, Kumar Sigalapalli D, Sridhar Goud N, et al. Ureidosulfocoumarin Derivatives As Selective and Potent Carbonic Anhydrase IX and XII Inhibitors. *ChemMedChem*. 2022; 17(5):e202100725. doi:10.1002/cmdc.202100725
123. Burleigh M, Smith MJ. The mechanism of the inhibitory action of salicylate on glutamyl-transfer ribonucleic acid synthetase in vitro. *J Pharm Pharmacol*. 1971; 23(8):590-594. doi:10.1111/j.2042-7158.1971.tb08722.x
124. Deutscher MP. Rat liver glutamyl ribonucleic acid synthetase. II. Further properties and anomalous pyrophosphate exchange. *J Biol Chem*. 1967; 242(6):1132-1139
125. Daina A, Michielin O, Zoete V. SwissADME: a free web tool to evaluate pharmacokinetics, drug-likeness and medicinal chemistry friendliness of small molecules. *Sci Rep*. 2017; 7:42717. doi:10.1038/srep42717
126. Qureshi R, Jakkula P, Sagurthi SR, Qureshi IA. Protein phosphatase 1 of Leishmania donovani exhibits conserved catalytic residues and pro-inflammatory response. *Biochem Biophys Res Commun*. 2019; 516(3):770-776. doi:10.1016/j.bbrc.2019.06.085
127. Van Der Spoel D, Lindahl E, Hess B, Groenhof G, Mark AE, Berendsen HJ. GROMACS: fast, flexible, and free. *J Comput Chem*. 2005; 26(16):1701-1718. doi:10.1002/jcc.20291
128. Trott O, Olson AJ. AutoDock Vina: improving the speed and accuracy of docking with a new scoring function, efficient optimization, and multithreading. *J Comput Chem*. 2010; 31(2):455-461. doi:10.1002/jcc.21334
129. Loren D, Mendelsohn, ChemDraw 8 ultra, windows and macintosh versions, *J. Chem. Inf. Comput. Sci*. 2004; 44(6) 2225–2226, https:/doi.org/10.1021/ci040123t
130. Berendsen HJC, Grigera JR, Straatsma TP, The missing term in effective pair potentials, *J. Phys. Chem*. 1987; 91:6269–6271. doi.org/10.1021/j100308a038
131. Vondenhoff GH, Van Aerschot A. Aminoacyl-tRNA synthetase inhibitors as potential antibiotics. *Eur J Med Chem*. 2011; 46(11):5227-5236. doi:10.1016/j.ejmech.2011.08.049

132. Hoepfner D, McNamara CW, Lim CS, et al. Selective and specific inhibition of the *plasmodium falciparum* lysyl-tRNA synthetase by the fungal secondary metabolite cladosporin. *Cell Host Microbe*. 2012; 11(6):654-663. doi:10.1016/j.chom.2012.04.015
133. Chadha S, Mallampudi NA, Mohapatra DK, Madhubala R. Genetic Validation of *Leishmania donovani* Lysyl-tRNA Synthetase Shows that It Is Indispensable for Parasite Growth and Infectivity. *mSphere*. 2017; 2(4):e00340-17. doi:10.1128/mSphereDirect.00340-17
134. Sharma A, Sharma M, Yogavel M, Sharma A. Protein Translation Enzyme lysyl-tRNA Synthetase Presents a New Target for Drug Development against Causative Agents of Loiasis and Schistosomiasis. *PLoS Negl Trop Dis*. 2016; 10(11):e0005084.. doi:10.1371/journal.pntd.0005084
135. Ho JM, Bakkalbasi E, Söll D, Miller CA. Drugging tRNA aminoacylation. *RNA Biol*. 2018; 15(4-5):667-677. doi:10.1080/15476286.2018.1429879
136. Rajendran V, Kalita P, Shukla H, Kumar A, Tripathi T. Aminoacyl-tRNA synthetases: Structure, function, and drug discovery. *Int J Biol Macromol*. 2018; 111:400-414. doi:10.1016/j.ijbiomac.2017.12.157
137. Cusack S, Härtlein M, Leberman R. Sequence, structural and evolutionary relationships between class 2 aminoacyl-tRNA synthetases. *Nucleic Acids Res*. 1991; 19(13):3489-3498. doi:10.1093/nar/19.13.3489
138. Ratinaud MH, Thomes JC, Julien R. Glutamyl-tRNA synthetases from wheat. Isolation and characterization of three dimeric enzymes. *Eur J Biochem*. 1983; 135(3):471-477. doi:10.1111/j.1432-1033.1983.tb07675.x
139. Gendron N, Breton R, Champagne N, Lapointe J. Adenylosuccinate lyase of *Bacillus subtilis* regulates the activity of the glutamyl-tRNA synthetase. *Proc Natl Acad Sci U S A*. 1992; 89(12):5389-5392. doi:10.1073/pnas.89.12.5389
140. Jakkula P, Narsimulu B, Qureshi IA. Biochemical and structural insights into 6-phosphogluconate dehydrogenase from Leishmania donovani. *Appl Microbiol Biotechnol*. 2021; 105(13):5471-5489. doi:10.1007/s00253-021-11434-4
141. Yadav S, Gupta S, Saxena JK. Monitoring thermal and chemical unfolding of *Brugia malayi* calreticulin using fluorescence and Circular Dichroism spectroscopy. *Int J Biol Macromol*. 2017; 102:986-995. doi:10.1016/j.ijbiomac.2017.04.053
142. Siddiqui MF, Bano B. Insight into the functional and structural transition of garlic phytocystatin induced by urea and guanidine hydrochloride: A comparative biophysical study. *Int J Biol Macromol*. 2018; 106:20-29. doi:10.1016/j.ijbiomac.2017.07.172

143. Narsimulu B, Qureshi R, Jakkula P, Are S, Qureshi IA. Biophysical and Structural Characterization of Ribulose-5-phosphate Epimerase from *Leishmania donovani*. *ACS Omega*. 2021; 7(1):548-564. doi:10.1021/acsomega.1c04967
144. Katze JR, Konigsberg W. Purification and properties of seryl transfer ribonucleic acid synthetase from Escherichia coli. *J Biol Chem*. 1970; 245(5):923-930
145. Lapointe J, Söll D. Glutamyl transfer ribonucleic acid synthetase of Escherichia coli. I. Purification and properties. *J Biol Chem*. 1972; 247(16):4966-4974
146. Ador L, Jaeger S, Geslain R, Martin F, Cavarelli J, Eriani G. Mutation and evolution of the magnesium-binding site of a class II aminoacyl-tRNA synthetase. *Biochemistry*. 2004; 43(22):7028-7037. doi:10.1021/bi049617+
147. Lovgren T. The effect of monovalent cations on isoleucyl transfer-RNA synthetase reaction from baker's yeast. Acta Chemica Scand B. 1976; 30:911–914
148. Kayne MS, Cohn M. Cation requirements of isoleucyl-tRNA synthetase from *Escherichia coli*. *Biochem Biophys Res Commun*. 1972; 46(3):1285-1291. doi:10.1016/s0006-291x(72)80114-1
149. Lenhard B, Filipić S, Landeka I, Skrtić I, Söll D, Weygand-Durasević I. Defining the active site of yeast seryl-tRNA synthetase. Mutations in motif 2 loop residues affect tRNA-dependent amino acid recognition. *J Biol Chem*. 1997; 272(2):1136-1141. doi:10.1074/jbc.272.2.1136
150. Borel F, Vincent C, Leberman R, Härtlein M. Seryl-tRNA synthetase from *Escherichia coli*: implication of its N-terminal domain in aminoacylation activity and specificity [published correction appears in Nucleic Acids Res 1994 Oct 25;22(21):4552]. *Nucleic Acids Res*. 1994; 22(15):2963-2969. doi:10.1093/nar/22.15.2963
151. Mailu BM, Ramasamay G, Mudeppa DG, et al. A nondiscriminating glutamyl-tRNA synthetase in the plasmodium apicoplast: the first enzyme in an indirect aminoacylation pathway. *J Biol Chem*. 2013; 288(45):32539-32552. doi:10.1074/jbc.M113.507467
152. Paravisi S, Fumagalli G, Riva M, et al. Kinetic and mechanistic characterization of *Mycobacterium tuberculosis* glutamyl-tRNA synthetase and determination of its oligomeric structure in solution. *FEBS J*. 2009; 276(5):1398-1417. doi:10.1111/j.1742-4658.2009.06880.x
153. Lapointe J, Söll D. Glutamyl transfer ribonucleic acid synthetase of *Escherichia coli.* Influence of the 46K protein on the affinity of the 56K glutamyl transfer ribonucleic acid synthetase for its substrates. *J Biol Chem*. 1972; 247(16):4982-4985

154. Yu XY, Hill JM, Yu G, et al. A series of quinoline analogues as potent inhibitors of C. albicans prolyl tRNA synthetase. *Bioorg Med Chem Lett*. 2001; 11(4):541-544. doi:10.1016/s0960-894x(00)00697-1
155. Farhanullah, Kim SY, Yoon EJ, et al. Design and synthesis of quinolinones as methionyl-tRNA synthetase inhibitors. *Bioorg Med Chem*. 2006; 14(21):7154-7159. doi:10.1016/j.bmc.2006.06.062
156. Pang L, Nautiyal M, De Graef S, et al. Structural Insights into the Binding of Natural Pyrimidine-Based Inhibitors of Class II Aminoacyl-tRNA Synthetases. *ACS Chem Biol*. 2020; 15(2):407-415. doi:10.1021/acschembio.9b00887
157. Bhat SY, Jagruthi P, Srinivas A, Arifuddin M, Qureshi IA. Synthesis and characterization of quinoline-carbaldehyde derivatives as novel inhibitors for leishmanial methionine aminopeptidase 1. *Eur J Med Chem*. 2020; 186:111860. doi:10.1016/j.ejmech.2019.111860
158. Bellamy A, Huggins AK, Smith MJ. salicylate and glutamate metabolism. *J Pharm Pharmacol*. 1963; 15:559-560. doi:10.1111/j.2042-7158.1963.tb12836.x
159. Burleigh M, Smith MJ. The site of the inhibitory action of salicylate on protein biosynthesis in vitro. *Biochem J*. 1970; 117(3):68P. doi:10.1042/bj1170068pa
160. Deutscher MP. Rat liver glutamyl ribonucleic acid synthetase. II. Further properties and anomalous pyrophosphate exchange. *J Biol Chem*. 1967; 242(6):1132-1139
161. Bhat SY, Qureshi IA. Mutations of key substrate binding residues of leishmanial peptidase T alter its functional and structural dynamics. *Biochim Biophys Acta Gen Subj*. 2020; 1864(1):129465. doi:10.1016/j.bbagen.2019.129465
162. Jakkula P, Qureshi R, Iqbal A, Sagurthi SR, Qureshi IA. *Leishmania donovani* PP2C: Kinetics, structural attributes and in vitro immune response. *Mol Biochem Parasitol*. 2018; 223:37-49. doi:10.1016/j.molbiopara.2018.06.005
163. Nachiappan M, Jain V, Sharma A, Yogavel M, Jeyakanthan J. Structural and functional analysis of Glutaminyl-tRNA synthetase (TtGlnRS) from *Thermus thermophilus HB8* and its complexes. *Int J Biol Macromol*. 2018; 120(Pt B):1379-1386. doi:10.1016/j.ijbiomac.2018.09.115
164. Myers JK, Pace CN, Scholtz JM. Denaturant m values and heat capacity changes: relation to changes in accessible surface areas of protein unfolding [published correction appears in Protein Sci 1996 May;5(5):981]. *Protein Sci*. 1995; 4(10):2138-2148. doi:10.1002/pro.5560041020

165. Moen SO, Edwards TE, Dranow DM, et al. Ligand co-crystallization of aminoacyl-tRNA synthetases from infectious disease organisms. *Sci Rep*. 2017; 7(1):223. doi:10.1038/s41598-017-00367-6
166. Sharma VK, Chhibber-Goel J, Yogavel M, Sharma A. Structural characterization of glutamyl-tRNA synthetase (GluRS) from *Plasmodium falciparum*. *Mol Biochem Parasitol*. 2023; 253:111530. doi:10.1016/j.molbiopara.2022.111530

8. Publications

International Journal of Biological Macromolecules xxx (xxxx) 127756

Contents lists available at ScienceDirect

International Journal of Biological Macromolecules

journal homepage: www.elsevier.com/locate/ijbiomac

Inhibition and structural insights of leishmanial glutamyl-tRNA synthetase for designing potent therapeutics

Bandigi Narsimulu [a, 1], Pranay Jakkula [a, 1], Rahila Qureshi [b], Fouzia Nasim [a], Insaf Ahmed Qureshi [a, *]

[a] Department of Biotechnology & Bioinformatics, School of Life Sciences, University of Hyderabad, Prof. C.R. Rao Road, Hyderabad 500046, India
[b] Centre for DNA Fingerprinting and Diagnostics, Hyderabad 500039, India

ARTICLE INFO

Keywords:
Leishmaniasis
Glutamyl-tRNA synthetase
Salicylate
Drug discovery

ABSTRACT

Aminoacyl-tRNA synthetases (aaRSs), essential components of the protein synthesizing machinery, have been often chosen for devising therapeutics against parasitic diseases. Due to their relevance in drug development, the current study was designed to explore functional and structural aspects of *Leishmania donovani* glutamyl-tRNA synthetase (*Ld*GluRS). Hence, *Ld*GluRS was cloned into an expression vector and purified to homogeneity using chromatography techniques. Purified protein showed maximum enzymatic activity at physiological pH, with more binding capacity towards its cofactor (Adenosine triphosphate, 0.06 ± 0.01 mM) than the cognate substrate (L-glutamate, 9.5 ± 0.5 mM). Remarkably, salicylate inhibited *Ld*GluRS competitively with respect to L-glutamate and exhibited druglikeness with negligible effect on human macrophages. The protein possessed more α-helices (43 %) than β-sheets (12 %), whereas reductions in thermal stability and cofactor-binding affinity, along with variation in mode of inhibition after mutation signified the role of histidine (H60) as a catalytic residue. *Ld*GluRS could also generate a pro-inflammatory milieu in human macrophages by upregulating cytokines. The docking study demonstrated the placement of salicylate into *Ld*GluRS substrate-binding site, and the complex was found to be stable during molecular dynamics (MD) simulation. Altogether, our study highlights the understanding of molecular inhibition and structural features of glutamyl-tRNA synthetase from kinetoplastid parasites.

1. Introduction

Leishmaniasis, caused by parasites belonging to the genus *Leishmania*, is a neglected tropical disease that infects millions of people worldwide [1]. Of the several forms, visceral leishmaniasis or kala azar is highly fatal as it affects visceral organs of the body and is also characterized by a wide range of clinical symptoms that include prolonged fever, hypergammaglobulinemia, hepatosplenomegaly, and pancytopenia [2]. Due to the absence of proper vaccines, chemotherapy is the only treatment available for this disease. However, drugs such as pentavalent antimonials, amphotericin B, and miltefosine besides being expensive pose side effects such as toxicity and the need for long-term administration [3]. Also, an increase in the development of resistance by the parasite to available therapeutics necessitates the identification of newer drug targets for treating leishmaniasis.

Aminoacyl-tRNA synthetases (aaRSs) are responsible for the ligation of amino acids to their cognate tRNAs that can further take part in protein synthesis. Apart from their role in protein synthesis, aaRSs are also associated with non-canonical functions such as signal transduction, RNA splicing, transcription, angiogenesis, apoptosis *etc*. [4], and are also known for their roles in immune regulation and diseases [5,6]. The twenty aaRSs have been categorized into two classes considering structural dissimilarities in their catalytic cores [7]. The class-I enzymes have a characteristic Rossmann fold, HIGH (His-Ile-Gly-His) and KMSKS (Lys-Met-Ser-Lys-Ser) motifs at their catalytic pocket for ligand binding, whereas the class-II enzymes have antiparallel β-sheets that are surrounded by α-helices. Moreover, these enzymes also differ with respect to the tRNA termini where they aminoacylate, *viz*., classes I and II correspondingly aminoacylate the 2'-OH and 3'-OH groups of adenosine nucleotide [8]. Two genes are present for each of the 20 aaRSs in

Abbreviations: aaRS, aminoacyl-tRNA synthetase; GluRS, glutamyl-tRNA synthetase; CD, circular dichroism; ORF, open reading frame; ATP, adenosine triphosphate; L-Glu, L-glutamate; tRNA, transfer ribonucleic acid; DTT, dithiothreitol; PPase, inorganic pyrophosphatase; Pi, inorganic phosphate; PPi, inorganic pyrophosphate; KI, potassium iodide; MTT, 3-(4,5-dimethyl-thiazol-2-yl)-2,5-diphenyltetrazolium bromide; PDB, protein data bank

* Corresponding author at: Department of Biotechnology & Bioinformatics, School of Life Sciences, University of Hyderabad, Hyderabad 500046, India.
E-mail address: insaf@uohyd.ac.in (I.A. Qureshi).

[1] These authors contributed equally to this article.

https://doi.org/10.1016/j.ijbiomac.2023.127756
Received 12 July 2023; Received in revised form 8 October 2023; Accepted 27 October 2023
0141-8130/© 20XX

International Journal of Biological Macromolecules 237 (2023) 124118

Contents lists available at ScienceDirect

International Journal of Biological Macromolecules

journal homepage: www.elsevier.com/locate/ijbiomac

Exploration of seryl tRNA synthetase to identify potent inhibitors against leishmanial parasites

Bandigi Narsimulu [a,1], Rahila Qureshi [b,1], Pranay Jakkula [a], Priti Singh [c], Mohammed Arifuddin [c,2], Insaf Ahmed Qureshi [a,*]

[a] Department of Biotechnology & Bioinformatics, School of Life Sciences, University of Hyderabad, Prof. C.R. Rao Road, Hyderabad 500046, India
[b] Centre for DNA Fingerprinting and Diagnostics, Hyderabad 500039, India
[c] Department of Medicinal Chemistry, National Institute of Pharmaceutical Education and Research, Hyderabad 500037, India

ARTICLE INFO

Keywords:
Leishmania donovani
Seryl tRNA synthetase
Ureidosulfocoumarin derivatives
Drug discovery

ABSTRACT

Aminoacyl-tRNA synthetases are crucial enzymes for cellular protein metabolism and have been considered as an attractive target for development of new antimicrobials. In the current study, seryl tRNA synthetase of *Leishmania donovani* (*Ld*SerRS) and its mutants were purified and characterized through biochemical and structural methods. Purified *Ld*SerRS was found to be enzymatically active and exhibited more alpha helices in secondary structure. The enzymatic activity of purified protein was observed as highest near physiological temperature and pH. Mutation in ATP binding residues (R295 and E297) demonstrated reduction in the affinity for cofactor with no significant deviation in secondary structure. In vitro inhibition studies with ureidosulfocoumarin derivatives helped to identify Comp 5l as a specific inhibitor for leishmanial SerRS that showed lesser potency towards purified *Hs*SerRS. The identified compound presented competitive mode of inhibition for *Ld*SerRS and also revealed druglikeness along with very low toxicity for human macrophages. Structural analysis of protein and ligand complex depicted the binding of Comp 5l into the cofactor binding site of *Ld*SerRS with high affinity succeeded by validation employing molecular dynamics simulations. Altogether, our study presents a promising scaffold to explore small molecules to target the enzymatic activity of leishmanial SerRS to develop the specific therapeutics.

1. Introduction

Leishmaniasis, a group of vector borne diseases, is caused by approximately twenty different species of leishmanial parasites worldwide. Visceral leishmaniasis (VL) or kala-azar is the most severe form of leishmaniasis that is engendered by *Leishmania donovani* and affects approximately 50,000 to 90,000 people worldwide annually [1]. It exhibits heterogenic life cycle requiring two diverse host systems, i.e. midgut of the sandfly and parasitophorous vacuole of the human macrophage [2]. Lack of effective vaccine renders the chemotherapy as extensively used practice to treat this neglected tropical disease. Pentavalent antimonials have been employed from few decades, however continuous practice of these drugs results in side effects as well as the development of resistance in parasite [3]. Thus, exploration and characterization of the proteins that are essential for the parasitic survival and virulence become utmost important as these could be helpful in designing specific inhibitors against leishmanial parasites.

Aminoacyl-tRNA synthetases (aaRSs) are considered as essential enzymes for protein biosynthesis as they connect a specific amino acid to the cognate tRNA that participates in the translation of the genetic code. When a tRNA is mischarged with noncognate amino acid due to the rare errors by aaRSs, it could be lethal for the cells [4]. Misfolded proteins and neurodegeneration are caused by editing-defective tRNA synthetase that has been experimentally proven in mouse by sticky mutation. This mutation has led to degeneration of cerebellar Purkinje and ataxia cells due to lack of activity of proofreading domain in alanyl-tRNA synthetase [5]. Majority of protein misfolding disorders including protein aggregation of amylin, Aβ peptide and α-synuclein leads to various human diseases like type II diabetes, Alzheimer's and Parkinson's [6]. Additionally, many studies have proved that aaRSs are also involved in

* Corresponding author.
E-mail address: insaf@uohyd.ac.in (I.A. Qureshi).
[1] These authors contributed equally to this article.
[2] Present address: Department of Chemistry, Directorate of Distance Education, Maulana Azad National Urdu University, Gachibowli, Hyderabad 500032, India

https://doi.org/10.1016/j.ijbiomac.2023.124118
Received 31 January 2023; Received in revised form 13 March 2023; Accepted 17 March 2023
Available online 23 March 2023

ACS OMEGA

http://pubs.acs.org/journal/acsodf

Article

Biophysical and Structural Characterization of Ribulose-5-phosphate Epimerase from *Leishmania donovani*

Bandigi Narsimulu, Rahila Qureshi, Pranay Jakkula, Sayanna Are, and Insaf Ahmed Qureshi*

Cite This: *ACS Omega* 2022, 7, 548−564

Read Online

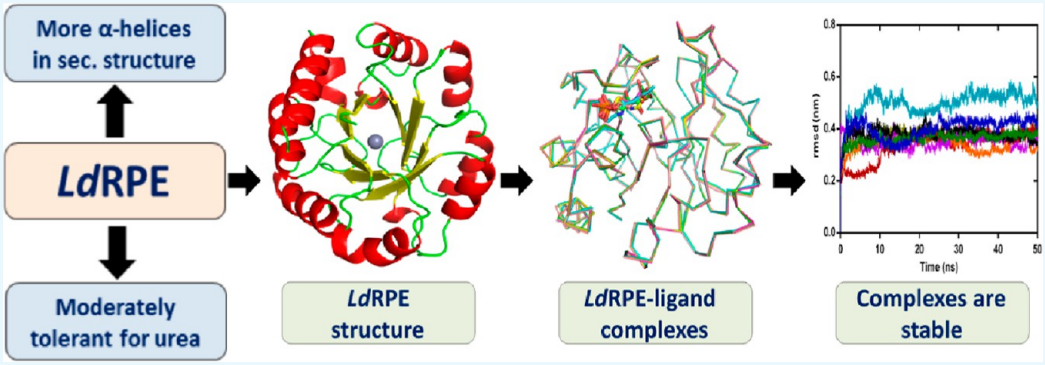

ABSTRACT: Pentose phosphate pathway (PPP) plays a crucial role in the maintenance of NADPH/NADP$^+$ homeostasis and provides protection against oxidative stress through detoxification of the reactive oxygen species. Ribulose-5-phosphate epimerase (RPE) participates in catalysis of the interconversion of ribulose-5-phosphate (Ru5P) to xylulose-5-phosphate (Xu5P) during PPP, however the structural attributes of this enzyme are still underexplored in many human pathogens including leishmanial parasites. The present study focuses upon cloning, purification and characterization of RPE of *Leishmania donovani* (*Ld*RPE) using various biophysical and structural approaches. Sequence analysis has shown the presence of trypanosomatid-specific insertions at the N-terminus that are absent in humans and other eukaryotes. Gel filtration chromatography indicated recombinant *Ld*RPE to exist as a dimer in the solution. Circular dichroism studies revealed a higher alpha helical content at physiological pH and temperature that comparatively varies with changing these parameters. Additionally, intrinsic fluorescence and quenching studies of *Ld*RPE have depicted that tryptophan residues are mainly buried in the hydrophobic regions, and the recombinant enzyme is moderately tolerant to urea. Moreover, homology modeling was employed to generate the three-dimensional structure of *Ld*RPE followed by molecular docking with the substrate, product, and substrate analogues. The modeled structure of *Ld*RPE unravelled the presence of conserved active site residues as well as a single binding pocket for the substrate and product, while an *in silico* study suggested binding of substrate analogues into a similar pocket with more affinity than the substrate. Additionally, molecular dynamics simulation analysis has deciphered complexes of *Ld*RPE with most of the ligands exhibiting more stability than its apo form and lesser fluctuations in active site residues in the presence of ligands. Altogether, our study presents structural insights into leishmanial RPE that could provide the basis for its implication to develop potent antileishmanials.

1. INTRODUCTION

Trypanosomatid protozoan parasite *Leishmania* is responsible for the disease leishmaniasis, which affect millions of people worldwide. The parasite causes a spectrum of diseases ranging from simple, self-healing innocuous oriental shore to fatal visceral leishmaniasis. It is transmitted to the mammalian hosts through the bite of sandfly belonging to the genus Phlebotomus.[1] The amastigote and promastigote stages of the parasite survive and propagate inside the parasitophorous vacuole of the host macrophage and midgut of the sandfly, respectively.[2,3] The infected macrophage provides a first-line antimicrobial defence through the production of reactive oxygen species (ROS) and creating the oxidative stress that is harmful for the survival of parasites. To overcome this problem in the parasite most of the glucose molecules undergo in pentose phosphate pathway (PPP) to produce NADPH that reduces the oxidative stress environment surrounding the parasite and makes the PPP a vital part of the defence

Received: September 8, 2021
Accepted: November 25, 2021
Published: December 17, 2021

Applied Microbiology and Biotechnology (2021) 105:5471–5489
https://doi.org/10.1007/s00253-021-11434-4

BIOTECHNOLOGICALLY RELEVANT ENZYMES AND PROTEINS

Biochemical and structural insights into 6-phosphogluconate dehydrogenase from *Leishmania donovani*

Pranay Jakkula[1] · **Bandigi Narsimulu**[1] · **Insaf Ahmed Qureshi**[1]

Received: 17 February 2021 / Revised: 19 May 2021 / Accepted: 13 June 2021 / Published online: 12 July 2021

Abstract

6-phosphogluconate dehydrogenase (6PGDH) participates in pentose phosphate pathway of glucose metabolism by catalyzing oxidative decarboxylation of 6-phsophogluconate (6PG) and its absence has been lethal for several eukaryotes. Despite being a validated drug target in many organisms like *Plasmodium*, the enzyme has not been explored in leishmanial parasites. In the present study, 6PGDH of *Leishmania donovani* (*Ld*6PGDH) is cloned and purified followed by its characterization using biochemical and structural approaches. *Ld*6PGDH lacks the glycine-serine-rich sequence at its C-terminal that is present in other eukaryotes including humans. Leishmanial 6PGDH possesses more affinity for substrate (6PG) and cofactor (NADP) in comparison to that of human. The enzymatic activity is inhibited by gentamicin and cefuroxime through competitive mode with functioning more potently towards leishmanial 6PGDH than its human counterpart. CD analysis has shown higher α-helical content in the secondary structure of *Ld*6PGDH, while fluorescence studies revealed that tryptophan residues are not completely accessible to solvent environment. The three-dimensional structure was generated through homology modelling and docked with substrate and cofactor. The docking studies demonstrated two separate binding pockets for 6PG and NADP with higher affinity for the cofactor binding, and Asn105 is interacting with substrate as well as the cofactor. Additionally, MD simulation has shown complexes of *Ld*6PGDH with 6PG and NADP to be more stable than its apo form. Altogether, the present study might provide the foundation to investigate this enzyme as potential target against leishmaniasis.

Key points

- *Ld6PGDH enzymatic activity is competitively inhibited by gentamicin and cefuroxime.*
- *It displays more helical contents and all structural characteristics of 6PGDH family.*
- *Interaction studies demonstrate higher affinity of cofactor than substrate for Ld6PGDH.*

Keywords *Leishmania donovani* · Pentose phosphate pathway · 6-phosphogluconate dehydrogenase · Enzyme kinetics · Antibiotics · Structural insights

Introduction

Leishmaniasis is a spectrum of diseases, caused by more than 20 species of *Leishmania* with three clinical manifestations, namely cutaneous, mucocutaneous, and visceral leishmaniasis. Among them, visceral leishmaniasis (VL) is caused by *L. donovani* and is characterized by weight loss, anemia, irregular bouts of fever, and enlarged liver and spleen. It is considered the most severe form of disease with an estimation of 50,000–90,000 new cases worldwide annually (https://www.who.int/news-room/fact-sheets/detail/leishmaniasis). Unavailability of effective vaccine makes the chemotherapy as widely recommended option for treatment of leishmaniasis. However, the currently used drugs such as pentavalent antimonials and amphotericin B are not satisfactory due to prolonged period of dosage, numerous side effects, and development of resistance by leishmanial parasite (Ponte-Sucre et al. 2017). Hence, there is an urgent need to explore proteins that are critical for the parasitic survival as well as infection and might provide the basis for designing specific inhibitors against leishmanial parasite.

✉ Insaf Ahmed Qureshi
insaf@uohyd.ac.in

[1] Department of Biotechnology & Bioinformatics, School of Life Sciences, University of Hyderabad, Prof. C.R. Rao Road, Hyderabad 500046, India

Department of Pharmaceuticals
Ministry of Chemicals and Fertilizers
Government of India

Azadi Ka Amrit Mahotsav

स्वच्छ भारत
एक कदम स्वच्छता की ओर

NIPER
HYDERABAD

National Institute of Pharmaceutical Education and Research (NIPER), Hyderabad

Department of Pharmaceuticals (DoP), Ministry of Chemicals and Fertilizers, Govt. of India
Balanagar, Hyderabad – 500037, Telangana, India

Poster Presentation Certificate

This is to certify that **Mr. Bandigi Narsimulu** has presented his work in the international conference on **"NextGen Therapeutics & Diagnostics Concept to Commercialization"** titled **"Evaluation of salicylate as potent inhibitor for glutamyl-tRNA synthetase of Leishmania donovani."** conducted by the National Institute of Pharmaceutical Education and Research, Hyderabad from 20th – 22nd April 2022

N Srinivas

DR. SRINIVAS NANDURI
Convenor

DR. SHASHI BALA SINGH
Director

International Symposium on Malaria Biology & 29th National Congress of Parasitology on Basic and Applied Aspects (ISMBNCP-2018)

This is to certify that Prof. / Dr. /Mr. / Ms. Bandigi Narsimulu ..... has participated / presented Invited talk / Oral / Poster session of **ISMBNCP-2018** held at School of Life Sciences, University of Hyderabad, Hyderabad – 500 046, India, from 1st - 3rd November 2018.

President
Indian Society for Parasitology

Convener
ISMBNCP-2018

Biochemical and structural attributes of leishmanial seryl and glutamyl tRNA synthetases

by Narsimulu B

Biochemical and structural attributes of leishmanial seryl and glutamyl tRNA synthetases

ORIGINALITY REPORT

50%	6%	48%	4%
SIMILARITY INDEX	INTERNET SOURCES	PUBLICATIONS	STUDENT PAPERS

PRIMARY SOURCES

1	Bandigi Narsimulu, Rahila Qureshi, Pranay Jakkula, Priti Singh, Mohammed Arifuddin, Insaf Ahmed Qureshi. "Exploration of seryl tRNA synthetase to identify potent inhibitors against leishmanial parasites", International Journal of Biological Macromolecules, 2023 Publication	45%
2	Submitted to University of Hyderabad, Hyderabad Student Paper	1%
3	www.ncbi.nlm.nih.gov Internet Source	1%
4	Girish Ch. Panigrahi, Rahila Qureshi, Pranay Jakkula, K. Amith Kumar, Nooruddin Khan, Insaf Ahmed Qureshi. "Leishmanial aspartyl-tRNA synthetase: Biochemical, biophysical and structural insights", International Journal of Biological Macromolecules, 2020 Publication	<1%

5	Samayaditya Singh, Insaf Ahmed Qureshi. "Identification of potent inhibitors against chorismate synthase of Toxoplasma gondii using molecular dynamics simulations", Journal of Molecular Graphics and Modelling, 2022 Publication	<1 %
6	dspace.uohyd.ac.in Internet Source	<1 %
7	James S. Pham, Karen L. Dawson, Katherine E. Jackson, Erin E. Lim et al. "Aminoacyl-tRNA synthetases as drug targets in eukaryotic parasites", International Journal for Parasitology: Drugs and Drug Resistance, 2014 Publication	<1 %
8	Jakkula Pranay, Rahila Qureshi, Atif Iqbal, S.R. Sagurthi, Insaf A. Qureshi. "Leishmania donovani PP2C: kinetics, structural attributes and in vitro immune response", Molecular and Biochemical Parasitology, 2018 Publication	<1 %
9	Shun-ichi Sekine, Mika Shichiri, Stéphane Bernier, Robert Chênevert, Jacques Lapointe, Shigeyuki Yokoyama. "Structural Bases of Transfer RNA-Dependent Amino Acid Recognition and Activation by Glutamyl-tRNA Synthetase", Structure, 2006	<1 %

Publication

10	Mayank Saini, Sayanna Are, Insaf Ahmed Qureshi. "Pyridoxal Kinase of Disease-causing Human Parasites: Structural and Functional Insights to Understand its Role in Drug Discovery", Current Protein & Peptide Science, 2022 Publication	<1 %
11	S. B. Rho, K. H. Lee, J. W. Kim, K. Shiba, Y. J. Jo, S. Kim. "Interaction between human tRNA synthetases involves repeated sequence elements.", Proceedings of the National Academy of Sciences, 1996 Publication	<1 %
12	Stefano Paravisi. "Kinetic and mechanistic characterization of *Mycobacteriumtuberculosis* glutamyl-tRNA synthetase and determination of its oligomeric structure in solution", FEBS Journal, 03/2009 Publication	<1 %
13	centlib.mui.ac.ir Internet Source	<1 %
14	d.docksci.com Internet Source	<1 %
15	Igor Cestari, Kenneth Stuart. "A Spectrophotometric Assay for Quantitative Measurement of Aminoacyl-tRNA Synthetase	<1 %

Activity", Journal of Biomolecular Screening, 2012
Publication

16	www.nature.com Internet Source	<1 %
17	Shomik Maruf, Soumik Kha Sagar, Md Utba Rashid, Md Rasel Uddin et al. "Assessment of treatment outcomes of visceral leishmaniasis (VL) treated cases and impact of COVID-19 on VL management and control services in Bangladesh", Journal of Infection and Public Health, 2023 Publication	<1 %
18	Carla Polycarpo. "Chapter 12 Highlights on Trypanosomatid Aminoacyl-tRNA Synthesis", Springer Science and Business Media LLC, 2014 Publication	<1 %

Exclude quotes	On	Exclude matches	< 14 words
Exclude bibliography	On		

University of Hyderabad
Hyderabad- 500 046, India

PLAGIARISM FREE CERTIFICATE

This is to certify that the similarity index of this thesis as checked by the Library of University of Hyderabad is 50%. Out of this, 45% similarity has been found to be identified from the candidate's own publication (B. Narsimulu) which forms the adequate part of the thesis. The details of student's publication are as follows:

Publication	% Similarity
Narsimulu B, Qureshi R, Jakkula P, Sign P, Arifuddin M, Qureshi IA (2023). Exploration of seryl tRNA synthetase to identify potent inhibitors against leishmanial parasites. ***International Journal of Biological Macromolecules*** **237(1): 124118.**	**45**

About 5% similarity was identified from external sources in the present thesis which is according to prescribed regulations of the University. All the publications related to this thesis have been appended at the end of the thesis. Hence the present thesis may be considered to be plagiarism free.

Dr. Insaf Ahmed Qureshi
Supervisor

Dr. INSAF A. QURESHI
Associate Professor
Dept. of Biotechnology & Bioinformatics
School of Life Sciences
University of Hyderabad
Hyderabad-500 046, India.